34

Preliminary Observations on the Niigata-Chuetsu Oki, Japan, Earthquake of July 16, 2007

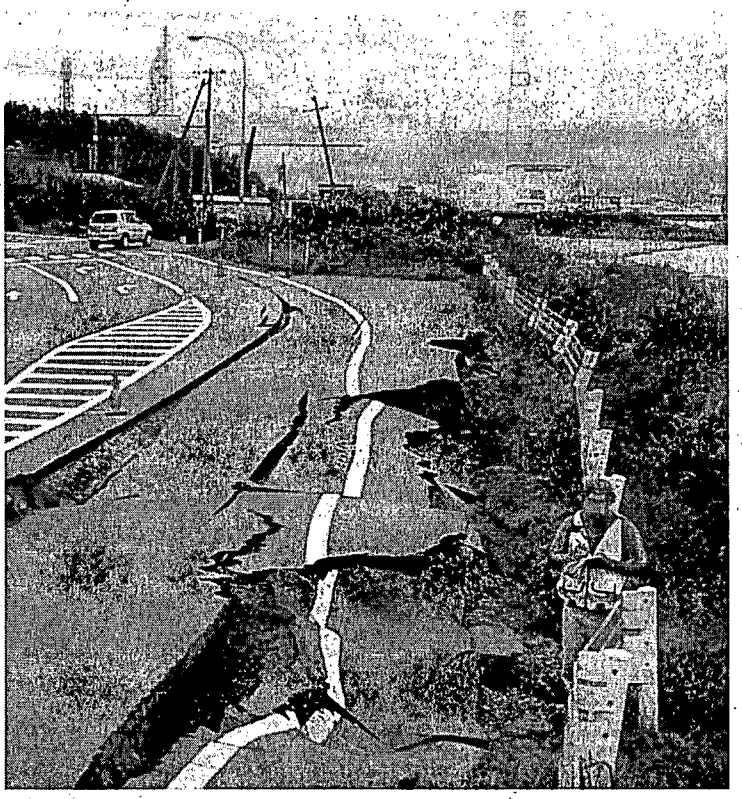

Robert Kayen (Leader), Santiago Pujol (Leader), Brian D. Collins, Norm Abrahamson, Scott Ashford, Scott J. Brandenberg, Stephen Dickenson, Laurie Johnson, Toshimi Kabeyasawa, Yohsuke Kawamata, Hidetaka Koumoto, Yasuo Tanaka, Nanako Marubashi, Kohji Tokimatsu, Ben Tsai, Peter Yanev, Mark Yashinsky, Kim Yousok

EERI-GEER Web Report 2007–1 v.8
October 9, 2007

B34

Additional site information and imagery at http://walrus.wr.usgs.gov/infobank/n/nii07jp/html/n-ii-07-jp.sites.kmz

Contents

Section 1 - Introduction 3

Section 2 - Seismological Aspects 9

Section 3 - Landslides 32

Section 4 - Liquefaction 44

Section 5 - Building and Industrial Structures 79

Section 6. Bridges 110

Section 7 -Tanks 153

Section 8 - Ports and Harbors 162

Section 9 - Transportation Systems 192

Section 10 - Lifeline Systems 207

Section 11 - Response and Recovery Issues 219

Preliminary Observations on the Niigata-Chuetsu Oki, Japan, Earthquake of July 16, 2007

Robert Kayen[1] (Leader), Santiago Pujol[2] (Leader), Brian Collins[1], Norm Abrahamson[3], Scott Ashford[4], Scott J. Brandenberg[5], Stephen Dickenson[4], Laurie Johnson[6], Yasuo Tanaka[7], Kohji Tokimatsu[8], Toshimi Kabeyasawa[9], Yohsuke Kawamata[4], Hidetaka Koumoto[7], Nanako Marubashi[10], Ben Tsai[3], Peter Yanev[12], Mark Yashinsky[11], Kim Yousok[8]

Section 1 - Introduction

1.1 Introduction

The M6.6 mainshock of the Niigata Chuetsu Oki (offshore) earthquake occurred at 10:13 a.m. local time on July 16, 2007, and was followed by a sequence of aftershocks that were felt during the entire time of the reconnaissance effort (USGS, http://earthquake.usgs.gov/eqcenter/eqinthenews/2007/us2007ewac/#details). The mainshock had an estimated focal depth of 10 km (USGS, 2007) and struck in the Japan Sea offshore Kariwa. Analysis of waveforms from source inversion studies indicate that the event occurred along a thrust fault with a NE trend. The fault plane is either a strike of 34 degrees with a dip of 51 degrees or a strike of 238 degrees with a dip of 41 degrees (http://wwweic.eri.u-tokyo.ac.jp/topics/20070716/). Which of these two planes is associated with the mainshock rupture is unresolved, although attenuation relationship analysis indicates that the northwest-dipping fault is favored. The quake affected an approximately 100-km-wide area along the coastal areas of southwestern Niigata prefecture. The event triggered ground failures as far as the Unouma Hills, located in central Niigata approximately 50 km from the shore and the source area of the 2004 Niigata Chuetsu earthquake. The primary event produced tsunami run-ups along the shoreline of southern Niigata that reached maximum heights of about 20 centimeters.

[1] U.S. Geological Survey
[2] Purdue University
[3] Pacific Gas and Electric Company
[4] Oregon State University
[5] University of California at Los Angeles
[6] Kyoto University
[7] Kobe University
[8] Tokyo Institute of Technology
[9] University of Tokyo
[10] Nagoya Institute of Technology
[11] California Dept. of Transportation
[12] Independent Consultant

The JMA (Japan Meteorological Agency) seismic intensity was 6+ (IX in MMI) in Kariwa-cho, Kashiwazaki city, and Nagaoka city in Niigata prefecture, and Ohzuna-machi in Nagano prefecture. An instrument maintained by K-NET (Kyoshin Network, National Research Institute for Earth Science and Disaster Prevention of Japan) recorded a value of peak ground acceleration of 0.67g near Kashiwazaki's city municipal building. The earthquake resulted in eleven fatalities and nearly two thousand injuries (http://www.pref.niigata.jp/seisaku/kokusai/english/). Close to 1,100 collapses of residential structures took place. These collapses occurred almost exclusively in old houses with wood and clay walls and heavy kawara, clay-tile roofs. In many cases, reconnaissance team members observed that collapses occurred in the store houses of the residences, rather than the residences themselves, although hundreds of homes also collapsed.

Damage occurred in lifeline utilities of gas, water, and electricity. Electric power generation recovered in areas without downed power lines within a day in most of the epicentral area. The water supply system and gas network were also damaged in areas of soft ground. Water service had not been restored in Kashiwazaki one week following the event. The team saw a strong presence of the Japan Self-Defense Forces distributing water at community centers throughout the city during the entire duration of the reconnaissance.

Kariwa village is home to the world's largest nuclear power plant with seven reactors and a total output of 8200 Megawatts. This facility is instrumented with 97 strong motion recorders that were triggered by the July 16, 2007 event. Records obtained by a number of these instruments were lost because of overwrites that occurred during aftershocks. Several members of our team visited Kashiwazaki-Kariwa nuclear power plant facility and preliminary observations are presented in Chapter 5. The power plant is located above the inferred fault planes in a region of high iso-seismal intensity, as inferred from the observed damage patterns in the area. Critical structures appeared to have performed well given the intensity of the ground shaking, large ground settlement, and evidence of liquefaction near the waterfront.

The reconnaissance was a combined effort of the Earthquake Engineering Research Institute (EERI) - Learning From Earthquakes, and the Geo-Engineering Earthquake Reconnaissance (GEER) activity of the National Science Foundation (NSF). EERI and GEER dispatched the first reconnaissance team to Niigata, Japan within three days of the earthquake. The EERI-GEER team was led by Robert Kayen of the United States Geological Survey (USGS) and composed of Scott Ashford, Steve Dickenson, and Yohsuke Kawamata from the School of Civil and Construction Engineering at Oregon State University; Brian Collins of the USGS; and Scott Brandenberg of the University of California at Los Angeles. EERI and PEER (Pacific Earthquake Engineering Research Center) supported the reconnaissance efforts of Santiago Pujol (co-leader) of Purdue University in collaboration with Toshimi Kabeyasawa, Nanako Marubashi, and Yousok Kim from the Japan Association of Earthquake Engineering (JAEE) to specifically examine the performance of buildings during the earthquake. The EERI-GEER team was joined by international GEER members Yasuo Tanaka and Hidetaka Koumoto of Kobe University, and Kohji Tokimatsu of Tokyo Institute of Technology. Norm Abrahamson

and Ben Tsai, of Pacific Gas and Electric Company synthesized the seismological information about the event. A third group of EERI participants - Laurie Johnson, Mark Yashinsky and Peter Yanev, visited the region in early August to document the emergency response and performance of bridges.

This earthquake reconnaissance effort was made possible by funding from the U.S. National Science Foundation, cost sharing by the U.S. Geological Survey, and volunteer work by the team participants. Cooperation with the following Japanese researchers and organizations was invaluable: Kazuo Konagai, University of Tokyo, Toshikatsu Ichinose of Nagoya Institute of Technology, Toshikazu Kabeyasawa and Toshinori Kabeyasawa of the University of Tokyo, Kobe University and the staff of the Research Center for Urban Safety and Security (RCUSS). This material is based upon work supported by the National Science Foundation under Grant No. CMS-032914 & National Science Foundation Grants supporting EERI. Any opinions, findings, conclusions or recommendations expressed in this material are those of the authors and do not necessarily reflect the views of the sponsoring organizations.

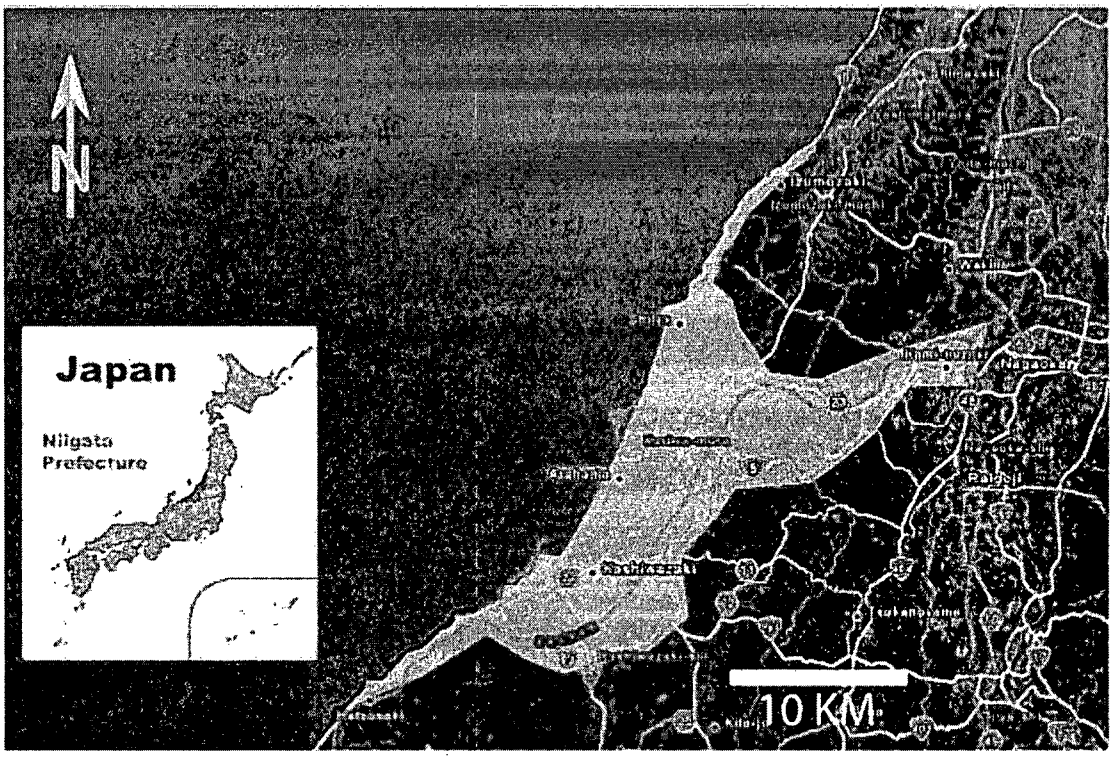

Figure 1.1: The reconnaissance effort covered the coastal region of southwest Niigata Prefecture, Japan. Coverage extends from the northern coastal town of Izumozaki-machi to the town of Hatsusaki to the south, and east to Nagaoka City.

1.2 Reconnaissance Method

A reconnaissance team sponsored by the National Science Foundation (NSF) was organized and sent to the epicentral region within the first 48 hours following the

earthquake to assess the geo-engineering and soil-related structural damage aspects of this event. The team's main goal was to quantify the spatial extent and amplitude of ground failures, soil liquefaction, landslides, and damage to bridges, piers, ports and harbors, lifeline systems and critical structures.

During the five-day reconnaissance, from July 20 through July 24, three vehicles were used to cover most of the roads of the epicentral region. On the ground, we sought to quantify the severity and abundance of damage associated with ground and ground-structure interaction. Each of the three vehicles had teams equipped with hand-held two-way radios, digital cameras, maps, computers for recording site logs, and GPS units for recording track logs and site locations. In the evening, the reconnaissance team held meetings where the GPS data, site logs and digital pictures were merged into a common database. In the field, we generated Google Earth KML mark-up language files to display all of the written observations on dynamic digital maps (Figure 1.2), and damage-specific maps (e.g., Google Earth map of liquefaction damage). By observing damage in the Google Earth program, we identified unexplored areas for the next days reconnaissance, spatial trends in the observations, and any errors in the GPS logs and typed observations. The .kml files were also sent by email to the United States so that EERI and GEER members working on the reconnaissance effort could take virtual tours of the damage zone and plan for following reconnaissance efforts. Using the city of Kashiwazaki's Google Earth community display of 3D buildings and residences, we were also able to identify the locations of critical facilities such as the waster water plant, municipal waste incinerator, schools, and other municipal buildings.

Readers of this report should download and open the .kmz Google Earth map file to navigate through the report observation sites as they are described in the text. Clicking on the individual site name in the waypoints folder will direct the program to fly to that site. http://walrus.wr.usgs.gov/infobank/n/nii07jp/html/n-ii-07-jp.sites.kmz The file n-ii-07-jp.sites.kmz will be updated regularly on the USGS server. Each time readers visit the data set, we recommend that you visit the url, above, and download the latest file. Then, remove any older versions of that file from Google Earth before uploading the newest .kmz file.

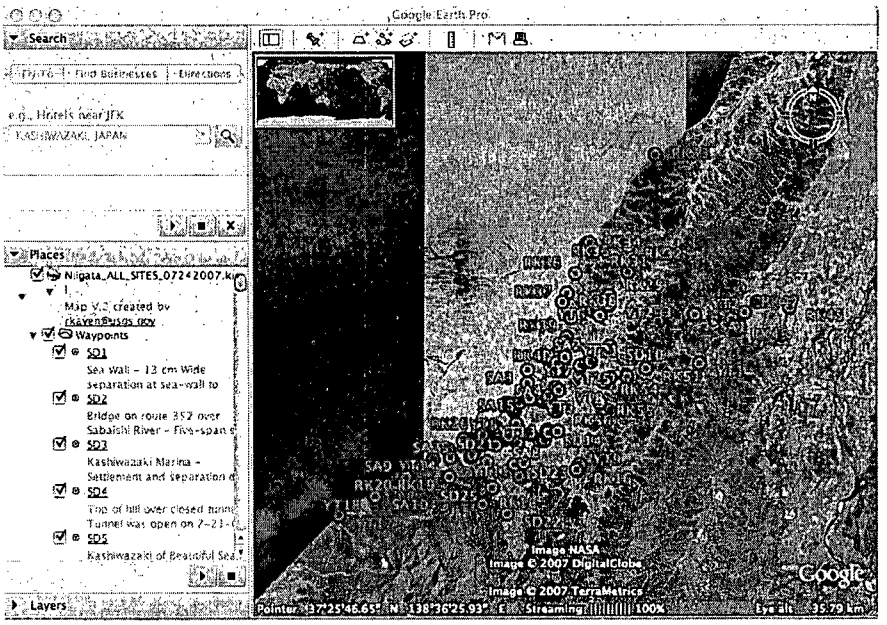

Figure 1.2: An interactive observation map of the Kashiwazaki, City area of Niigata Prefecture, Japan affected by the July 16, 2007 earthquake can be viewed at http://walrus.wr.usgs.gov/infobank/n/nii07jp/html/n-ii-07-jp.sites.kmz

Four teams of delegates from EERI and JAEE followed the team supported by NSF to document details of damage to structures, industrial facilities, bridges, and emergency response. These teams used the .kml file created with Google Earth to guide and map their observations.

High-resolution topographic data sets of the most significant damage features were collected for preservation of the event using the USGS terrestrial LiDAR (Light Detection and Ranging) system. Terrestrial LiDAR data were collected for the Omigawa landslide (Site RK20, Shin-etsu Train Station Landslide N37.34480°, E138.48888°); the Ozumi-Mishimayamachi Landslide (Site RK2, N37.44057°, E138.70467°); the Kashiwazaki incinerator lateral spread (Site RK6, N37.39343°, E138.58555°); and the Kashiwazaki South Harbor liquefaction induced lateral spread (Site RK25, N37.36713°, E138.53210°). The terrestrial LiDAR data collection technique consists of sending and receiving laser pulses to build a point file of three-dimensional coordinates of virtually any reflective surface. The time of travel for a single pulse reflection is measured along a known trajectory such that the distance from the laser and consequently the location of a point of interest is computed. The USGS system consisted of a Riegl Z210 instrument mounted on a tripod platform and linked with a set of Topcon DGPS RTK receivers. The instrument captured data at approximately 8000 points per second with a typical range of several hundred meters and at an accuracy of 15 mm for each point. Data from these sites will be made available in digital format once processed.

This reconnaissance report has been organized into sections that describe geotechnical and structural aspects of the damage caused by the earthquake. The report begins with a description of the seismological aspects of the earthquake in Section 2.

Section 3 describes landslides, Section 4 describes liquefaction, Section 5 describes damage and performance of buildings, Section 6 describes damage to bridges, and Section 7 describes damage to tanks. Section 8 describes damage to ports and harbors, Section 9 describes damage to transportation systems, Section 10 describes damage to lifeline systems, and Section 11 describes response and recovery issues.

Section 2 - Seismological Aspects

2.1 Tectonic Setting

The Niigata Chuetsu Oki, Japan earthquake occurred on July 16, 2007 at 10:13:22 local time (01:13:22 URC) along the west coast of Honshu (Fig. 2.1) in an area of relative high seismic activity.

Tectonically, Niigata is in a region of compressional deformation that is associated with the boundary between the Amur plate and the Okhotsk plate (two relatively small plates that lie between the larger Eurasia and Pacific plates). Figure 2.1 shows the seismicity in central Japan from 1990 to present. Overall, the pattern of seismicity shows a general deepening of hypocenters from east to west associated with the subducting slab (yellow, green, blue and purple symbols). The shallow crustal earthquakes in the Niigata region are shown by the orange symbols in the center of the figure. The seismic hazard in the Niigata region at long return periods is related to crustal earthquakes since they can be closer but less frequent.

2.2 Mainshock

The mainshock moment magnitude of this event was estimated to be 6.6 using teleseismic data (USGS) and estimated to be 6.7 using regional Japanese data. The JMA magnitude is 6.8. For comparisons with earthquakes around the world, the moment magnitude is used: for this event, we use a moment magnitude of 6.6.

The Niigata earthquake was a buried reverse-slip earthquake. The estimated hypocenter was at a depth of 8 km (NRI ESDP, 2007) which is slightly shallower than the USGS depth of 10 km from teleseismic data. The focal mechanism leads to two potential fault planes: the first at strike = 215°, dip = 49°, rake = 80°; and the second at strike = 49°, dip = 42°, rake = 80°. Which of these two planes is associated with the mainshock rupture is unresolved. Aftershock locations fell along both planes, although the majority of the aftershocks were located along the SE dipping plane (49°/42°/80°). However, aftershocks from reverse earthquakes often occur along backthrusts on the conjugate plane.

A finite source inversion based on the nearby strong motion data (NRI ESDP, 2007) could not resolve the mainshock rupture plane (Fig. 2.2). The fit of the velocity waveforms is similar for the two planes. The rupture length is 30 km and the down-dip fault width is 22 km for both planes. The hypocenter is at the northeast end of either plane and the rupture was toward the southwest. The slip models for both rupture planes show a single strong asperity in the western-end of the rupture. The top of rupture for the two models is 1 km for the northwest dipping model and 3 km for the southwest dipping model. The maximum computed slip was 3.5 m. For both models, there is an asperity in the southwest-end of the rupture.

2.3 Strong Motion Recordings

The Japanese nationwide strong motion network, K-net, recorded the earthquake at 390 stations, with 20 stations within 50 km. A subset of the regional K-net stations that recorded the event are shown in Figure 2.3 and the nearby stations to the epicentral area are shown in Figure 2.4. Estimates of the V_{S30} values were provided by Strasser (2007). The KiK-Net station locations are shown in these figures as open circles. We had not completed compiling the KiK-net data at the time this report was prepared. Most of the stations within 30 km of the rupture are the K-Net stations.

Acceleration time series are shown in Figure 2.5 for the four closest stations. The accelerograms at station NIG018 (close to the fault plane and within the observed damaged area) show strong low-frequency content, suggesting features associated with liquefaction in foundation soils below the instrument. A soil profile reported by K-Net for the site is shown in Figure 2.6. The spiky acceleration behavior of NIG018 in Figure 2.5 is consistent with the known behavior of sandy soils undergoing cyclic mobility in undrained loading, although no surficial observation of liquefaction was observed at the site. The accelerograms at the other stations are more consistent with one other and show durations of 10-15 seconds. The 5% damped response spectra for 20 of the nearby stations are shown in Figures 2.7a-e. Observe the unusual frequency content for NIG018.

The attenuation of peak ground acceleration (PGA) and spectral ordinates (at T=0.2 sec and T=1.0 sec) is shown in Figures 2.8a,b,c for the rupture plane dipping to the southeast (red plane in Fig. 2.4) and in Figures 2.9a,b,c for the rupture plane dipping to the northwest (blue plane in Fig. 2.4). The attenuation is compared to the Abrahamson and Silva (2007) model developed as part of the NGA project (Power et al, 2006). At PGA and SA(T=0.2 sec), the ground motions from the Niigata earthquake are higher than estimated when using the southeast dipping source model (Fig. 2.8a,b). Using the northwest dipping source model, the PGA and T=0.2 sec data are in better agreement with the Abrahamson & Silva model. The T=1 sec data are equally well modeled by both source models. This is consistent with the inability of the source inversion, based on velocity time series, to distinguish between the two source models. Assuming that the Abrahamson and Silva (2007) model is applicable to crustal earthquakes in Japan at short distances, then the short period data suggest that the northwest dipping is favored.

2.4 Ground Motions at the Kashiwazaki-Kariwa Nuclear Power Plant

The seven-unit Kashiwazaki-Kariwa nuclear power plant, owned by Tokyo Electric Power Company (TEPCO) is located about 16 km from the epicenter determined by JMA (Japan Meteorological Agency) for this event. Figure 2.10 shows an aerial photograph from the Japanese Geographical Survey Institute (GSI) taken after the main shock. The plant has seven generators (Units 1 through 7) with a total output capacity of 8.2 GW located within a 4.2 km^2 area. There are two seismic instrument systems at the plant: an older system and a new system. The motions at 33 locations from the new system were recorded, but unfortunately, the recordings obtained at the other 66 locations from the older system, including two free-field down-hole arrays and most structural arrays were lost with the exception of the peak values. The recovered 33 recordings

Additional site information and imagery at http://walrus.wr.usgs.gov/infobank/n/nii07jp/html/n-ii-07-jp.sites.kmz

included 27 from a majority of the reactor and turbine buildings and one 4-depth free-field array at the Service Hall. The ground motion data from the old system could not be automatically transmitted due to communication congestion and system overwrite settings - the aftershocks caused additional triggers of the recorders, which overwrote the mainshock recordings in the buffer as new data came in. Thus, the mainshock recordings were lost.

The peak acceleration on the foundations for the seven units, as well as down hole array and Units 1 and 5 arrays, are listed in Table 2.1 and Figure 2.11. The NS and EW directions of the seismometers were set in the two principal axes of the plant buildings as opposed to being aligned with true NS and EW directions. The data indicate a large range in the foundation motions for the EW components with PGA values ranging over a factor of two. On the other hand, the NS components show values more similar to one another. The large range in the EW component values is likely due to different SSI effects at the different units and spatial variation of the ground motion over short distances probably due to the near-fault rupture mechanism. The large range of PGA values on the EW component shows the need for multiple recordings at NPP sites to reliably determine the input ground motions for the structures.

At the Service Hall, the horizontal peak ground accelerations recorded at the surface were smaller than the accelerations measured 250 m below grade. In contrast, the up-down (UD) ground accelerations were larger near the surface (Fig. 2.11). Horizontal ground acceleration measured in the downhole arrays at Units 1 and 5 are shown in Figs. 2.12 and 2.13. Here, the accelerations were amplified more in the turbine building than in the reactor building. However, there is no consistent trend in the variations of measured peak horizontal acceleration with depth.

Table 2.1. Peak accelerations from the foundations of the seven units at the Kashiwazaki Kariwa nuclear power plant (from TEPCO, 2007)

	PGA (gal)		
Unit	NS	EW	Vertical
K-1	311	680	408
K-2	304	606	282
K-3	308	384	311
K-4	310	492	337
K-5	277	442	205
K-6	271	322	488
K-7	267	356	355

2.5 References

Abrahamson, N.A., and Silva, W.J., (2007). Abrahamson & Silva NGA Ground Motion Relations for the Geometric Mean Horizontal Component of Peak and Spectral Ground Motion Parameters: PEER Report 200x/xx, Pacific Earthquake Engineering Research Center, College of Engineering, University of California, Berkeley, July 9, 2007, Draft Version 2, 378p. http://peer.berkeley.edu/pdf/AbraSil_2007_v2.pdf.

NRI ESDP (2007) Source Process of the 2007 Niigata-ken Chuetsu-oki Earthquake Derived from Near-fault Strong Motion Data, http://www.k-net.bosai.go.jp/k-net/topics/chuetsuoki20070716/inversion/

Power, M., B. Chiou, N. Abrahamson, and C. Roblee (2006). The next generation of ground motion attenuation models (NGA) project: An overview. Proc. Eighth National Conf., Earthquake Engineering, Paper No. 22.

Strasser, F. (2007). Estimates of VS30 values for the K-Net stations based on extrapolation of the velocity profile, personal communication.

TEPCO (2007). Report on analysis of observed records at Kashiwazaki-Kariwa Nuclear Power Plant during the Niigata-Chuetsu-Oki earthquake 2007.

USGS, (2007). U.S. Geological Survey, Earthquake Hazards Program, http://neic.usgs.gov/neis/eq_depot/2007/eq_070716_ewac/neic_ewac_h.html.

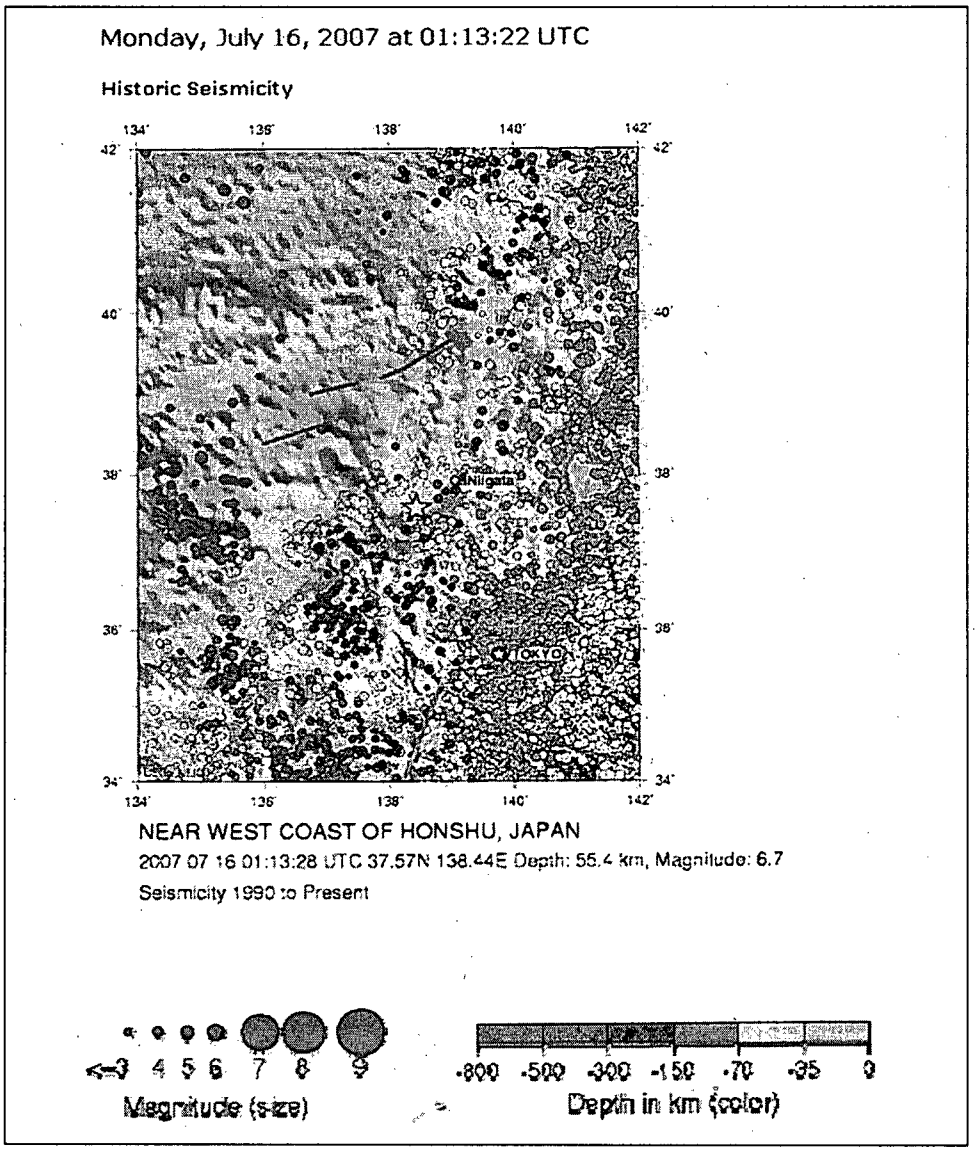

Figure 2.1: Seismicity in the Niigata region (Source: USGS, 2007).

Additional site information and imagery at http://walrus.wr.usgs.gov/infobank/n/nii07jp/html/n-ii-07-jp.sites.kmz

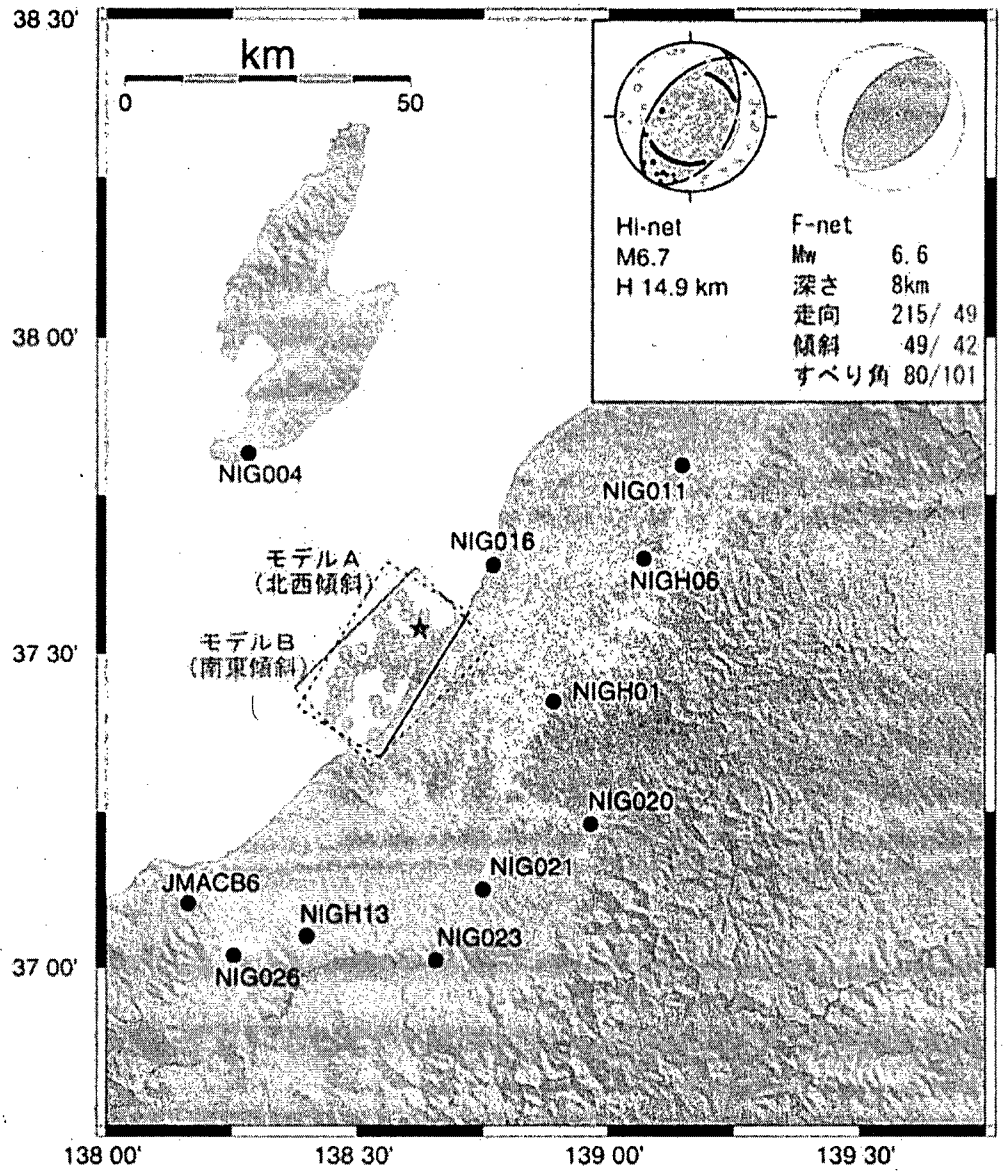

Figure 2.2: Strong motion stations used in the source inversion. The red and blue rectangles show the two alternative plausible fault planes with the solid line indicating the top of the rupture. (From NRI ESDP, 2007)

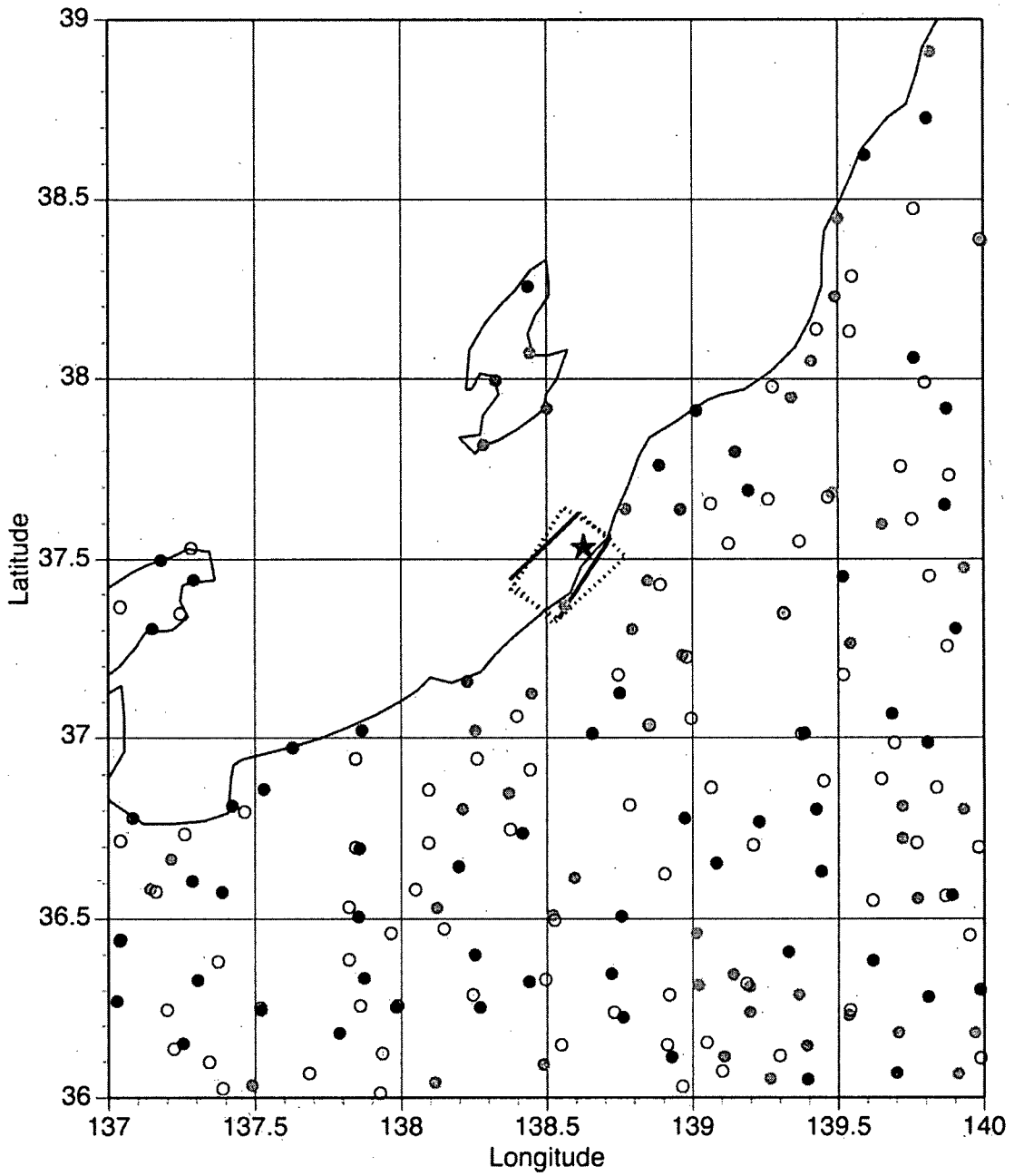

Figure 2.3: Regional subset of the K-net stations that recorded the Niigata earthquake. (Red: V_{S30}<180 m/s; Green: 180≤V_{S30}<360; Blue: 360≤V_{S30}<760). The open black circles are the Kik-Net stations. The two alternative mainshock rupture planes are shown by the blue and red rectangles.

Additional site information and imagery at http://walrus.wr.usgs.gov/infobank/n/nii07jp/html/n-ii-07-jp.sites.kmz

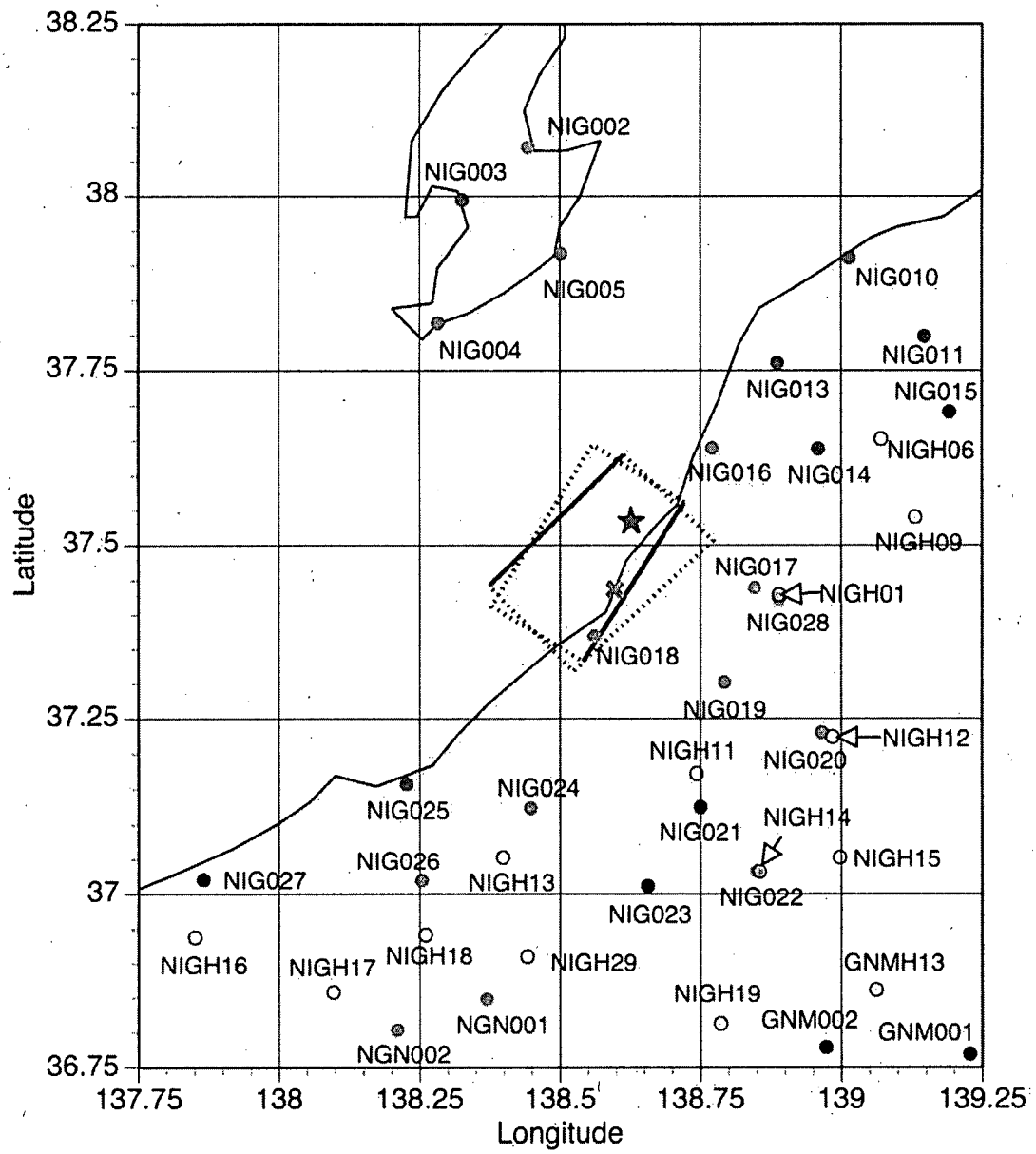

Figure 2.4: Nearby K-net stations that recorded the Niigata earthquake. (Red: V_{s30}<180 m/s; Green: 180≤V_{S30}<360; Blue: 360≤V_{S30}<760). The open black circles are the Kik-Net stations. The two alternative mainshock rupture planes are shown by the blue and red rectangles.

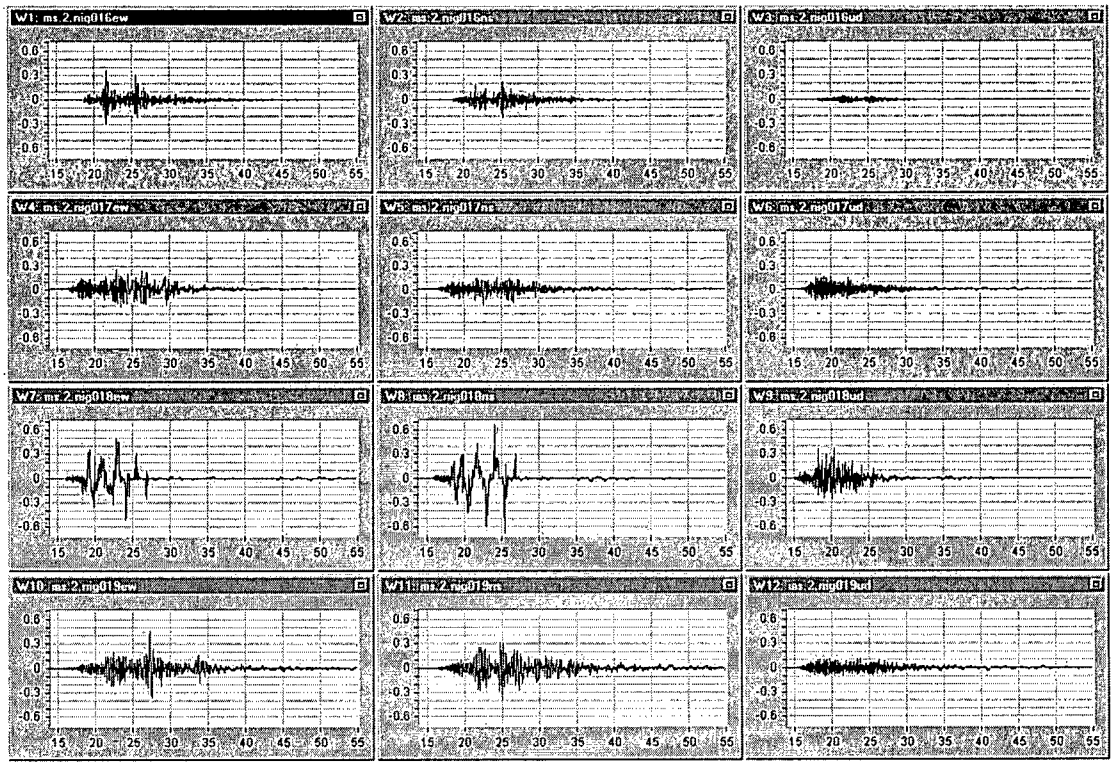

Figure 2.5: Example acceleration time histories of the near-source stations. From top to bottom: NIG016, NIG017, NIG018, NIG019. The horizontal axes represent time, in seconds, and the vertical axes represent ground acceleration as a fraction of the acceleration of gravity. The left panel is the EW component, middle panel is the NS component, right panel is the Z component.

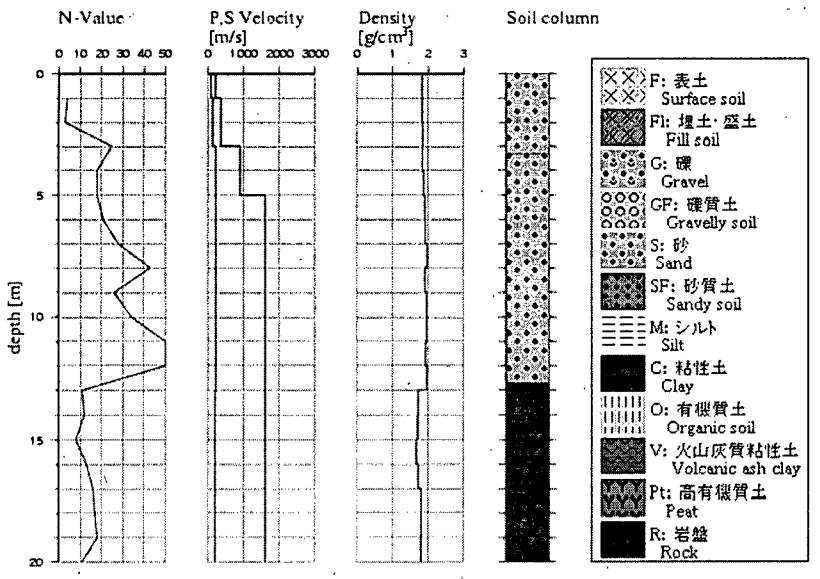

Figure 2.6. Soil profile at the K-NET Kashiwazaki Station (Source: K-NET)

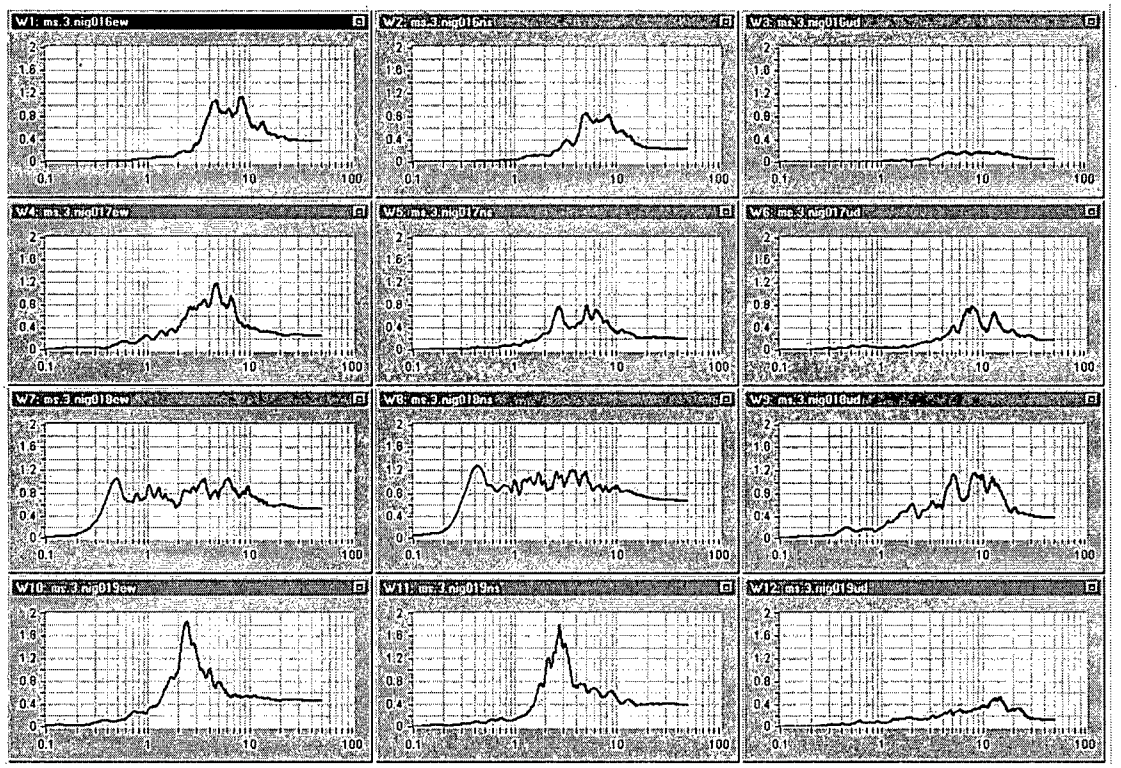

Figure 2.7a: 5% damped acceleration response spectra. From top to bottom: NIG016, NIG017, NIG018, NIG019. The horizontal axes represent frequency, in Hz, and the vertical axes represent absolute acceleration as a fraction of the acceleration of gravity. The left panel is the EW component, middle panel is the NS component, right panel is the Z component.

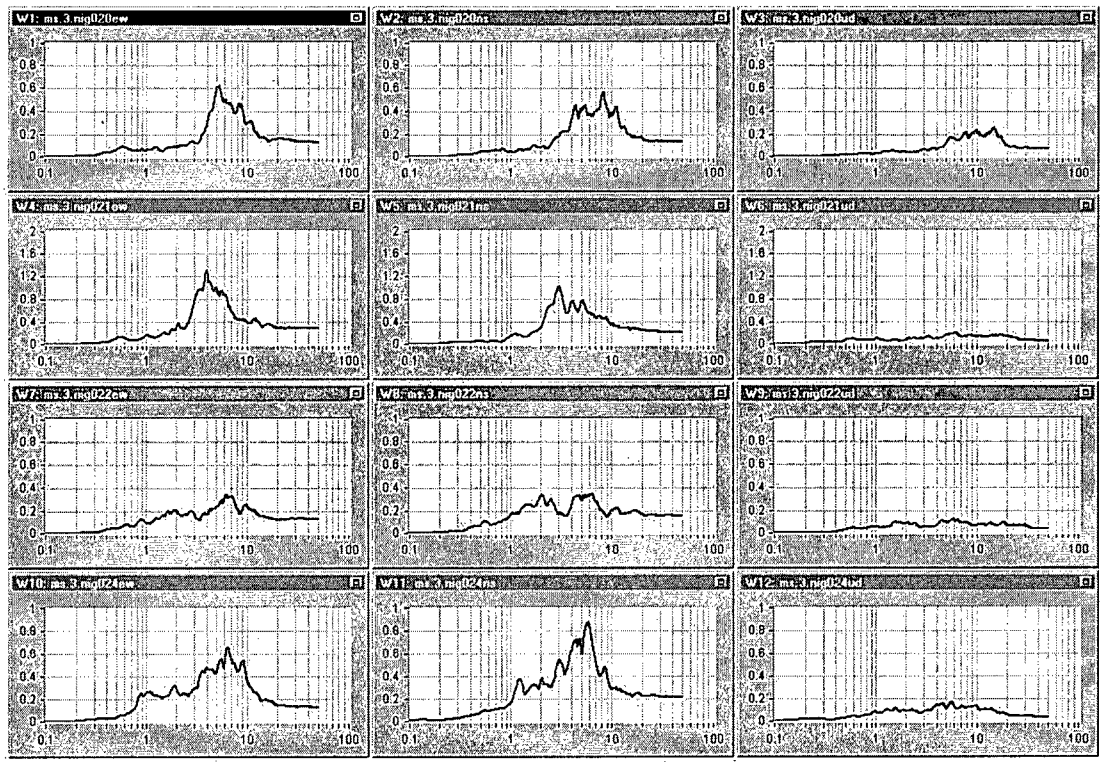

Figure 2.7b: 5% damped acceleration response spectra. From top to bottom: NIG020, NIG021, NIG022, NIG024. The horizontal axes represent frequency, in Hz, and the vertical axes represent absolute acceleration as a fraction of the acceleration of gravity. The left panel is the EW component, middle panel is the NS component, right panel is the Z component.

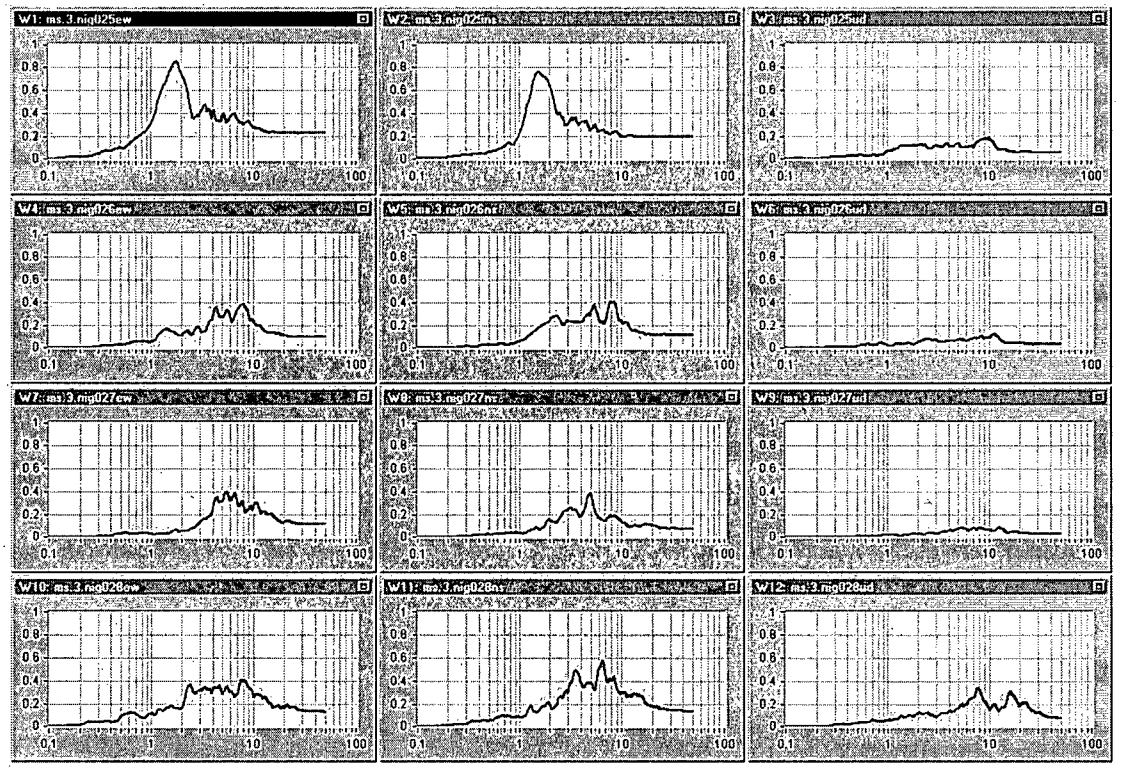

Figure 2.7c: 5% damped acceleration response spectra. From top to bottom: NIG025, NIG026, NIG027, NIG028. The horizontal axes represent frequency, in Hz, and the vertical axes represent absolute acceleration as a fraction of the acceleration of gravity. The left panel is the EW component, middle panel is the NS component, right panel is the Z component.

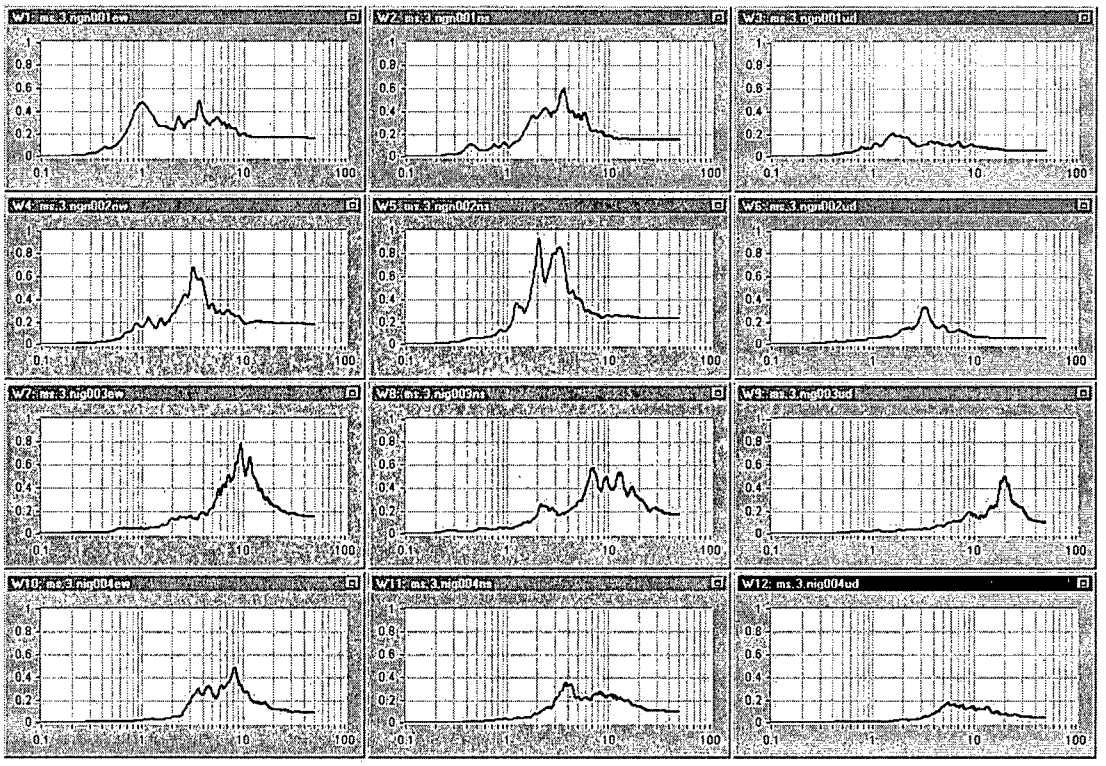

Figure 2.7d: 5% damped acceleration response spectra. From top to bottom: NGN001, NGN002, NIG003, NIG004. The horizontal axes represent frequency, in Hz, and the vertical axes represent absolute acceleration as a fraction of the acceleration of gravity. The left panel is the EW component, middle panel is the NS component, right panel is the Z component.

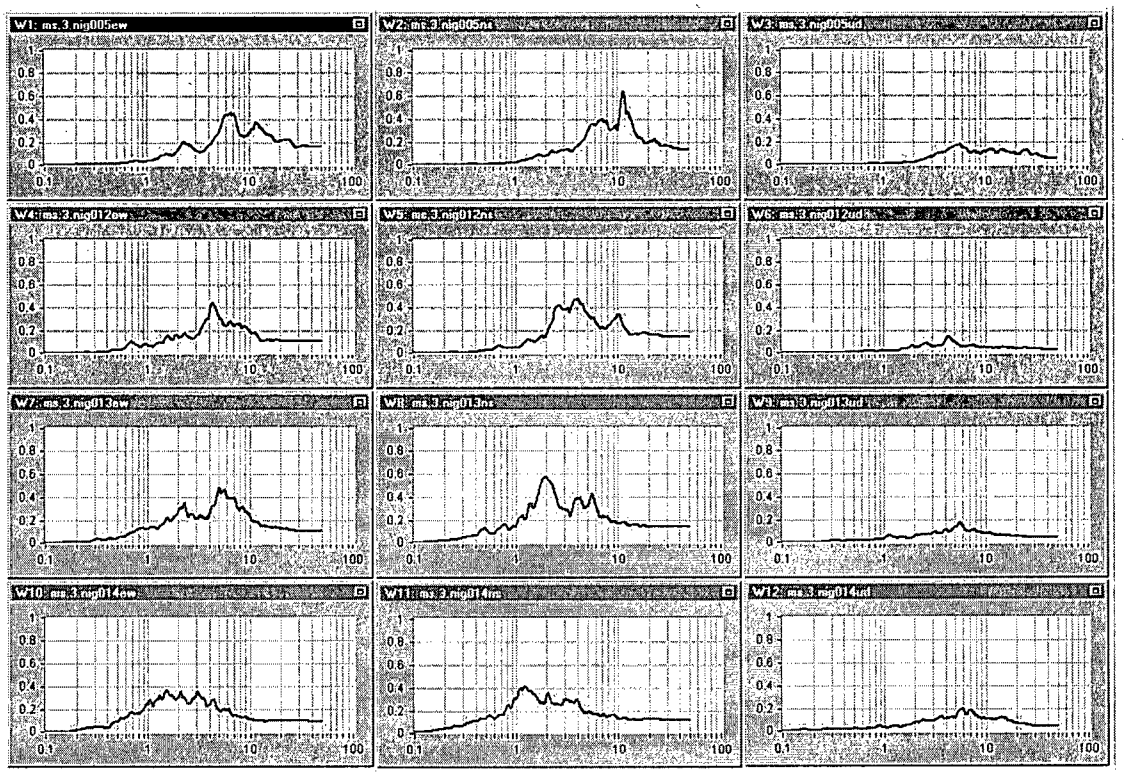

Figure 2.7e: 5% damped acceleration response spectra. From top to bottom: NIG005, NIG012, NIG013, NIG014. The horizontal axes represent frequency, in Hz, and the vertical axes represent absolute acceleration as a fraction of the acceleration of gravity. The left panel is the EW component, middle panel is the NS component, right panel is the Z component.

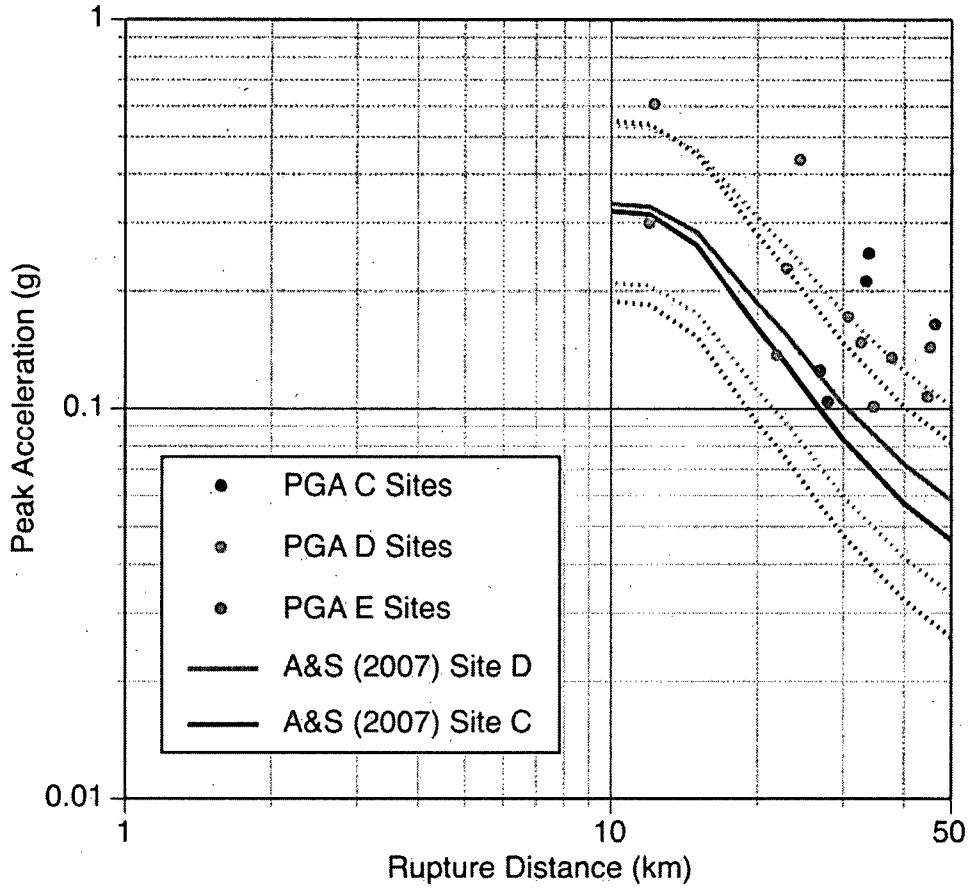

Figure 2.8a: PGA attenuation based on the southeast dipping source model. The Abrahamson and Silva model is for the hanging wall (HW) since most recording are on the HW side.

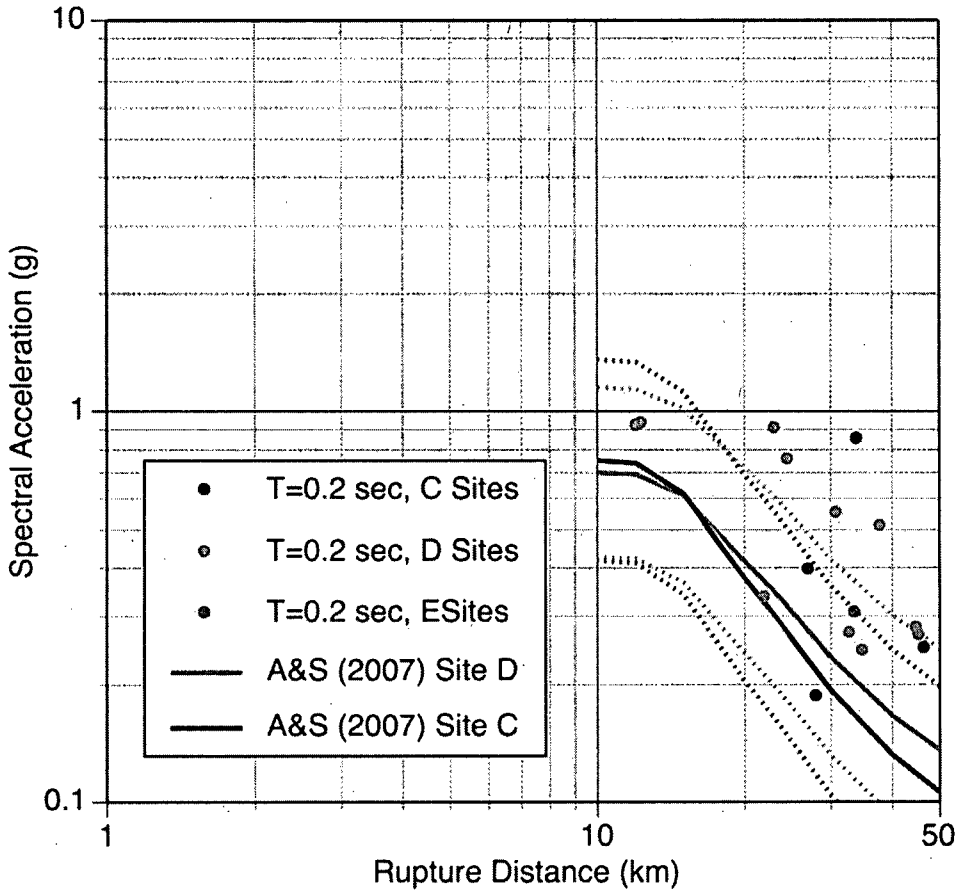

Figure 2.8b: T=0.2 attenuation based on the southeast dipping source model. The Abrahamson and Silva model is for the HW since most recording are on the HW side.

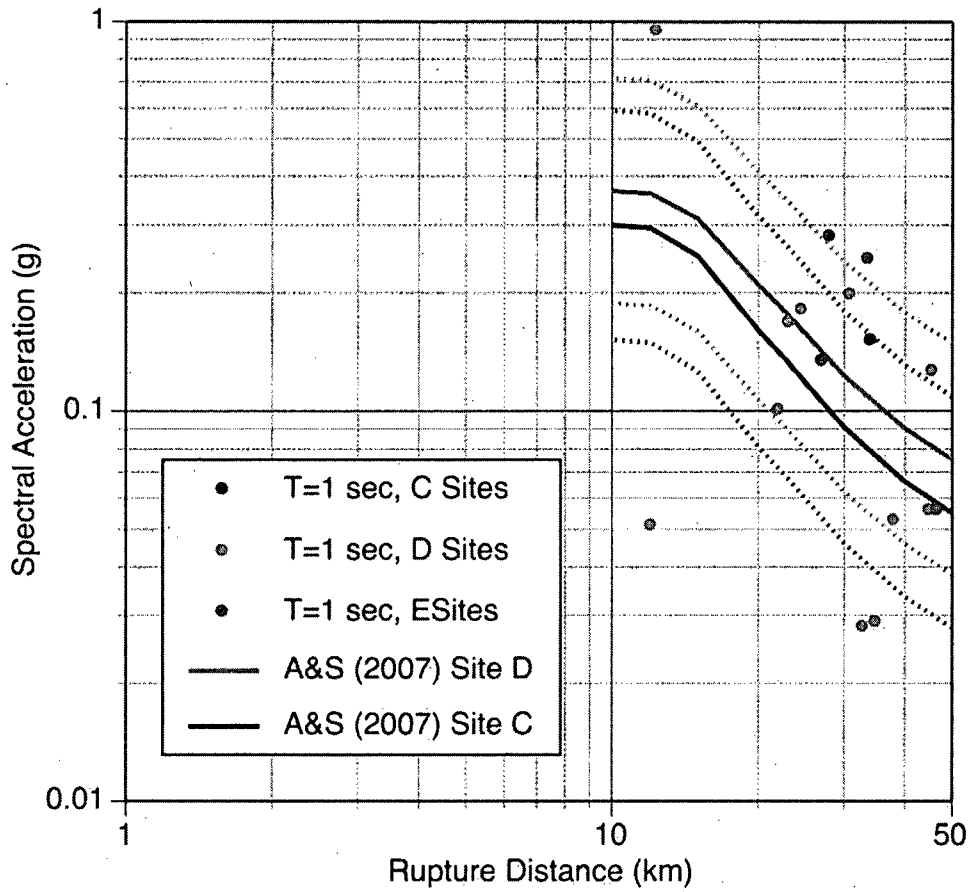

Figure 2.8c: T=1 sec attenuation based on the southeast dipping source model. The Abrahamson and Silva model is for the HW since most recording are on the HW side.

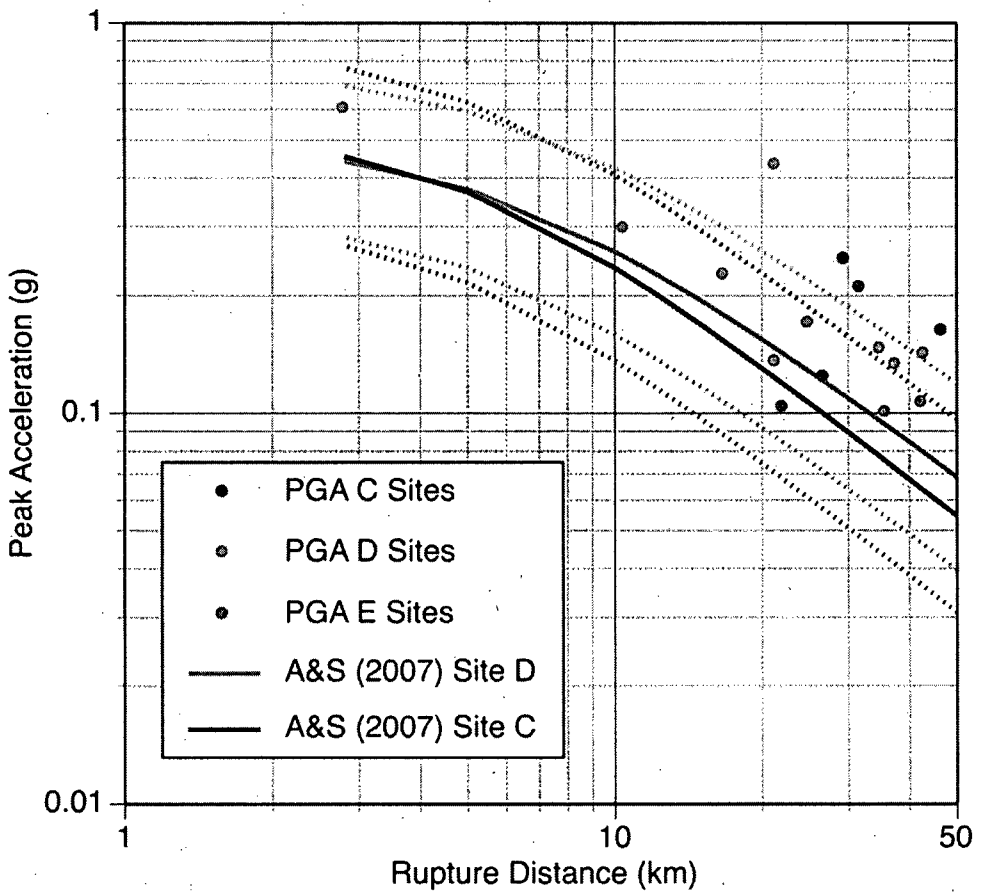

Figure 2.9a: PGA attenuation based on the northwest dipping source model. The Abrahamson and Silva model is for the FW since most recording are on the FW side.

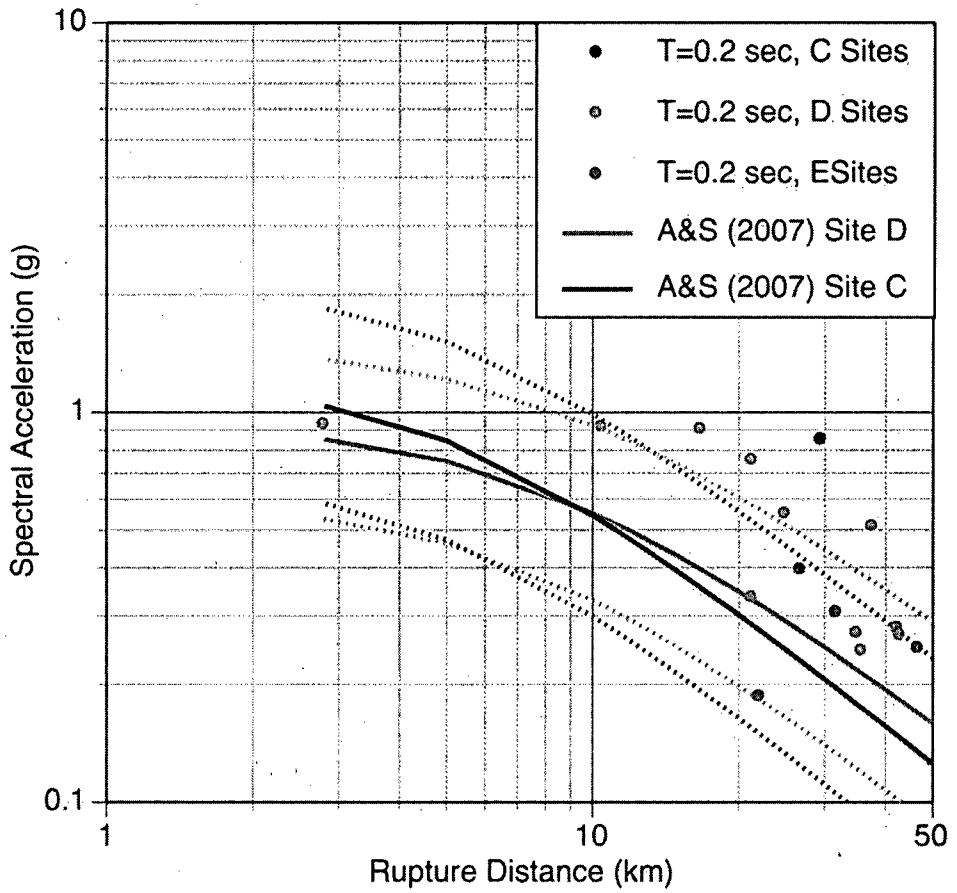

Figure 2.9b: T=0.2 sec attenuation based on the northwest dipping source model. The Abrahamson and Silva model is for the FW since most recording are on the FW side.

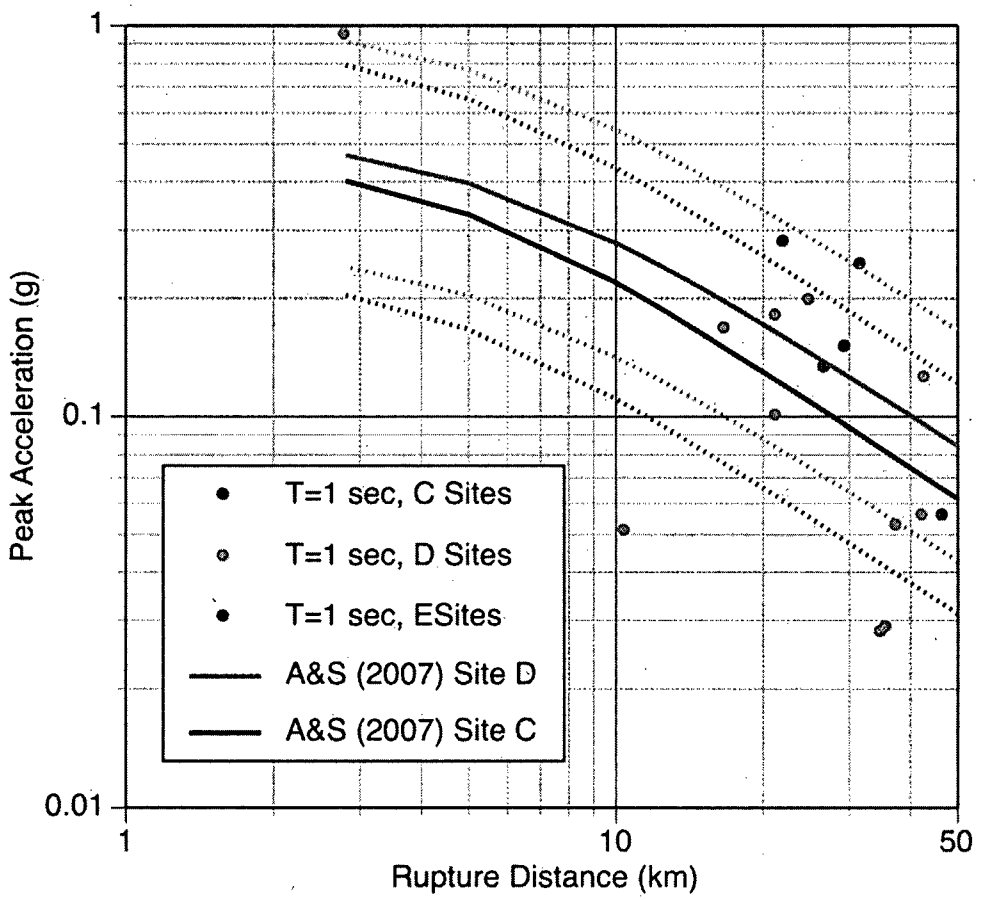

Figure 2.9c: T=1.0 sec attenuation based on the northwest dipping source model. The Abrahamson and Silva model is for the FW since most recording are on the FW side.

Fig. 2.10: Aerial Photograph of Kashiwazaki-Kariwa Nuclear Power Plan Area (GSI, 2007)

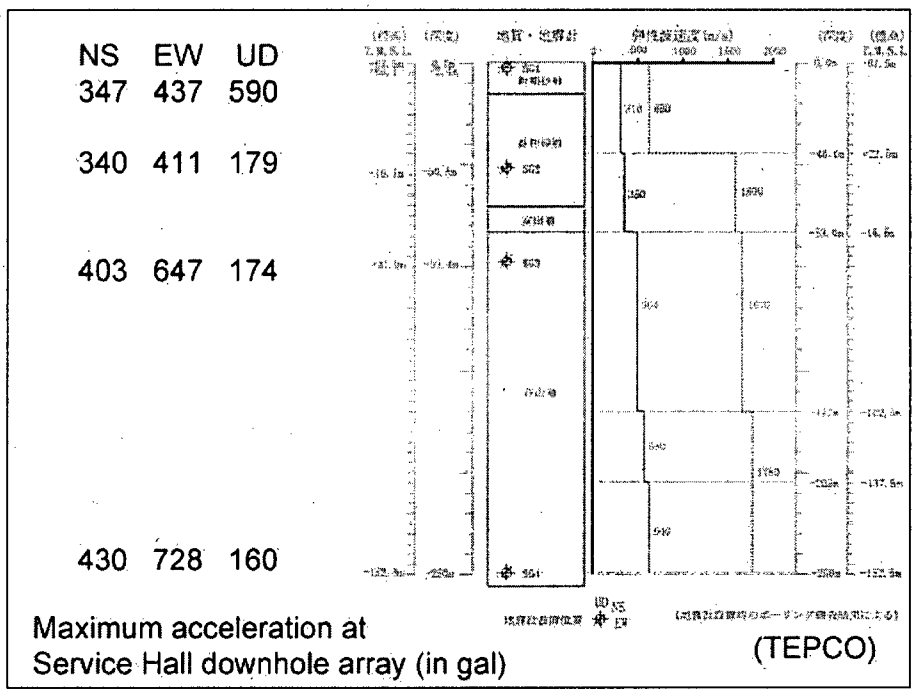

Fig. 2.11: Peak accelerations at Service Hall downhole array (after TEPCO,2007)

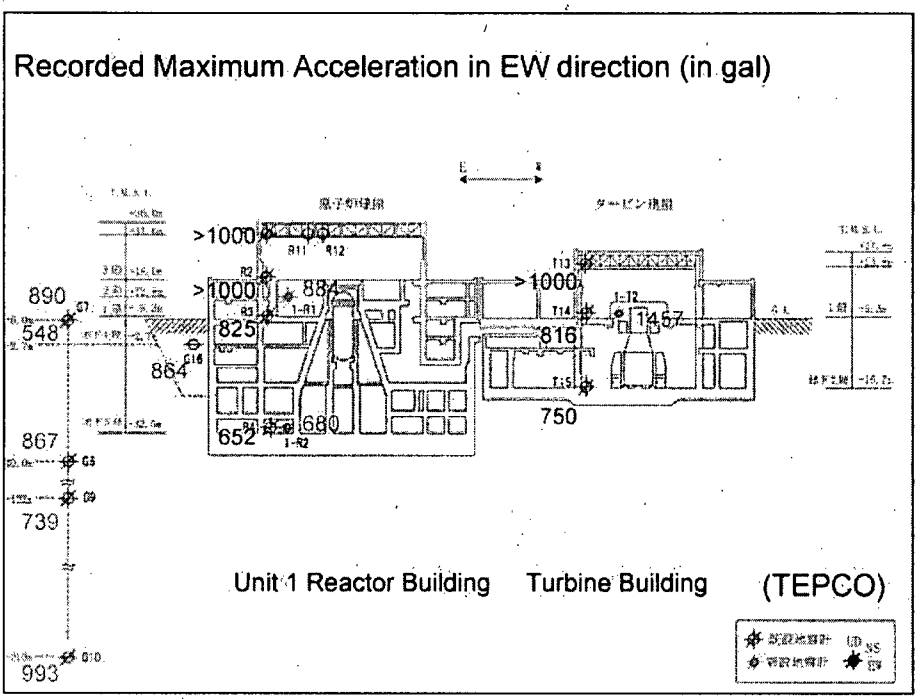

Fig. 2.12: Peak accelerations in and around Unit 1 (from TEPCO, 2007)

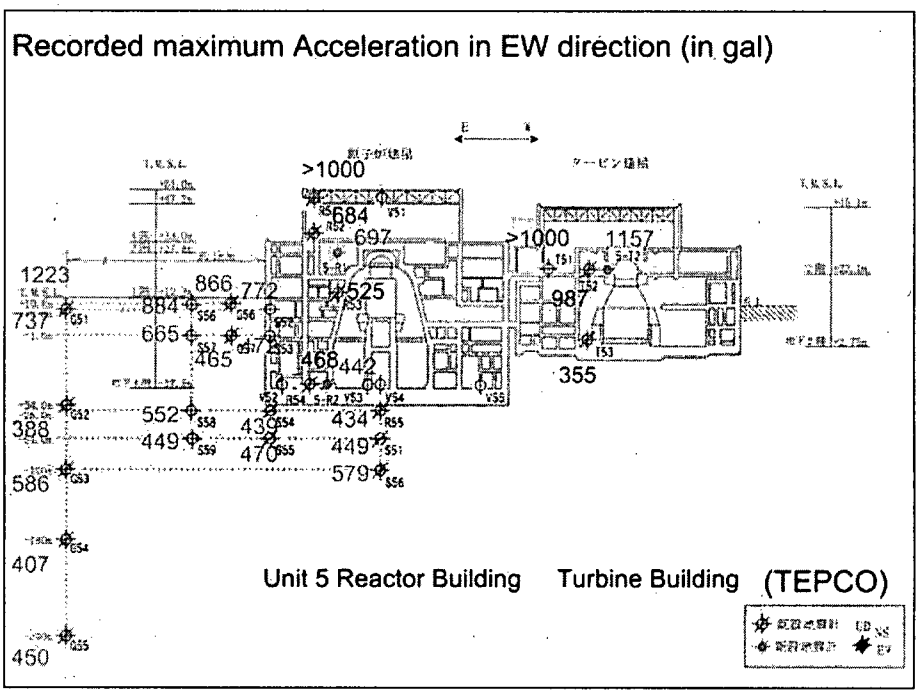

Fig. 2.13: Peak accelerations in and around Unit 5 (From TEPCO, 2007)

Section 3 - Landslides

Landslides caused by the earthquake consisted of shallow translational slides, debris slumps, and deep-seated rotational slides. Although the area had experienced a recent typhoon, soils were generally not sufficiently wet to cause debris flows.

In general, landslide activity was focused near the coast, with many steep (50° +) slopes experiencing shallow landsliding of overlying colluvial debris and residual soils (Figs. 3.1 - 3.4). Additional landslides also occurred some distance away from the main damaged areas (~10 km northeast of Kashiwazaki and 7 km east of the Kashiwazaki-Kariwa Nuclear Power Plant) in an upland, mountainous region. These slides also generally consisted of shallow translational events, but with at least one debris slump. Where transportation lines crossed areas of steep terrain, landslides often blocked or destroyed whole sections of roadways and railways. Three major transportation routes were blocked by landsliding in the region - the coastal road (Route 353) to the north of the Kashiwazaki-Kariwa Nuclear Power Plant (Fig. 3.2), the railway to the south of Kashiwazaki, at the Oumigawa train station on the Shin-etsu Line (Fig. 3.5) and Highway 8, north of the intersection with Route 252 located inland from the coast (Fig. 3.6).

An area of dense landslide activity not investigated by the field reconnaissance team, but identified through helicopter reconnaissance by the Japanese Public Works Research Institute (PWRI - a research agency under the Japanese Ministry of Infrastructure) was identified approximately 20 km to the southeast of Kashiwazaki in the Takayanagi-Machi region. Their photos identify at least 10 landslides in this area and were graciously lent to the reconnaissance team for study. According to the images, each of the slides appears to be relatively shallow and translational in movement and occurred within heavily vegetated upland areas. Because this area is located a significant distance away from other observed landslides from the earthquake, it is anomalous to the general pattern of observed seismic-induced geotechnical and structural damage and should be investigated more thoroughly.

Shallow coastal landslides were observed to be between 0.5 to several meters deep in colluvial and residual soils and ranged from 5 m^3 to several thousand cubic meters in volume. Typical slope surface and failure plane inclinations were between 50° and 70°, failing in translation as debris slides and slumps. These types of landslides were of sufficient size to close major transportation routes in the region, among them, the southern, coastal rail line and the coastal road (Route 352) located north of the Nuclear Power Station.

A large, deep, rotational slide occurred in weak mudstones and colluvial materials fairly far (~10 km) inland from the coast. The Ozumi Senbon landslide (Fig. 3.6) consisted of approximately 150,000 m^3 of total displaced material and led to destruction of a large road section on Route 8. According to on-site construction personnel, the slide plane was located at a depth ranging between 6 and 11 meters. Nearby to this site, several debris slumps/colluvial slides were also observed, however these required only

minimal grading efforts and maintenance to keep channels open for rice farming irrigation (Fig. 3.7).

Embankment failures were typical in road fills along the coast (Fig. 3.8), and were also observed at three sites located further inland (e.g. Figs. 3.9 - 3.10). Embankments underwent from 10 cm up to one meter of vertical displacement (Fig. 3.8), extending between 10 and to 60 meters in length. Three embankment failures required full closures of roads, and/or protection with tarps to reduce rainfall infiltration and the associated potential for additional movement. Among these was a 15-meter high, 97.5-meter wide, earth-fill dam located to the east of the region (Fig. 3.9), where cracking through the midpoint of the crest was observed. However, the dam was not storing water at the time of our visit and the reservoir had not been filled recently. Further, from on-site design documents, it appears that the normal water level is typically 8 meters below the crest of the dam. At a water supply dam located southwest of the city of Kashiwazaki (Fig. 3.10), cracking of the crest was also observed along with minor concrete cracking and spalling on the upstream side. Here, the reservoir water level was within several meters of the dam crest at the time of observation.

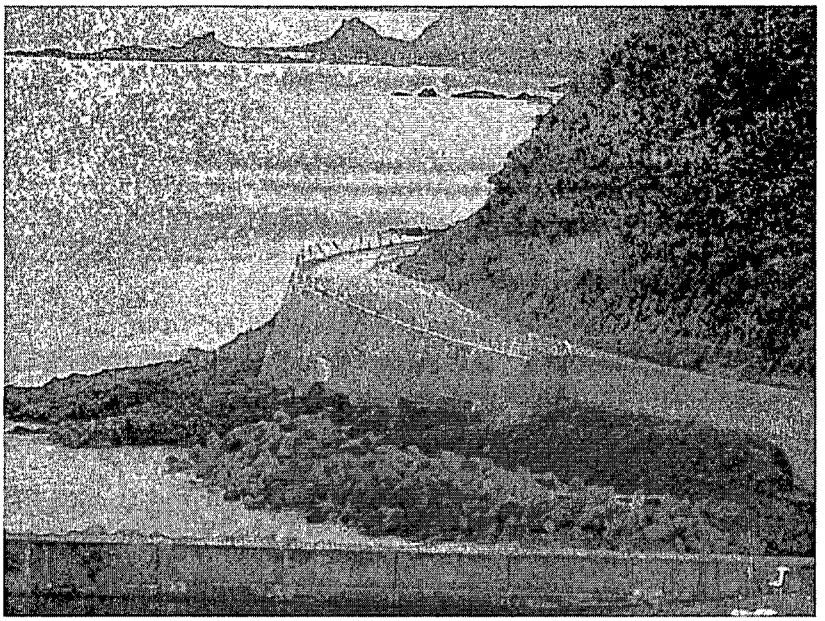

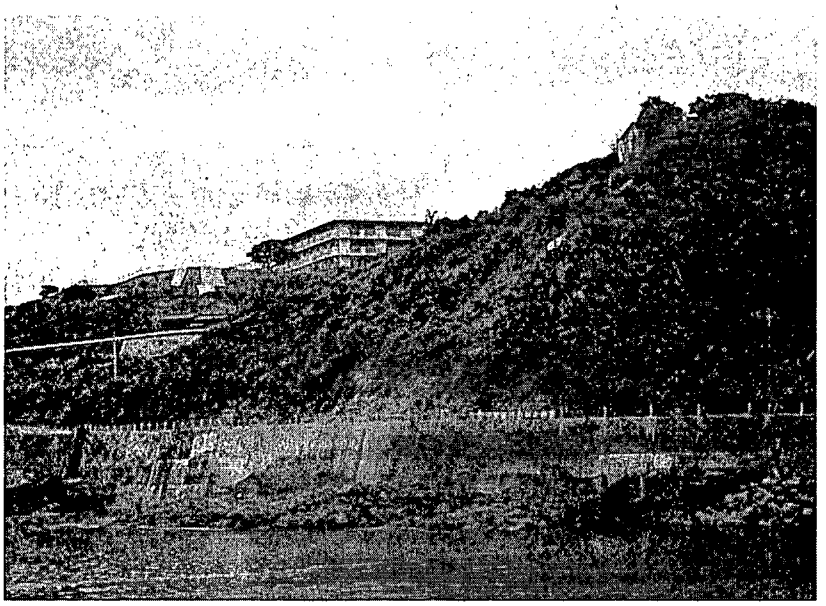

Figure 3.1: Shallow colluvial landslide located just north of the Kasashima Fishing Village, Site RK22/SA10; N37.33802° E138.46995°, photos taken 7/20/07 15:57 (top) and 7/21/07 13:35 (bottom). Dimensions are approximately 36 m wide, 24 m tall, 2 m thick. The lithology is composed of 24 m of weak mudstone overlying 6 m of more indurated, brecciated mudstone, which outcrops at the road. A 10 m tall concrete seawall leads down to the brecciated mudstone shore platform. The slide occurred in weak mudstone/colluvium, sliding over the brecciated mudstone, onto the road, and over the edge of the concrete seawall, spilling debris onto the shore platform at oceans edge.

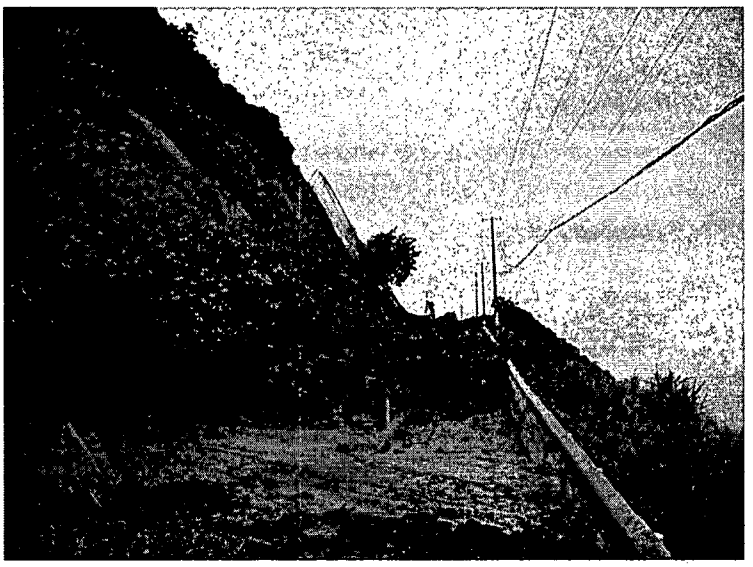

Figure 3.2: Coastal landslides on Highway 352 north of Kashiwazaki-Kariwa Nuclear Power Plant at road closure south of Route 373 (Site RK34; N37.48455° E138.62435°, photos taken 7/22/07 at approx. 10:45). This area consisted of at least eight individual slides. The landslide shown in the bottom photo consists of a slide in an area of previous instability - a shotcrete stabilization system is in effect for the bottom 50 m of this slope (total slope height is ~115 m), and overlain with a wire-mesh rock deflection system. The slide is approximately 50 to 60 m wide, 65 m long, and less than 1 meter thick. The landslide initiated above the shotcrete slope, moved into the wire-mesh and caused failure of the meshing and pull-out of the steel supports. The wire-mesh restrained most of debris, depositing the majority on the road, with only a slight quantity of the debris sliding over the road edge. The failure plane inclination is approximately 60°.

Figure 3.3: Coastal landslides on Highway 352 north of Kashiwazaki-Kariwa Nuclear Power Plant at road closure south of Route 373 (Site RK34-Slide 4; N37.48455° E138.62435°, photos taken 7/22/07 at approx. 10:45). This landslide is typical of many of those observed along the coast, and in this case did not damage transportation lines. Slide is approximately 10 m wide, 25 m long, and 0.5 m thick. Failure plane has approximate 50° inclination.

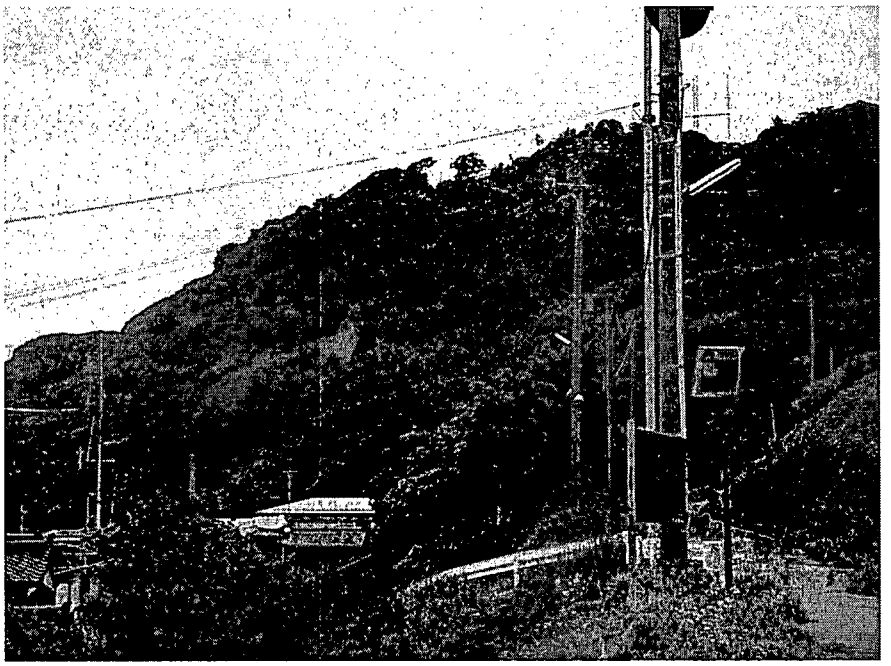

Figure 3.4: Yoneyama Landslide, located south of Kashiwazaki (Site YT17; N37.32223° E138.43828°, photos taken 7/21/07 at approximately 15:20). This slide marked the southwest-most limit of observed landslides along the Sea of Japan coast. The slide extended to the full height of the slope and blocked a paved coastal access road.

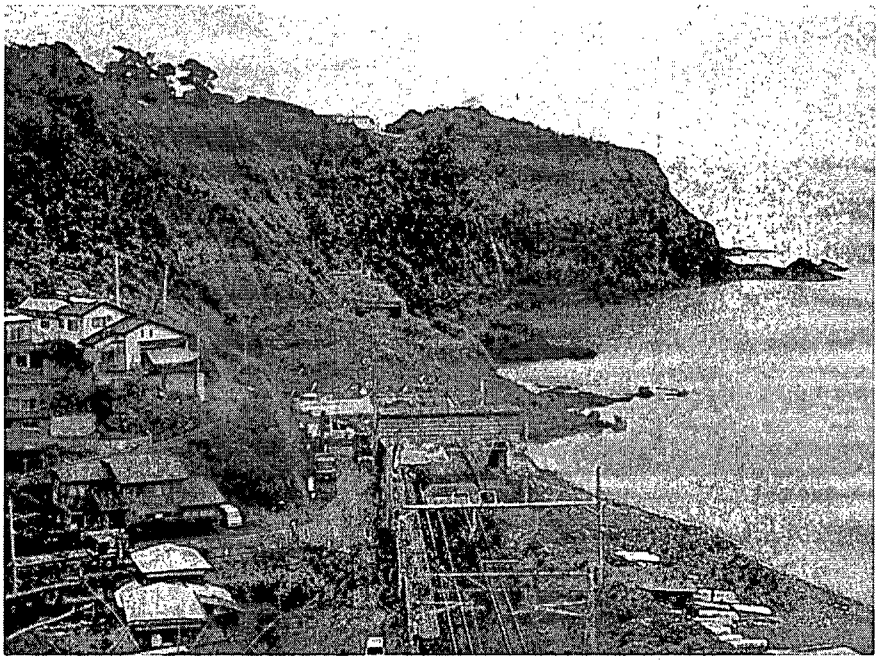

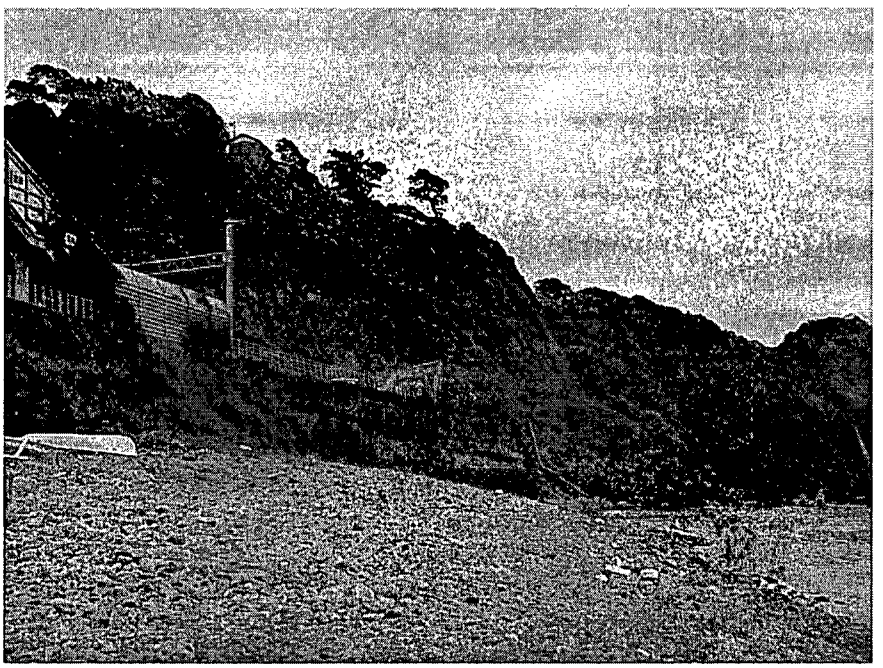

Figure 3.5: Landslide at the Oumigawa Train Station on the Shin-etsu Line (Site RK20/SA9/YT16; N37.34200° E138.48888°, photos taken 7/21/07 12:48 (top) and 7/24/07 15:00 (bottom)). This was among the larger of the coastal landslides to the south of Kashiwazaki. Site access was not possible due to construction repairs. Note that slope stability in this area has been a problem, as seen by the railway tunnel protection structure immediately behind (to the south) of this landslide. Many more smaller landslides were observed to the north and south of this location.

Figure 3.6: Ozumi Senbon Landslide at Highway 8 north of intersection with Route 252 (Site RK1/YT1; N37.41422° E138.71347°, photos taken 7/20/07 10:24 (top) and 7/23/07 13:04 (bottom)). This slide is approximately 150 meter wide, 100 meters long and 10 meters deep. According to construction personnel at the site during the reconnaissance, the slide plane occurred near the colluvial/bedrock interface, at a depth of between 6 and 11 meters. Signs of rotational movement were noted from back-rotated guardrails at the toe of the slide. This landslide forced closure of both lanes of traffic along Highway 8, just north of the intersection with Route 252, however both lanes had been reopened as early as 8 days following of the earthquake when reconnaissance team members revisited the site. Bottom photo shows excavated slide and subsurface bedrock lithology and structure.

Figure 3.7: Ozumi-Mishimayamachi Landslides (Site RK2/YT2; N37.44057° E138.70467°, photos taken 7/20/07 at approximately 11:30). These slides occurred on a native hill slope and consisted of debris slumps in mudstone/siltstones and colluvium materials. High-resolution, topographic data was collected of these landslides using the terrestrial LiDAR scanning method.

Figure 3.8: Road embankment failure off Route 8 on the way to Kasashima (Site YT18; N 37.33325 ° E 138.46500°, photos taken 7/21/07 at approximately 15:40). The slope appears to have undergone previous stabilization using slope grading and gabion baskets to support the toe.

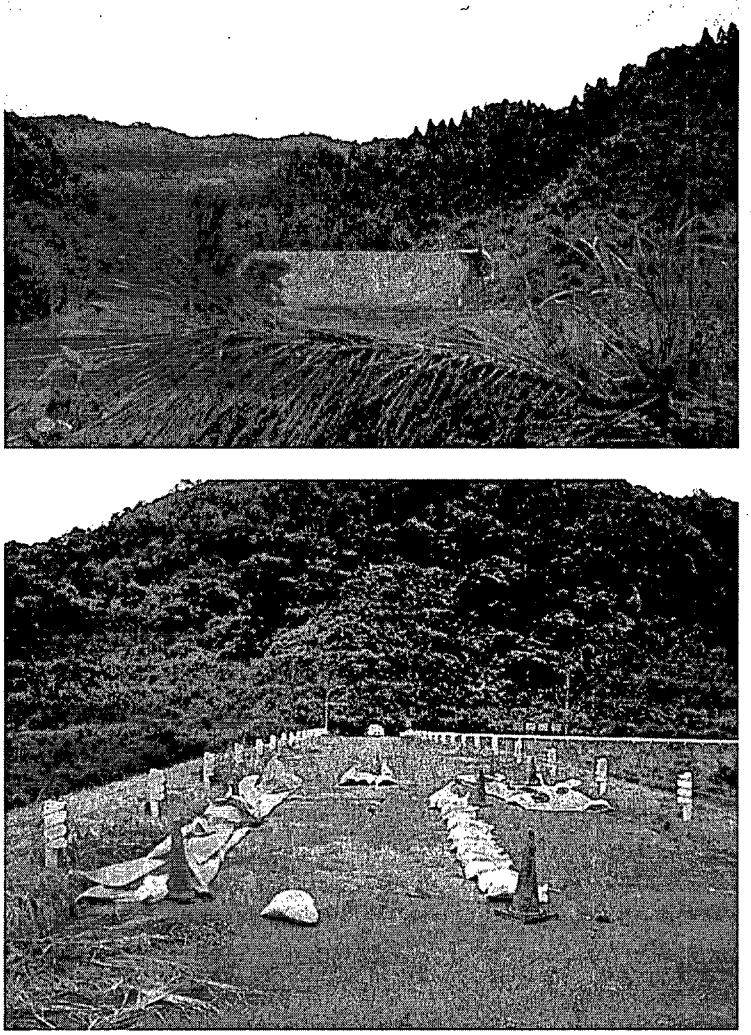

Figure 3.9: Embankment cracking and settlement of South Dam near Miyamo Parking Area along Highway 8, Nagaoka-Shi region (Site RK50; N37.43267° E138.73674°, photos taken 7/23/07 at approximately 11:15). The dam is a 15-meter tall, 97.5-meter wide earth fill structure with 3(H):1(V) downstream and 3.5(H):1(V) upstream benched slopes. Crest elevation is 63 meters and normal pool elevation is 55 meters. Observations were made of an embankment slope failure along the crest of this dam, through half the crest width (~4 m). Settlement and deformation occurred along a 10 m long section with up to 4 cm each of lateral and vertical deformation in the down slope direction. Contour-parallel ground cracking (2-4 cm wide, 1-2 m long) along the ground-spillway interface were also observed, two-thirds of the way down the dam face. The reservoir was empty and appeared to not have been filled in some time judging by the height of vegetation growing in the reservoir area.

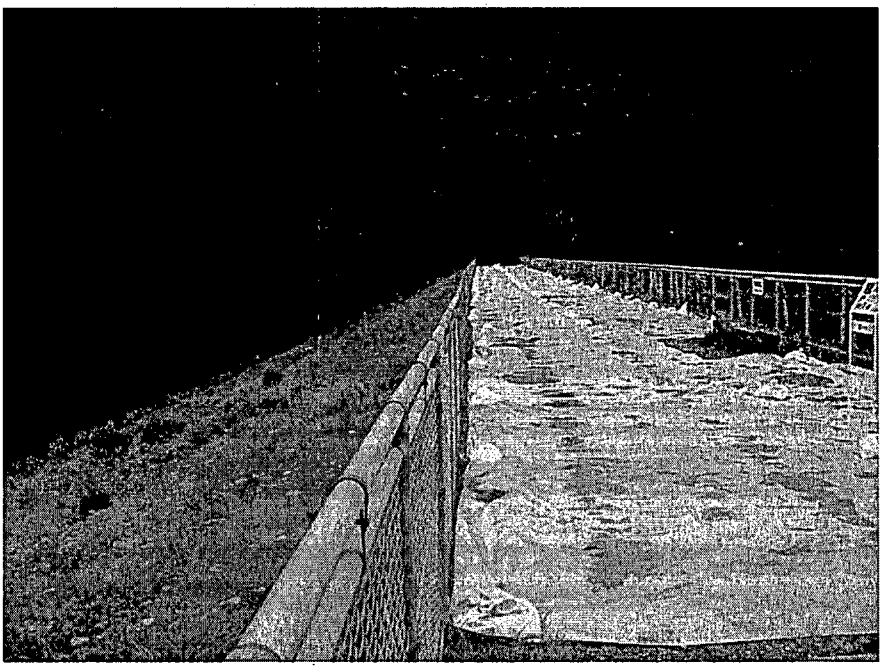

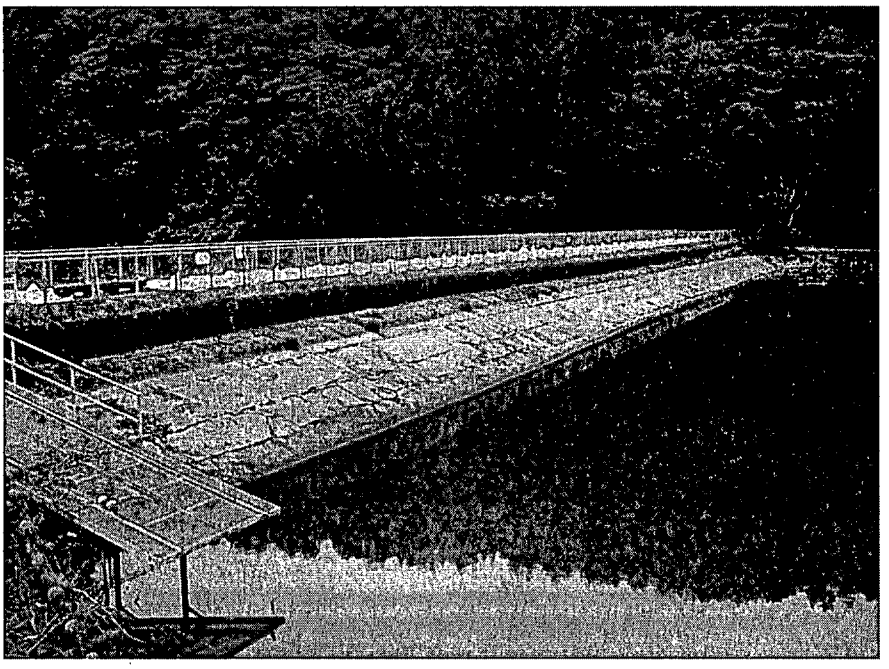

Figure 3.10: Embankment cracking at the crest of Kawauchi Dam, constructed in 1938. (Site YT19; N37.33635° E138.52410°, photos taken 7/21/07 at approximately 16:20).

Section 4 - Liquefaction

Liquefaction was observed from the southern port of Kasashima to Shiya village, north of the Kashiwazaki-Kawira Nuclear Power Plant. Liquefaction evidence was seen in four general settings, riverbank deposits, beach deposits, dune sand, and placed fill. Locations where liquefaction was observed are noted in the Google Earth file accompanying this report. A photo log showing major sites of liquefaction is included in Figures 4.1 through 4.39.

Along the Sabaishi River, located to the north of the city of Kashiwazaki, liquefaction and lateral spreading features were observed for approximately five kilometers from the river mouth to the village of Shimo-Oshinden. River deposits near the mouth of the river underwent extreme settlement at the Kashiwazaki wastewater treatment plant (Figs. 4.15 - 4.17; Site RK9) on the south bank of the Sabaishi River. Nearby, on the north bank, settlement of the river levee embankment west of the Kai-Un Bridge (Figs. 4.3 - 4.9; Site RK4) led to up to one meter of lateral displacement. On the opposite side of the river, east of the bridge, embankment settlement led to pipe separation of a large water main crossing the river. Extensive evidence of liquefaction was observed in this area with ejecta of the underlying sand and an uplifted underground tank near the base of the water-pipe bridge abutment. Moving inland towards the east and across the river, on the north side, a large lateral spread (Figs. 4.11 - 4.13; Site RK6) along the river bank cut into the neighborhood immediately east of the municipal incinerator (Site RK5). The trend of the head scarp of the lateral spread was in alignment with the edge of the levee settlement on the south side of the river. It may be that the liquefaction observed in this portion of the Sabaishi River occurred along an old meandering channel of the river that now underlies the neighborhoods adjacent to the trained-river.

The U River, located in the southwestern portion of Kashiwazaki City, was further from the epicentral region and exhibited less liquefaction damage. All liquefaction sites along this river were observed within one kilometer of the mouth of the river (Site SA13). In general, these sites experienced relatively small amounts of settlement, with the exception of a localized failure at a bridge located to the north of the nearby JR rail line (SA13), which experienced nearly one meter of settlement.

A long, coast-parallel, surficial unit of dune sand extends north of the city. This deposit was the source of numerous liquefaction failures, particularly along the edge of the modern flood plain. The sand was typically very soft under foot, and may have been reworked in areas by the ancient, meandering Sabaishi River. One site of liquefaction, (Figs. 4.33 - 4.35; Site RK40), had 40 cm of settlement, and minor lateral spreading around the foundation pile cap of a large high-voltage power transmission tower. Though the soil pulled away from the cap, the pile cap and tower had no indication of deformation. On the eastern slope of this dune, south of the tower, a lateral spread damaged a shopping center structure, buckling the floor slab in a compression failure (Figs. 4.36 - 4.39; Site RK41). Approximately one quarter of this warehouse discount shopping center building was damaged by the lateral movement of the ground and closed

to the public.

Sandy fill deposits used for backfill performed poorly throughout the epicentral region. Poorly compacted backfill of the wastewater and storm water drain network resulted in hundreds of uplifted manholes. These failures were localized to the backfilled trench of the drain, and had no apparent impact on surrounding structures. Uplifted manholes were a hazard to drivers and impeded traffic, as one-lane controls and resurfacing were needed to level the road grade around the manhole.

Ports and harbors suffered moderate levels of settlement and liquefaction-related lateral spreading. Following the event, all piers remained operable. In the south harbor of Kashiwazaki (Figs. 4.18 - 4.26; Site RK25/SA25), we saw evidence of caisson movement and lateral spreading towards the harbor. This site was scanned by terrestrial LiDAR for further analysis. At several locations north of the Kashiwazaki-Kawira Nuclear Power Plant (Figs. 4.27 - 4.32; Sites RK35, RK37), I-wall type seawalls founded on liquefied beach sand failed and rotated seaward between 50 and 70 cm. We observed diminishing severity of liquefaction effects as the teams drove away from Kashiwazaki and the nuclear power plant (Site RK33).

Liquefaction Figures

The following photo log is a catalog of example observations of liquefaction within these four settings: riverbank deposits, beach deposits, dune sand, and placed fill.

Site RK16 - Fujii Weir downstream from Tashiou Bridge crossing of river.

N 37.34875° E 138.61670°

Extensive cracking of levee embankment. Repairs were taking place to the levee/weir intersection with sand bags to support an embankment failure. We observed good performance of the weir, with no signs of damage. The control building suffered damage to the foundation with settlement of fill beneath the structure: 15 cm on downstream side of building at the retaining wall, 30 cm at the building, and 30 cm at the upstream side retaining wall that formed contributory channel. Three to four sets of transverse cracks parallel to the river ran through the embankment fill that the structure was built upon. Liquefaction and lateral spreading with ground cracks were observed upstream of the operations building and the contributory channel to the south.

Figure 4.1: Fujii Weir downstream from Tashiou Bridge crossing of river. (Site RK16; N N37.34875° E138.61670°, visited 7/21/2007 11:28 am UTZ+8). Extensive cracking of levee embankment.

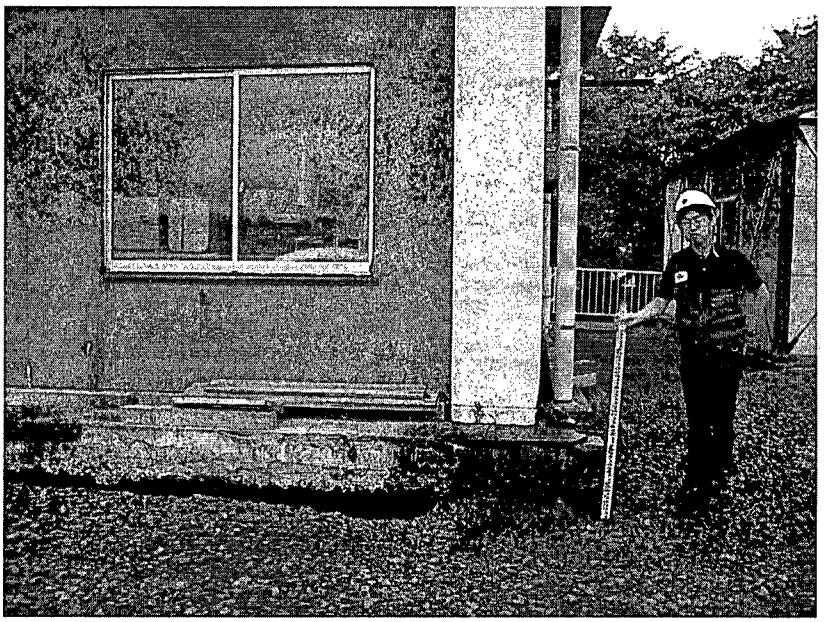

Figure 4.2: Fujii Weir downstream from Tashiou Bridge crossing of river. (Site RK16; N N37.34875° E138.61670°, visited 7/21/2007 11:28 am UTZ+8). The control building exhibited damage to the foundation with settlement of fill beneath the structure.

Site RK4 - Kai-Un Bridge over Sabaishi River with water pipeline and surrounding area

N 37.39233° E 138.58063°

This area experienced liquefaction, lateral spreading, bridge-ground differential settlement, pavement cracking, structural damage, and embankment failure. We observed approximately one meter of ground extension consisting of several 10-20 cm wide cracks (covered by tarps) in a river levee embankment over a distance of 45 meters associated with lateral spreading. Near an adjacent bridge, we measured pipeline rupture and pipe offsets of 13 cm in the horizontal direction, 10 cm in the vertical direction, and with 40 cm of associated nearby settlement between the pipeline and the ground. In a nearby house to the south, extensive signs of liquefaction were observed with sand boils, uplifted manholes, and large-scale ground cracking. A nearby home had been red-tagged due to distortions that appeared to line up with ground cracks.

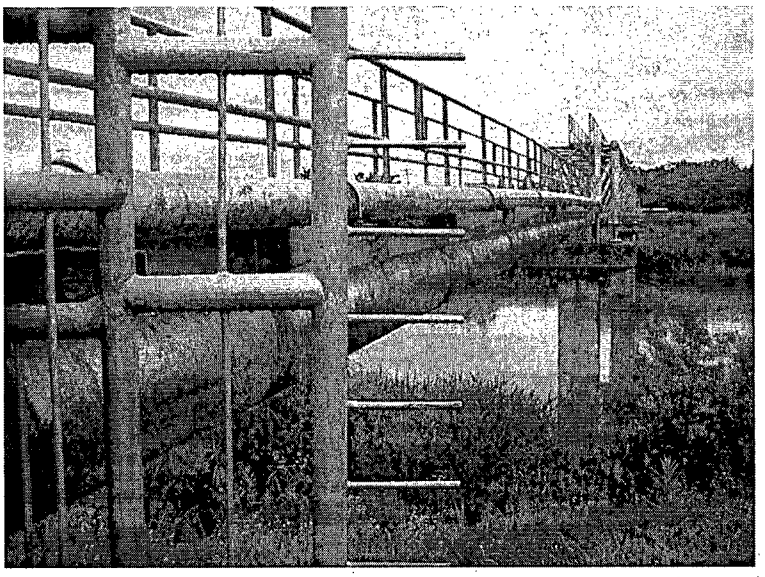

Figure 4.3: Kai-Un Bridge over Sabaishi River (Site RK4 N37.39233°,E 138.58063°, 7/19/2007, 1:40 p.m.). A water pipeline rupture was found with pipe offsets of 13 cm in the horizontal direction, 10 cm in the vertical direction, and with 40 cm of associated nearby settlement between the pipeline and the ground.

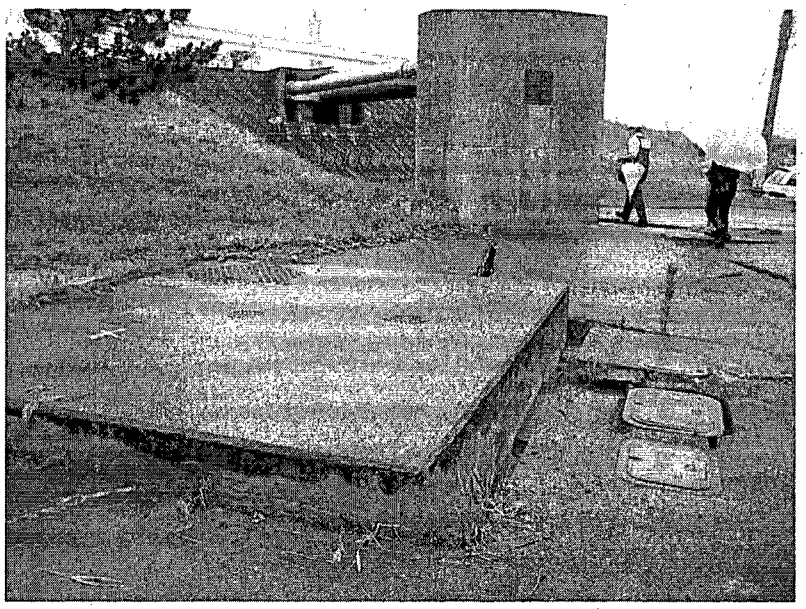

Figure 4.4: Kai-Un Bridge over Sabaishi River (Site N37.39233°, E138.58063°, 7/19/2007, 1:40 p.m.). A water cistern near the pipeline rupture uplifted in liquefied ground.

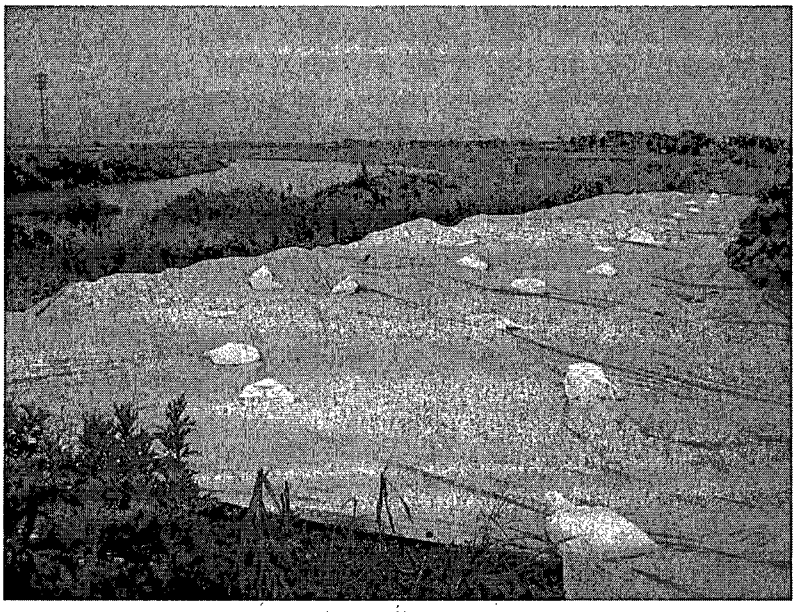

Figure 4.5: Kai-Un Bridge over Sabaishi River (Site RK4 N37.39233° E 138.58063°, 7/19/2007, 1:40 p.m.). Liquefaction induced crest cracking on the levee embankment near the northwest side of the bridge.

Figure 4.6: Kai-Un Bridge area Sabaishi River (Site RK4 N37.39233° E138.58063°, 7/19/2007, 1:40 p.m.). Numerous manholes on the southeast bank near the Sabaishi River uplifted in liquefied ground.

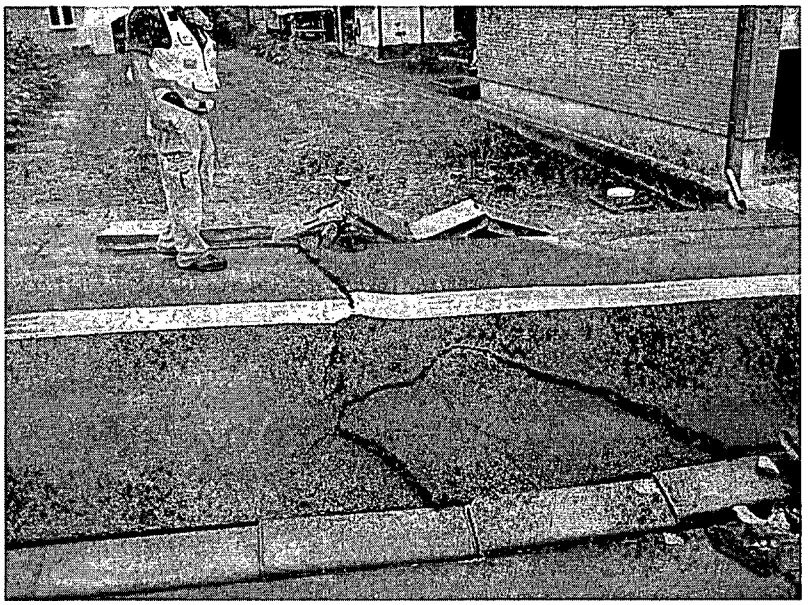

Figure 4.7: Kai-Un Bridge area Sabaishi River (Site RK4 N37.39233° E138.58063°, 7/19/2007, 1:40 p.m.). A sub-linear zone of lateral spreading, sand boils and settlement that may be associated with a buried shoestring sand deposit from the former channel of the Sabaishi River resulted in damage in the neighborhood immediately south of the Kai-Un Bridge.

Figure 4.8: Kai-Un Bridge area Sabaishi River (Site RK4 N37.39233° E138.58063°, 7/19/2007, 1:40 p.m.). A sub-linear zone of lateral spreading, sand boils and settlement that may be associated with a buried shoestring sand deposit from the former channel of the Sabaishi River resulted in damage in the neighborhood immediately south of the Kai-Un Bridge.

Figure 4.9: Kai-Un Bridge area Sabaishi River (Site RK4 N37.39233° E138.58063°, 7/19/2007, 1:40 p.m.). A sub-linear zone of lateral spreading, sand boils and settlement that may be associated with a buried shoestring sand deposit from the former channel of the Sabaishi River resulted in damage in the neighborhood immediately south of the Kai-Un Bridge. Here, settlement caused damage to a residential structure.

Site RK6 - Lateral spread on road to Kashiwazaki Incinerator Plant

N 37.39343° E 138.58555°

We observed lateral spreading, liquefaction, slope failures, and associated retaining wall failures at this site. This site was scanned with terrestrial LiDAR for documentation purposes and for further analysis. A massive embankment failure was observed to have occurred from liquefaction and lateral spread slope movement in aeolian sands. Movement was from north to south, from sand quarry area towards river. Vertical displacement of head scarp was a maximum of 2.8 m and diminished in height moving away from road crossing of head scarp. Measurements were made of total lateral displacement along a representative track-line through the failure representing the maximum likely displacement of the failure ~10 m over 55 m distance between head scarp and river edge (approximately 18% strain). The inclination of slope from road to river was measured to be approximately 14°. Nearby, a slope lateral spread caused failure of a 2.6-meter-tall, concrete block, gravity retaining wall, that resulted in the red-tagging of an otherwise undamaged home. The damaged retaining wall section was 25 meters in length and constructed of 40 cm by 30 cm by 100 cm sized concrete blocks. No backfill, drainage, or tieback reinforcement were observed.

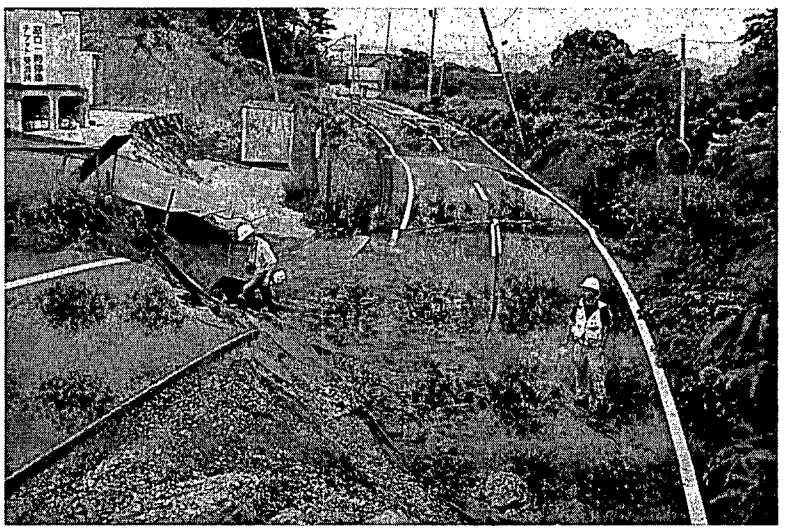

Figure 4.11: North side of Kai-Un Bridge area of the Sabaishi River - Lateral Spread on road to Kashiwazaki Municipal Incinerator (Site RK6, N37.39343° E138.58555°, 7/19/2007). A zone of lateral spreading, sand boils and settlement crossing the present-day Sabaishi River, and that may be associated with a buried shoestring sand deposit of a former channel, resulted in failure of a road on the north side of the river adjacent to the Kashiwazaki Municipal Incinerator.

Figure 4.12: North side of Kai-Un Bridge area of the Sabaishi River - Lateral Spread on Road to Kashiwazaki Incinerator (Site RK6, N37.39343° E138.58555°, 7/19/2007). A zone of lateral spreading, sand boils and settlement crossing the present-day Sabaishi River, and that may be associated with a buried shoestring sand deposit of a former channel, resulted in failure of a road on the north side of the river adjacent to the Kashiwazaki Municipal Incinerator.

Figure 4.13: North side of Kai-Un Bridge area Sabaishi River - Lateral Spread on Road to Kashiwazaki Incinerator (Site RK6, N37.39343° E138.58555°, 7/19/2007). Lateral spreading on the north side of the river adjacent to the Kashiwazaki Municipal Incinerator damaged the access road of the facility.

Site RK9 - Kashiwazaki Wastewater Treatment Plant

N 37.38748° E 138.56587°

We observed structural failures to the main building, liquefaction of ground resulting in extensive road damage, and minor tank damage. The main feature at this site was the complete separation of two adjacent, yet integrated, three-story buildings with associated building and ground settlements, as well as pipe breaks between the two sections of the building. Severe road and pavement damage were also observed as a result of liquefaction - nearby areas of sand boils were noted.

Figure 4.15: Kashiwazaki Wastewater Treatment Plan on the south side of Sabaishi River near the Sea of Japan (Site RK9 N37.38748° E138.56587°, 7/19/2007). Damage to the main building from liquefaction of ground resulted in meter-scale ground settlements.

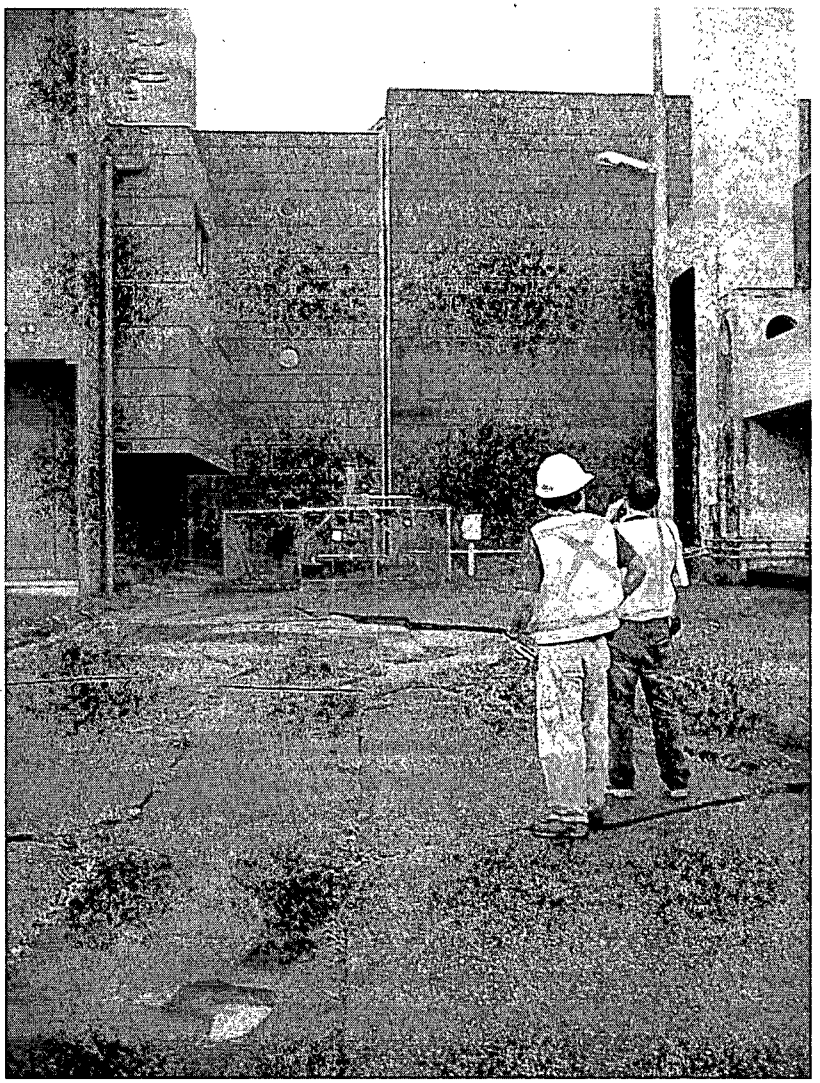

Figure 4.16a: Kashiwazaki Wastewater Treatment Plan on the south side of Sabaishi River near its outlet to the Sea of Japan (Site RK9 N37.38748° E138.56587°, 7/19/2007). Damage to the main building from liquefaction of ground resulted in the complete separation of two sections of the adjacent, yet integrated, three-story buildings with associated building and ground settlements.

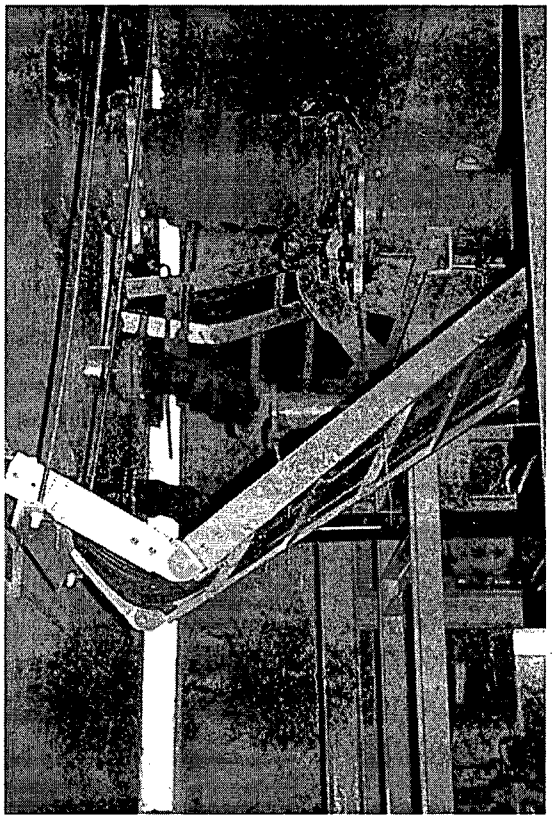

Figure 4.16b: Kashiwazaki Wastewater Treatment Plan on the south side of Sabaishi River near its outlet to the Sea of Japan (Site RK9 N37.38748° E138.56587°) Pipe breaks are due to separation of two adjacent building sections (Photo taken at 7/21/07 9:15)

Figure 4.17: Kashiwazaki Wastewater Treatment Plan on the south side of Sabaishi River near its outlet to the Sea of Japan (Site RK9 N37.38748° E138.56587°, 7/19/2007). Liquefaction features were abundant near the wastewater treatment facility.

Site RK25/SA25 - Kashiwazaki Harbor - South area

N37.36713° E138.53210°

This area experienced ground damage from liquefaction induced lateral spreading. We observed sand boils in the grassy area behind the port office building and on the west end of the pier between separated pier slab sections. Some areas of concrete had 15 cm of vertical and 20 cm of lateral displacement. A track-line measurement was performed with a cloth tape. Measurements indicate that 0.7 m of lateral displacement occurred over 79 meters resulting in 0.9% strain, as measured between the seawall on the west to the edge of the pier to the east. The displacement direction was inland to the east. Terrestrial LiDAR scanning was performed at this site.

Figure 4.18: Kashiwazaki Harbor - South area experienced ground damage from liquefaction induced lateral spreading and settlement of separated pier slab sections (Site RK25, N37.36713° E138.53210°, 7/20/2007).

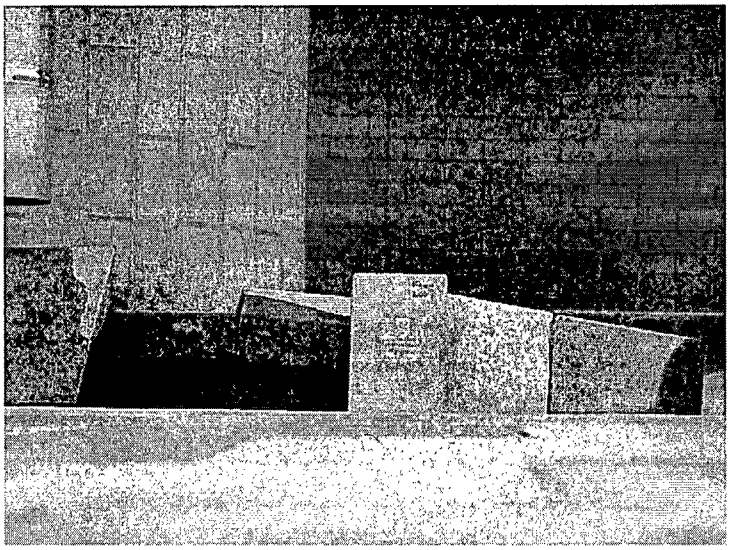

Figure 4.19: Kashiwazaki Harbor - South area experienced ground damage from liquefaction-induced lateral spreading and settlement immediately adjacent to the pile-supported port office building. (Site RK25, N37.36713° E138.53210°, 7/20/2007).

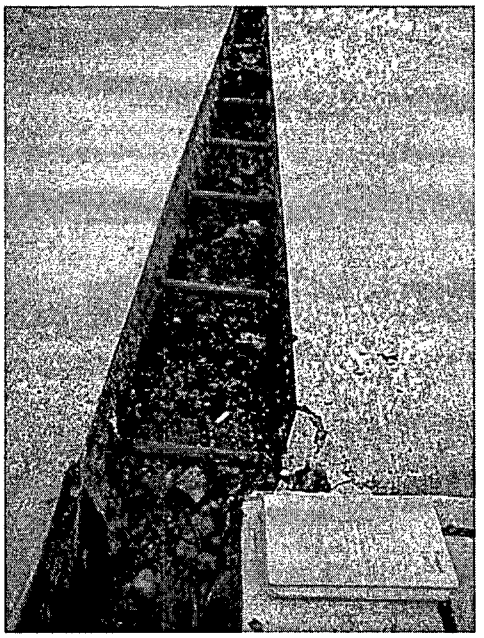

Figure 4.20: Kashiwazaki Harbor - South area experienced ground damage from liquefaction-induced lateral spreading resulting in separated pier slab sections (Site RK25, N37.36713° E138.53210°, 7/20/2007).

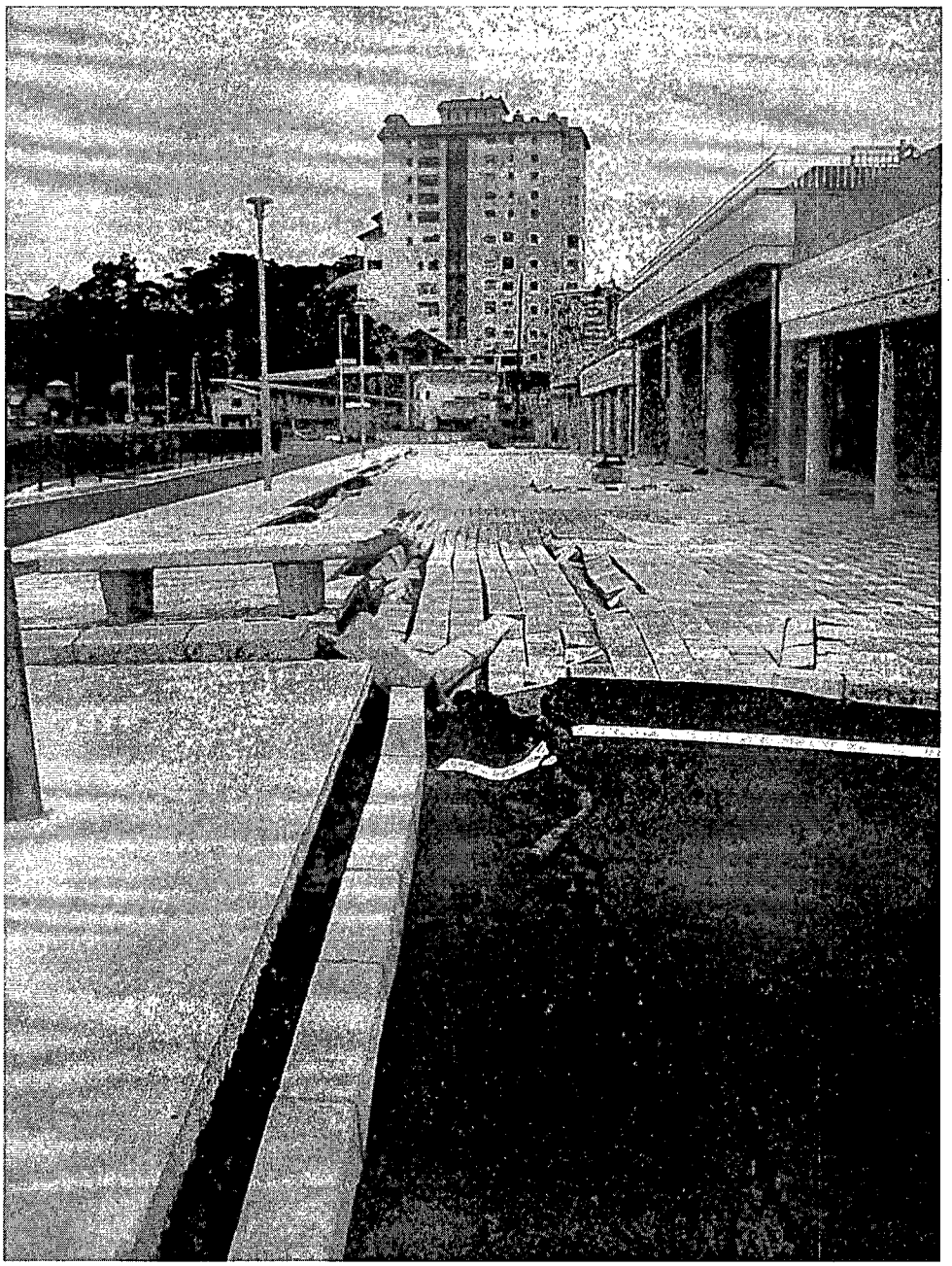

Figure 4.21: Kashiwazaki Harbor - The southern area experienced ground damage from liquefaction-induced lateral spreading and settlement. A harbor-front caisson rotated toward the harbor, to the left of the photo, initiating lateral displacement of the soil behind it, between the caisson and port building (Site RK25, N37.36713° E138.53210°, 7/20/2007).

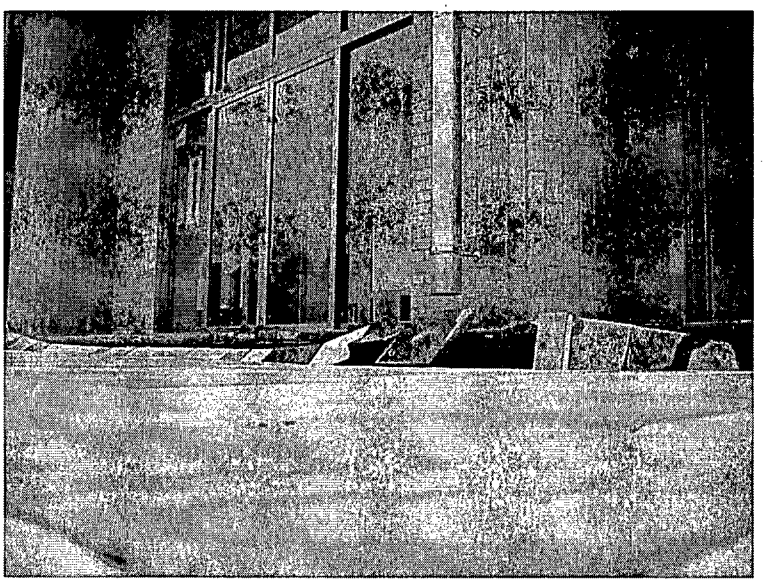

Figure 4.22: Kashiwazaki Harbor - The southern area experienced ground damage from liquefaction-induced lateral spreading and settlement. We observed settlement immediately adjacent to the pile supported port office building. (Site RK25, N37.36713° E138.53210°, 7/20/2007).

Figure 4.23: Kashiwazaki Harbor - The southern area experienced ground damage from liquefaction-induced lateral spreading and settlement. A harbor-front caisson rotated toward the harbor, uplifting the asphalt and tiled section shown here and initiating lateral displacement of the soil behind it, between the caisson and port building (Site RK25, N37.36713° E138.53210°, 7/20/2007).

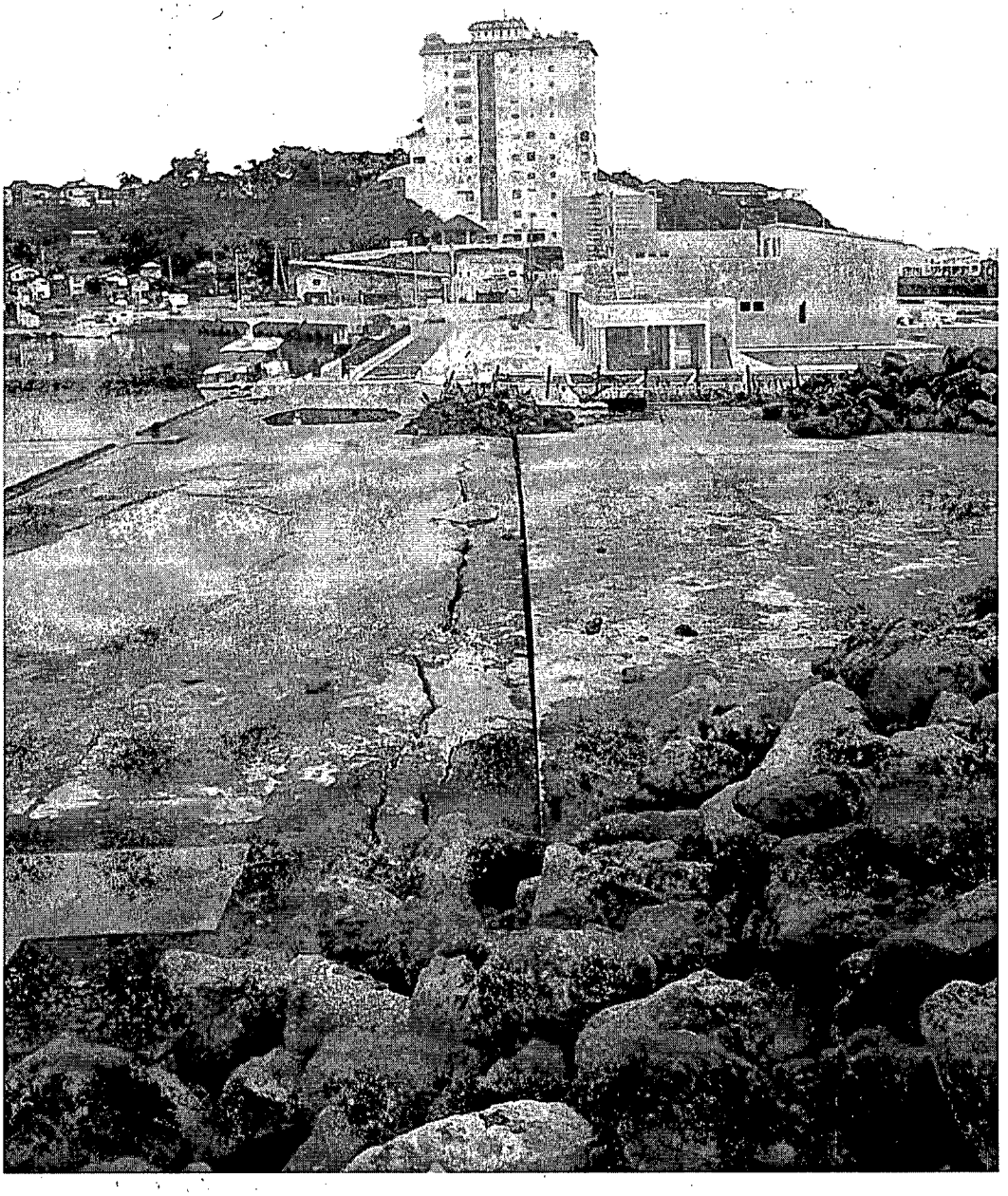

Figure 4.24: Kashiwazaki Harbor - South area experienced ground damage from liquefaction-induced lateral spreading and settlement, here seen from a mound of riprap (Site RK25, N37.36713° E138.53210°, 7/20/2007).

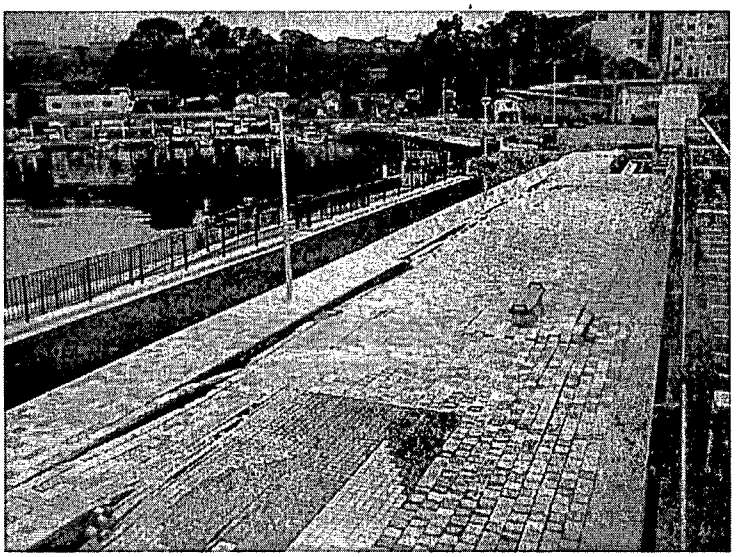

Figure 4.25: Kashiwazaki Harbor - South area experienced ground damage from liquefaction-induced lateral spreading and settlement. A harbor front caisson rotated toward the harbor, to the left of the photo, initiating lateral displacement of the soil behind it, between the caisson and port building. Settlements can also be seen in this photo. (Site RK25, N37.36713° E138.53210°, 7/20/2007)

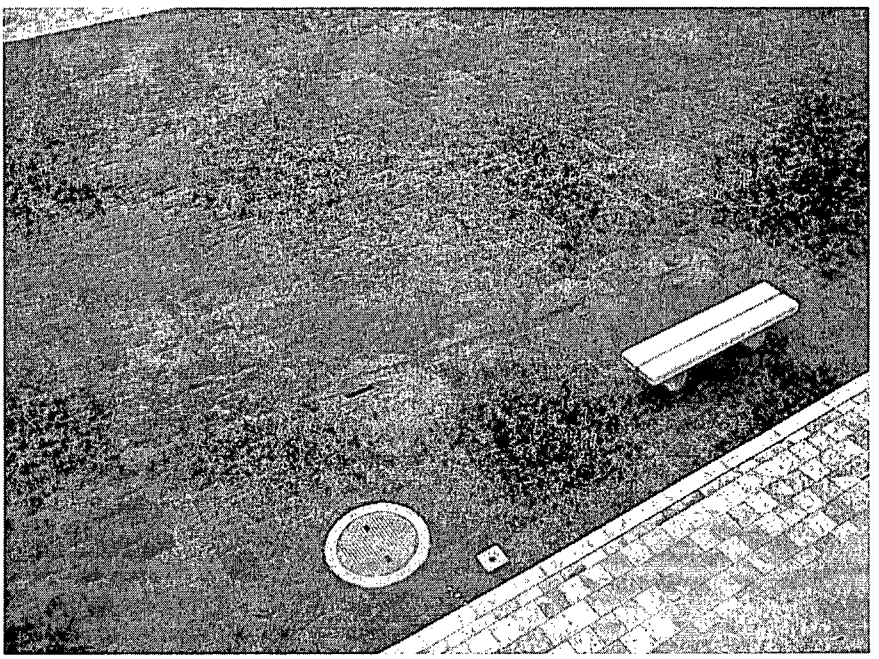

Figure 4.26: Kashiwazaki Harbor - South area exhibited surficial features of liquefaction on all sides of the port building. (Site RK25, N37.36713° E138.53210°, 7/20/2007).

Site RK35 - Road and Seawall Failure

N37.48497° E138.62645°

Liquefaction of beach sand led to lateral spreading of a road embankment and both rotation and translation of a 30-meter-long segment of concrete seawall. Deformations were on the order of 25 cm vertical, and up to 64 cm horizontal, with a component of rotation as measured by 32 cm lateral deformation at the base of wall and 64 cm lateral deformation at 2m height of wall.

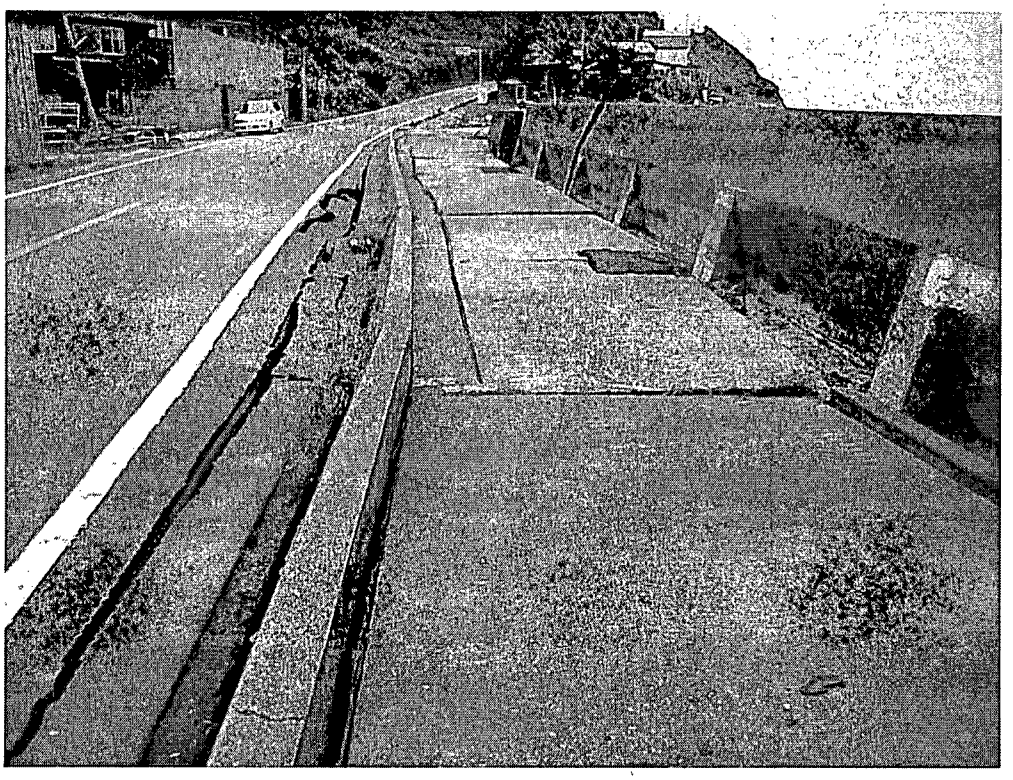

Figure 4.27: Liquefaction of beach sand led to lateral spreading of a road embankment and both rotation and translation of a 30-meter-long segment of concrete seawall. (Site RK35, N37.48497° E138.62645°, 7/22/2007).

Figure 4.28: Liquefaction of beach sand resulted in lateral spreading, above, in front of a 30-meter-long segment of concrete seawall. (Site RK35, N37.48497° E138.626°, 7/22/2007)

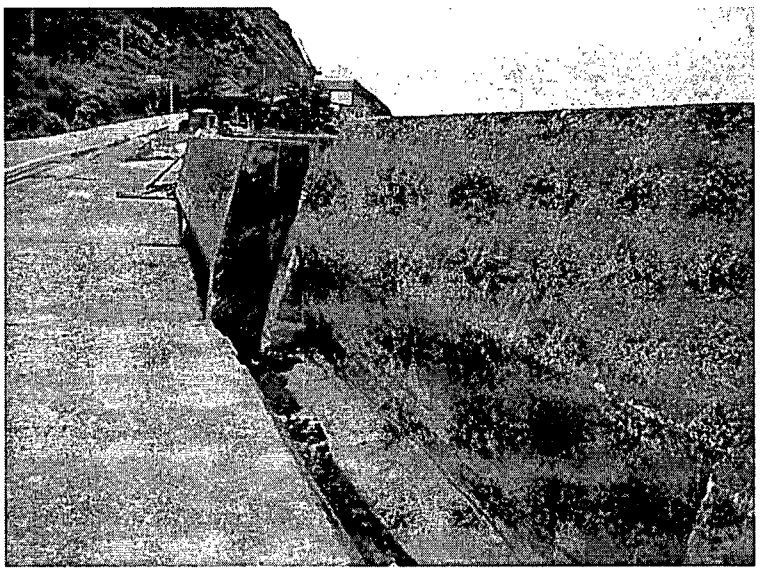

Figure 4.29: Liquefaction of beach sand led to lateral spreading of a road embankment and both rotation and translation of a 30-meter-long segment of concrete seawall. (Site RK35, N37.48497° E138.62645°, 7/22/2007). Deformations were on the order of 25 cm vertical, and up to 64 cm horizontal, with a component of rotation as measured by 32 cm lateral deformation at the base of wall and 64 cm lateral deformation at 2 m height of wall.

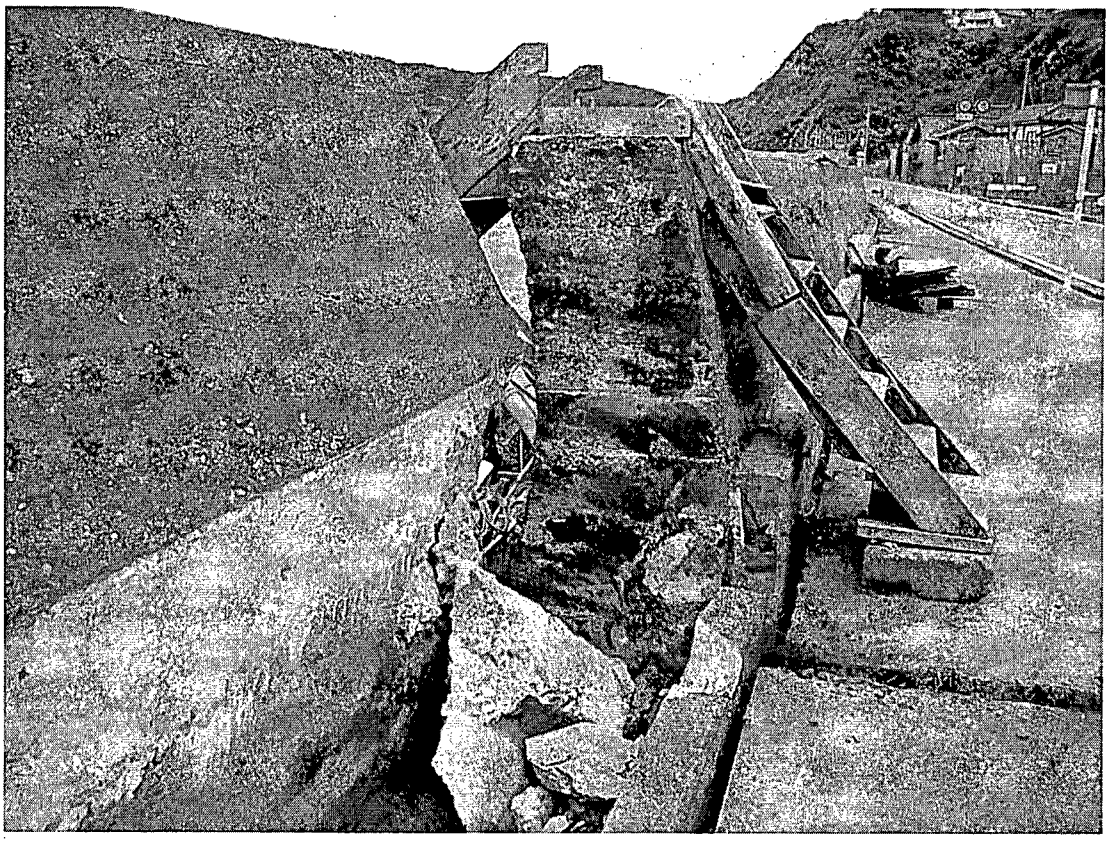

Figure 4.30: Concrete seawall deformations were on the order of 25 cm vertical (failed section up), and up to 64 cm horizontal, with a component of rotation as measured by 32 cm lateral deformation at the base of wall and 64 cm lateral deformation at 2 m height of wall. (Site RK35, N37.48497° E138.62645°, 7/22/2007).

Site RK37 - Seawall Failure

N 37.45478° E138.60927°

Embankment failure and lateral spread from liquefaction of beach sands at toe of seawall. We measured 21 cm of vertical displacement and 55 cm of horizontal displacement of a wall section from an adjacent non-failed wall section. The total length of failed sections was 40 m.

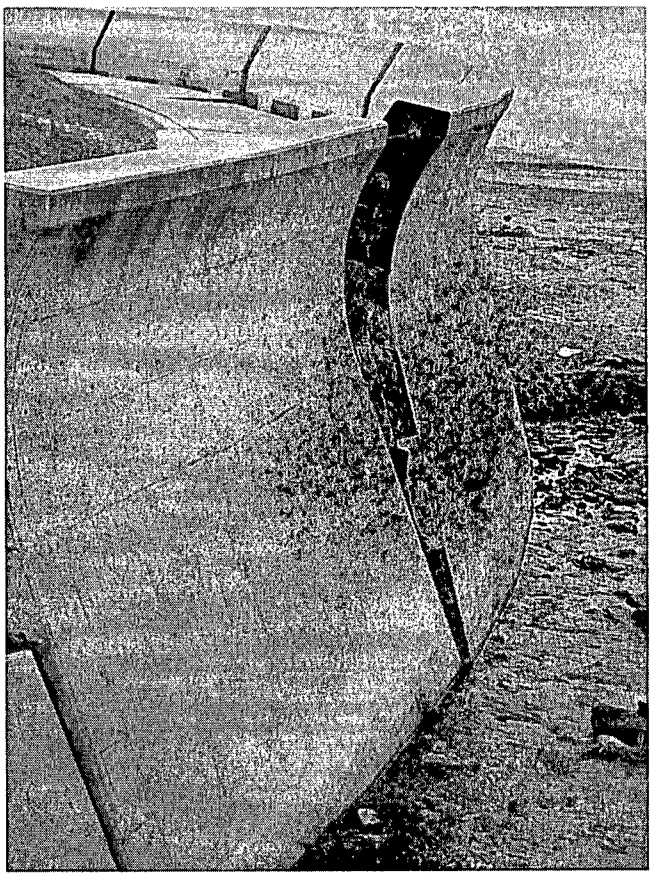

Figure 4.31: Seawall Failure as a result of embankment movement into a seawall founded on top of liquefied beach sands. (Site RK37, N37.45478° E138.60927°, 7/22/2007).

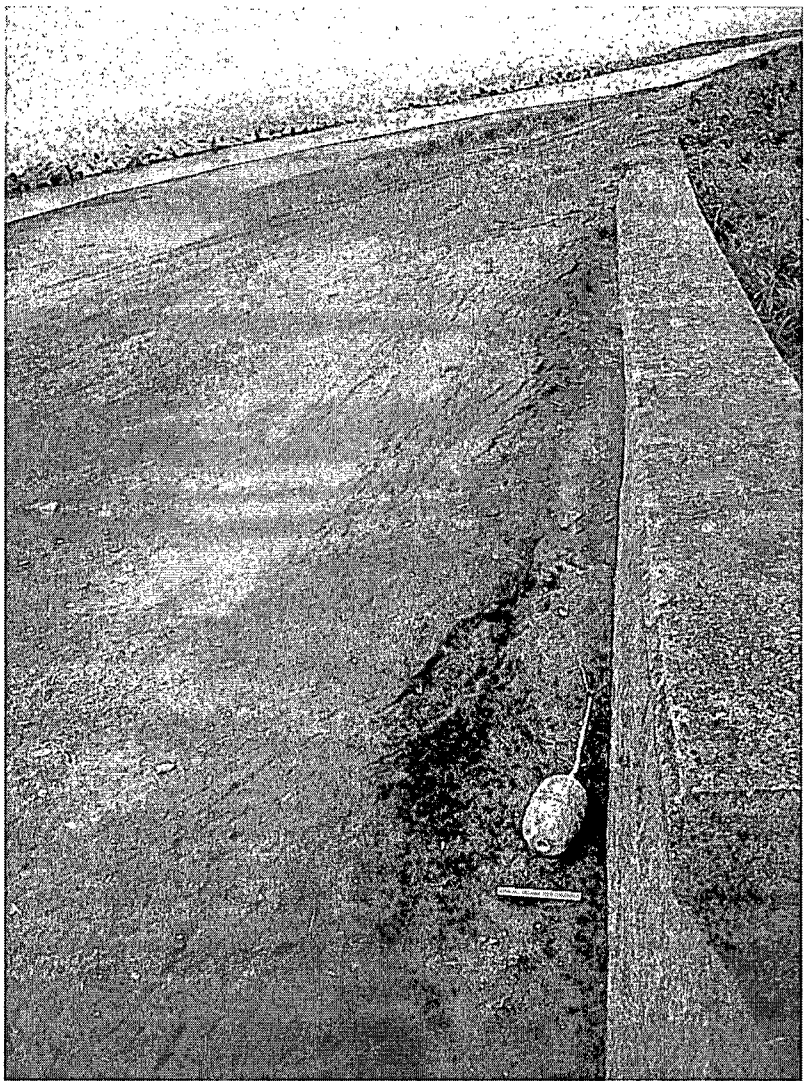

Figure 4.32: Lateral spreading related ground cracking in front of seawall. (Site RK37, N37.45478° E138.60927°, 7/22/2007).

Site RK40 - High Voltage Transmission Line Tower and Railroad Tracks

N 37.41633° E138.60792°

Liquefaction and lateral spread of dune sand adjacent to tower footings. We measured 40 cm of vertical displacement and 12 cm of horizontal displacement over a 20-meter track-line moving away from the footing for 0.6% of measured ground strain.

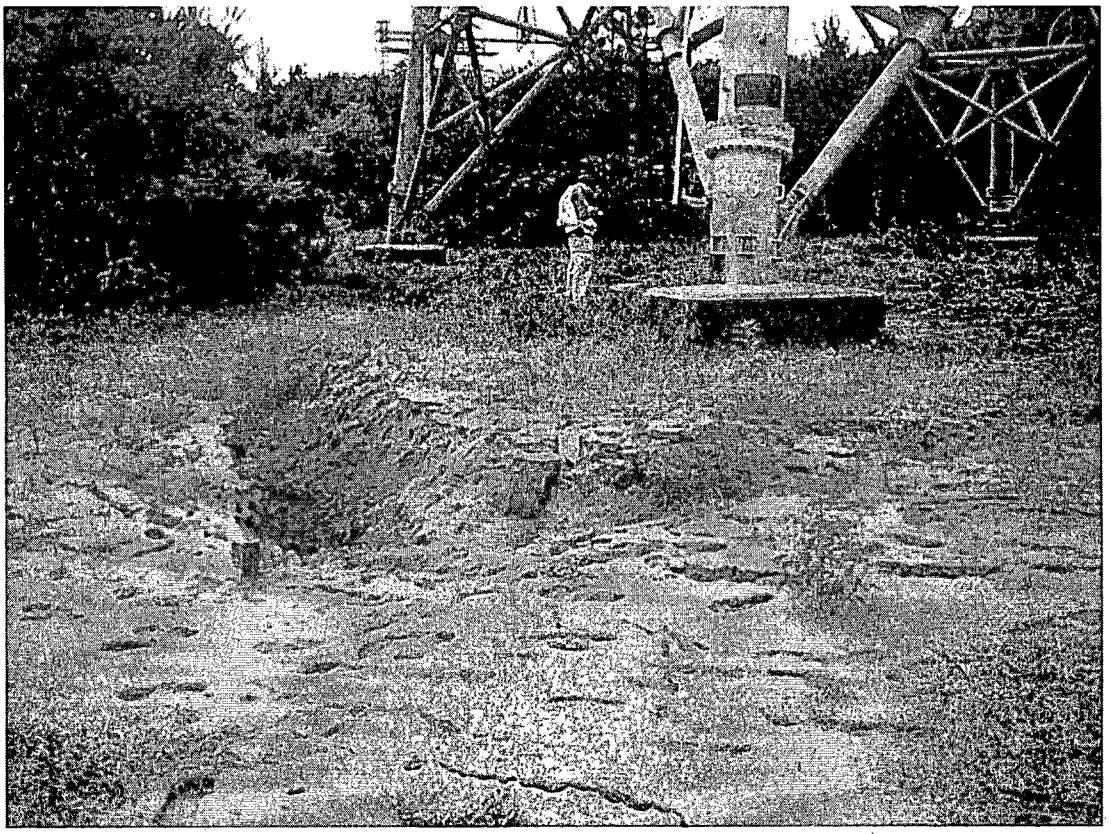

Figure 4.33: Liquefaction and lateral spread of ground adjacent to High Voltage Transmission Line Tower (Site RK40, N37.41633° E138.60792°, 7/22/2007).

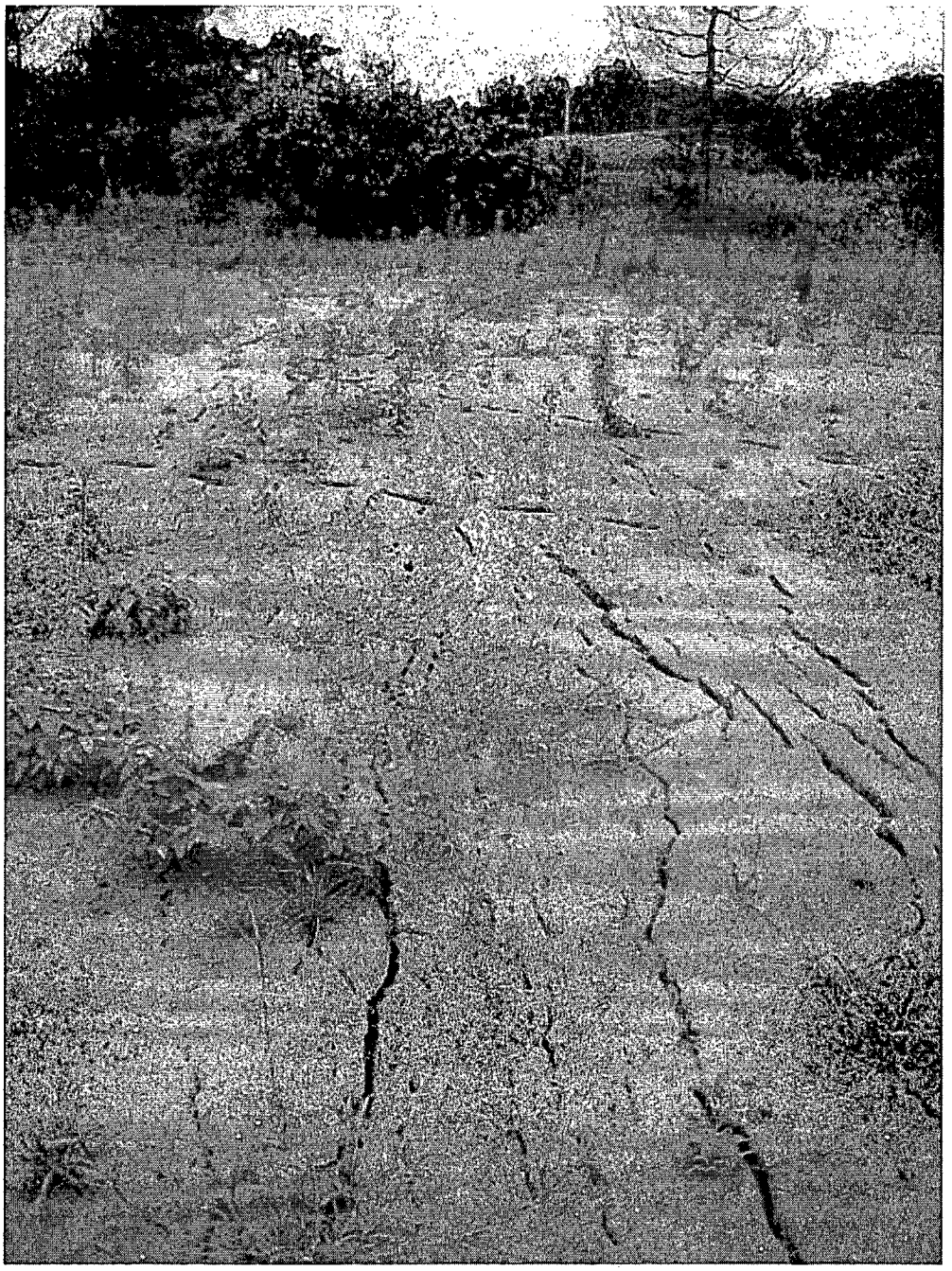

Figure 4.34: Lateral spreading in dune sand down slope of high voltage power transmission tower. We measured 0.6% of ground strain at the site. (Site RK40, N37.41633° E138.60792°, 7/22/2007).

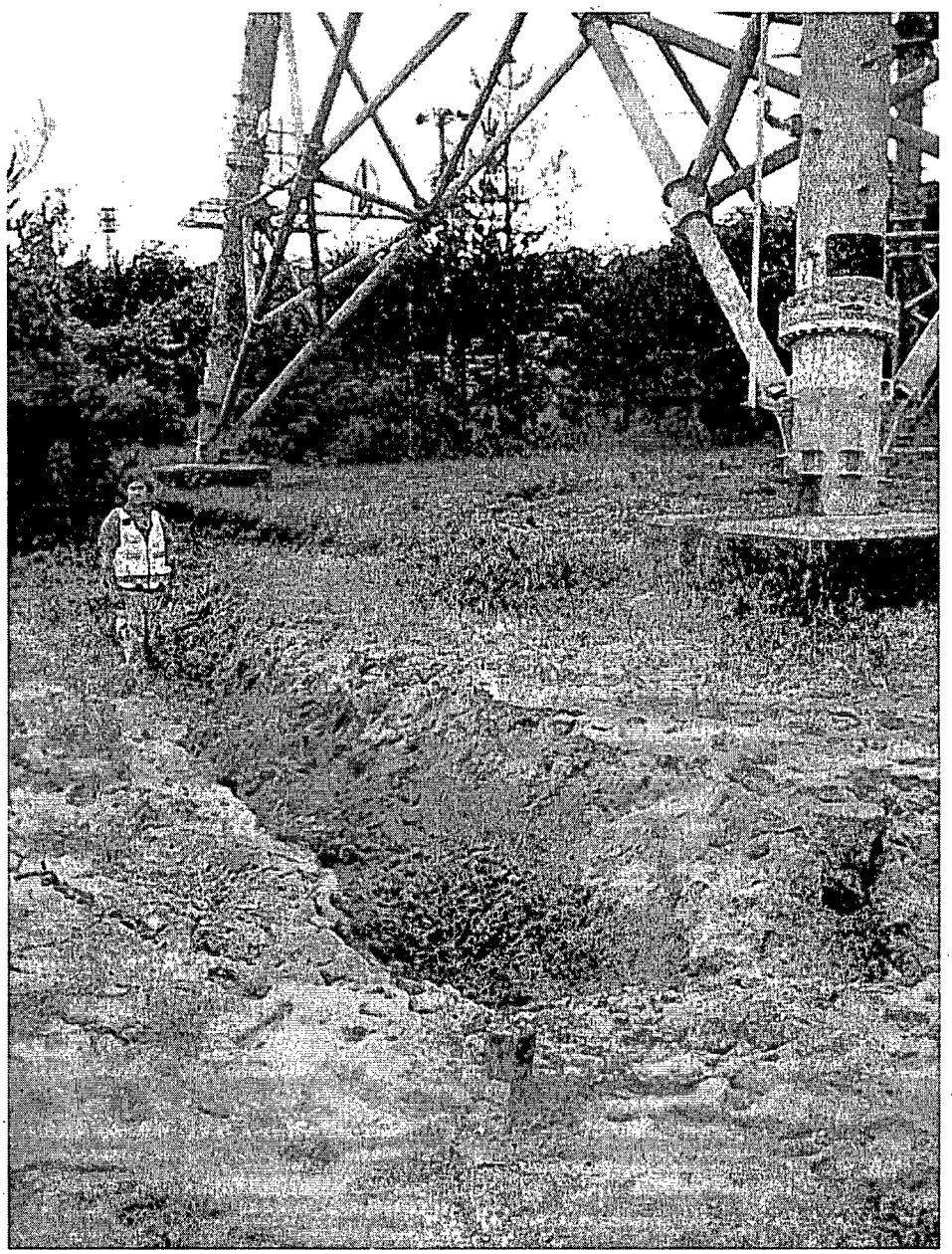

Figure 4.35: Settlement of ground adjacent to grade beam between footings of a high voltage transmission line tower (Site RK40, N37.41633° E138.60792°, 7/22/2007).

Site RK41 - Plant 5 Store

N37.41468° E138.60840°

We observed structural damage and ground settlement of a large warehouse-type department store. The interior columns were deformed and leaning, and the interior floor slab reinforcing bars had buckled and were exposed. Reinforcing bars and concrete also failed at a corner of the building. Ground settlement was observed around the building and an underground storage tank had been uplifted (this was the only obvious sign of liquefaction).

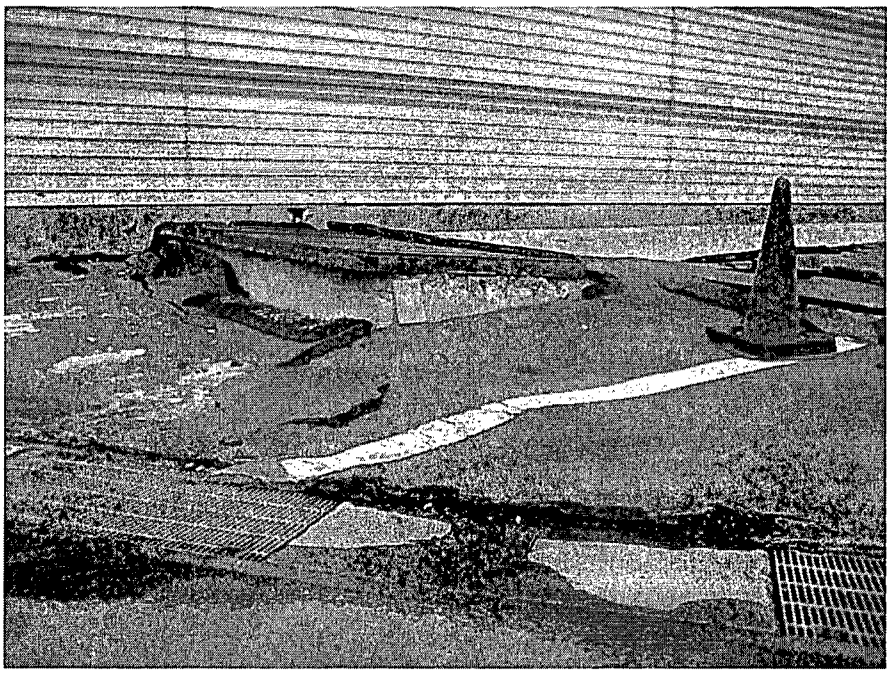

Figure 4.36: Plant 5 Store - Ground settlement in dune sand was observed around the building and an underground storage tank had been uplifted (Site RK41, N37.41468° E138.6084°, 7/22/2007).

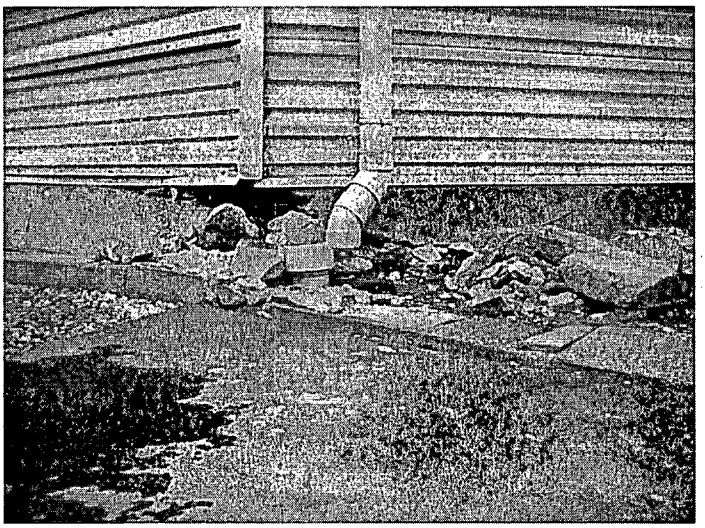

Figure 4.37: Plant 5 Store showing foundation corner area of failed reinforced concrete. (Site RK41, N37.41468° E138.60840°, 7/22/2007).

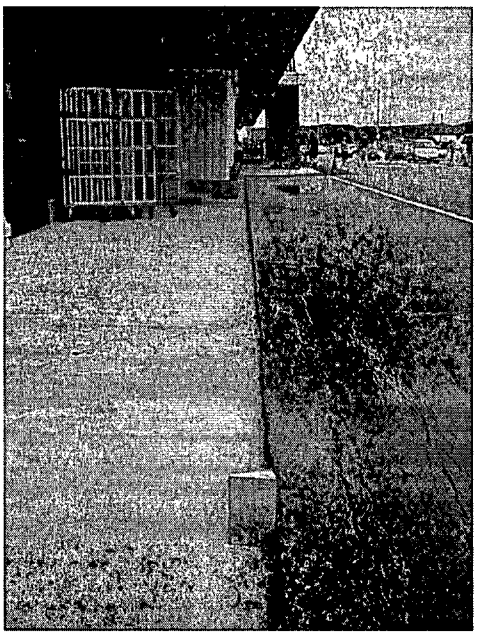

Figure 4.38: Plant 5 Store - Ground settlement in dune sand was observed around the building and an underground storage tank had been uplifted (Site RK41, N37.41468° E138.60840°, 7/22/2007).

Figure 4.39: Plant 5 – Failure of slab on grade with buckled reinforcing bars. (Site RK41, N37.41468° E138.60840°, 7/22/2007).

Site YT24 – Deep-seated Lateral Flow of Kashiwazaki Downtown Nishi-Honmachi Area
N 37.36896° E 138.54829°at center

Damage to old wooden houses were concentrated in the downtown area of Kashiwazaki City where the old sand dune deposit is thought to cover the most of the area. Because of strong shaking in these sand deposits with water level at some depth below the surface, a deep seated lateral flow of ground appears to have occurred, resulting in various surface ground distortions in the Nishi-Honmachi area. This hypothesis was first presented by Prof. Konagai of Univ. of Tokyo who conducted a reconnaissance of the area immediately after the quake (July 17, 2007). Yellow markers in Fig. 4.40 show the locations where EERI & GEER team identified signs of ground lateral flow. Photos of each of these areas can be viewed in the Google Earth database available through the USGS website. The ground movement occurred typically from areas of higher elevation to lower elevation, and we observed open tension cracks at higher ground and compressive heaves in lower ground. Fig.4.41 (SiteYT24_YT_19 as shown in Fig. 4.40) shows the ground distortion near a department store building that seems to be supported by deep foundation and shows no major structural damage. The road on the hill side (northern side) settled and moved downwards to result in the large opening and distortion at the road side.

The reconnaissance was made to define the extent of such a deep-seated lateral flow from ground surface distortions. Fig. 4.42 (Site YT24-YT_03 in Fig. 4.40) shows damage at the north-western limit, whereas Fig. 4.43 (Site YT24-YT_14 in Fig. 4.40) shows damage at the south-eastern limit. Thus, the area covered between Fig. 4.42 and Fig. 4.43 may have suffered deep seated lateral flow from higher ground to lower ground. The damages due to such lateral flow extend to the north-eastern direction of downtown. The arcaded street next to (east) Fig. 4.43 (Site YT24-YT_14 in Fig. 4.40) was closed because of heavy structural damages of shops along the street.

Fig. 4.40: Downtown Kashiwazaki Lateral Spread Overview (Adapted from Google Earth©)

Fig. 4.41: Downtown Kashiwazaki Lateral Spread (SiteYT24, N37.36949°, E138.5541°, photo taken 7/22/07, SiteYT24_YT_19 as shown in Fig. 4.40).

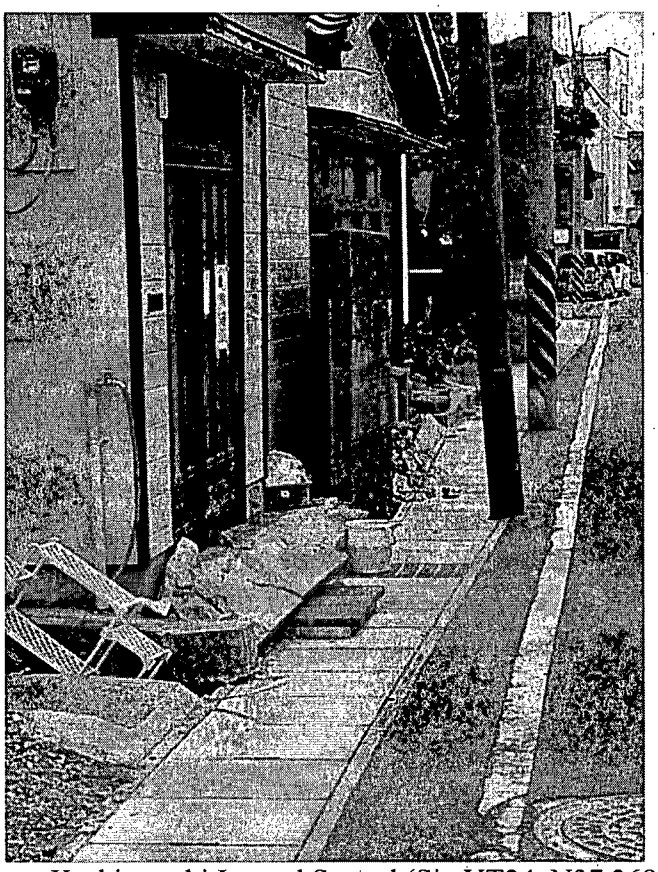

Fig. 4.42: Downtown Kashiwazaki Lateral Spread (SiteYT24, N37.36963°, E138.5486°, photo taken 7/22/07, SiteYT24_YT_03 as shown in Fig. 4.40).

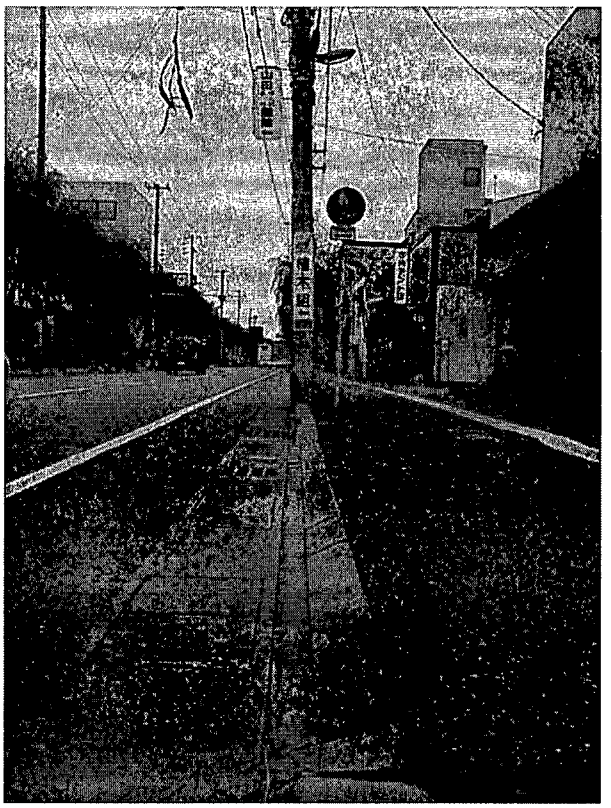

Fig. 4.43: Downtown Kashiwazaki Lateral Spread (SiteYT24, N37.36731°, E138.5522°, photo taken 7/22/07, SiteYT24_YT_14 as shown in Fig. 4.40).

Section 5 - Building and Industrial Structures

5.1 Introduction

The Earthquake of July 16 2007 caused the collapse of nearly eleven hundred houses in the Niigata prefecture in Japan. This section concentrates on observations made by a team of researchers sponsored by JAEE, EERI, and PEER on the response of engineered building structures, the Kashiwazaki-Kariwa Nuclear Power Plant and a smokestack at a recycling facility. Damage to one-to-three story wood buildings was observed along the 30-kilometer-long coastal region between Hatsusaki, to the south, and Shiya, to the north. Damage extended inland to western Nagaoka, 12 kilometers west of the coast.

On the fringes of the damage zone, damage to tile roofs and isolated collapses of residential storage structures and older houses were observed. Kashiwazaki reported the highest number of collapses in the region. Table 5.1 provides information on the distribution of fatalities and damage reported by the local press.

Table 5.1. Distribution of fatalities and damage reported by the local press

Town	Impact on Population		Impact on Housing		
	Fatalities	Injuries	Total Collapse	Partial Collapse	Other Damage
Niigata		12		1	28
Nagaoka		243	8	281	2694
Sanzyo		32			347
Kashiwazaki	10	1339	908	1912	20198
Oziya		40			99
Tokamachi		8		5	58
Tsubame		10	2	4	628
Myoko		0		2	26
Zyoetsu		132	13	43	2220
Uonuma		6			2
Minamiuonuma		4			4
Izumosaki		10	17	84	719
Kariwa	1	105	148	347	436
Kamo		0			
Yuzawa		1			
Mitsuke		14			341
Sado		0			
Agano		0			1
Itoigawa		1			6
TOTAL	11	1957	1096	2679	27807

5.2 Observations

The Kashiwazaki-Kariwa Nuclear Power Plant (Sites SP35-SP39)

Kashiwazaki is home to one of the largest nuclear power plants in the world (Figs. 5.1 and 5.2). The plant is owned by Tokyo Electric Power Corporation (TEPCO) and, with an operational capacity of 8,200 megawatts, can provide electricity for 2 to 3 million households. The power plant is located 10 to 20 km above the potential plane of

the fault dipping southeast (see the fault plane solutions from Section 2 of this report, and the Google Earth map that accompanies this report and is available at EERI's website.). The NW dipping plane is about 3 km below the site.

Initial reports on the performance of the facility were mixed, with reports of fire and radiation leaks, and reports of successful shutdown of reactors. The reported fire was in an electrical transformer located in the periphery of one of the seven reactors that make up the plant. Radiation leaks were caused by spilling of water from spent fuel pools, failure of joints in exhaust pipes, and the falling of drums containing low-radiation nuclear waste. Some of these drums lost their lids when they fell (http://www.world-nuclear-news.org, TEPCO news releases).

Acceleration records obtained at the site indicated that the peak acceleration at the bases of these structures reached values as high as about 0.69g. Figures 2.11 and 2.12 show that accelerations measured away from the structures and at foundation level varied from 388 to 867 cm/sec/sec over a distance of approximately 1.7 kilometers. Table 5.2 shows peak accelerations measured at the bases of the reactors. Observe that, at least in one instance, accelerations varied by more than 50% between bases of adjacent reactors (located approximately 200 m from one another). Bases of reactors sit on bedrock at depths of 45 m (Unit No.1), 44 m (Unit 2), 43 m (Units No.3-4), 36 m (Unit 5) and 26 m (Units No.6-7) below the surface and the buildings that house the reactors reach approximately 31 m to 39 m above ground. Table 5.2 also shows estimates of peak acceleration reported to have been used in the design of the reactors. Observe that the measured values are as much as 3.6 times larger than the assumed values. The discrepancy between the measured and the assumed, and the apparent absence of structural damage indicate that the designs resulted in redundant structures with large "overstrength". A large fraction of the overstrength is attributable to the use of an "importance factor" equal to 3 in the equivalent static design procedure used in Japan.

Table 5.2. Values of peak acceleration at bases of reactors reported by TEPCO

Reactor	PEAK ACCELERATION MEASURED NS	EW	UD	DESIGN NS	EW	UD	RATIO MEAS/ASSUMED NS	EW	UD
	cm/sec/sec								
1	311	680	408	(274)	(272)	(235)	1.1	2.5	1.7
2	304	606	408	(167)	(167)	(235)	1.8	3.6	1.7
3	308	384	311	(192)	(193)	(235)	1.6	2.0	1.3
4	310	492	337	(193)	(194)	(235)	1.6	2.5	1.4
5	277	442	205	(249)	(254)	(235)	1.1	1.7	0.9
6	271	322	488	(263)	(263)	(235)	1.0	1.2	2.1
7	267	356	355	(263)	(263)	(235)	1.0	1.4	1.5
						MAX	1.8	3.6	2.1
						MEAN	1.3	2.1	1.5
						MIN	1.0	1.2	0.9

One of the authors of this report (Prof. Kabeyasawa of the University of Tokyo) is a member of The Working Group for Building Structures in Japan's Nuclear and Industrial Safety Agency and, as such, was granted access to the immediate vicinity of the reactors. Damage was observed, but it appeared to be related almost exclusively to problems with the soils (Figs. 5.3 through 5.6).

We observed signs of liquefaction (sand boils near the shore), distorted roads, tilted isolated footings, and a small landslide in a man-made hill that separates reactors 1-4 from reactors 3-7 (this hill was constructed with soils excavated to construct the plant). In a two-story steel building used for administration, drop-ceilings fell and windows broke (http://www.world-nuclear-news.org) (Fig. 5.7). Joints of piping resting on isolated footings and expansion joints in covered pathways failed. Access through doors was impaired by ground settlements of up to 40 cm. And underground pipes supplying fire retardant to reactors broke because of the relative movement between the soils that surrounded the pipes and the foundations of the reactors.

In summary, there were problems at the TEPCO power plant, but official accounts indicate that the main structures did not suffer damage. There was no loss of life and the emergency shutdown system, which had been set to be triggered by accelerations exceeding 120 gal, operated successfully.

The Failure of a Reinforced Concrete Tower (Stack) at the Kashiwazaki Municipal Recycling Plant (Site SP31)

The stack is one of the tallest reinforced concrete structures in the area, and its failure was noticeable from afar (Fig. 5.8). The structure was 59 m tall. It had a square cross section with 4.6-meter sides. The thickness of the walls was 18 cm at the top and 36.6 cm at the bottom. At the bottom of the east face, a large frame reinforced an opening for a gate. Through its west face and at a sixth of its height, the stack was connected to the adjacent plant by a large duct. The failure took place at a height of approximately 17 m, where the longitudinal reinforcing bars were lap spliced (Fig. 5.9). The failure caused the upper part of the stack to fall 6 to 7 meters. Some transverse reinforcing bars, which also had lap splices, were observed to have ruptured.

Apparently, the stack was designed in accordance with modern design standards. Current Japanese standards require lap splices to have a length equal to forty times the diameter of the largest bar spliced. Splice failures in similar conditions have been reported to have caused the collapse of a stack in Turkey during the 1999 Kocaeli Earthquake (Kilic and Sozen, 2003).

Houses

The earthquake caused the collapse of nearly eleven hundred houses in the Niigata prefecture in Japan. Damage to one-to-three story wood buildings was observed along the 30-kilometer long coastal region between Hatsusaki, to the south, and Shiya, to the north. Damage extended inland to western Nagaoka, 12 kilometers west of the coast. The city of Kashiwazaki reported the highest number of collapses in the region. The

structures that collapsed were almost exclusively wooden structures (Fig. 5.10) and unreinforced masonry fences. Preliminary estimates of collapse rate were between 5 and 7% for buildings and houses in the vicinity of the K-NET instrument in Kashiwazaki. One team documented more than 200 collapses of houses, fences, sheds, and canopies near this location. Photos of all of the sites visited are linked to the Google Earth map available through the USGS link provided in this report. The direction of collapse or permanent displacement for many of these sites can be queried through the site map, although no clear trend is visible regarding overall displacement direction.

A large fraction of the houses affected were of old-style heavy clay-tile kawara roofs with walls constructed of wood, and walls of soil and bamboo-lathe known in Japanese as tsuchi-kabe or "soil wall" (Fig. 5.11). The clay-wood combination can be used effectively if provided with braces for lateral strength and stiffness, however in general, results in heavy and brittle building components. Soft story collapses were observed in buildings with open businesses on the ground floor. The business arcade of Higashi-Honcho Dori was particularly hard hit, accompanied by ground movement/settlement on the south side of the street that was located on the shoulder of sand dunes.

Dense concentrations of structural damage to houses located on slopes of sand dunes as well as flat artificial reclaimed/alluvial sandy deposits that cross the Kashiwazaki-Kariwa area were observed. Many houses suffered from soil performance problems such as those caused by soil liquefaction, vertical settlement, and dynamic displacements of structures built on the slopes of these deposits. An example of residential houses affected by soil-related damage is found in the district of Nishi-Hon-machi. There, collapse or large deformation of old temples and houses occurred, both, along the steep north-slope and along a more gentle slope towards the south. Nishi-Hon-machi experienced deep-seated ground movements from high to low elevations and collapses of homes were due to the softening or liquefaction of the underlying sand deposits (e.g. see Site YT24, 37.36712°, 138.54590°).

Steel Structures

In Kashiwazaki, steel structures were not as common as concrete structures at the time of our visit. None of the few steel structures we saw collapsed. One of these structures was a gymnasium built in the 1950's (Site SP2), located 1.1 km away from the K-NET NIG018 station. The structure was composed of a series of 2D trusses running in the EW direction. Trusses running NS connected the EW trusses at the roof (Fig. 5.12). Finishes did not allow viewing of additional structural elements. But windows along the NS direction made it evident that, at least in this direction, the structure was provided with no braces. The structure survived the earthquake with an estimated permanent drift ratio of 2.5% to the north.

Another example of a surviving steel structure is illustrated in Fig. 5.13 (Site SP29). This structure was located at approximately 270 m from the K-NET NIG018 station, which measured PGV=100m/s. The two-story structure included nine, one-bay

frames parallel to the EW direction. The five frames closer to the front of the structure had no moment connections. The four frames closer to the back did have moment connections. The frames were connected to one another by a concrete slab cast on a steel deck at the second level and presumably by the roof. The slab had a step in the span that connects the moment resisting frames in the back and the gravity frames in the front. Braces were visible along the NS walls of the structure. The braces were connected to the webs of columns in the front frames through brackets as shown in Figure 5.13.

We inspected another gymnasium (Fig. 5.14 - Site SP7) with a steel structure. In this structure, located 430 m from the K-NET station, we observed buckling of steel braces in the lower of the two stories in the structure. The braces had T-shape cross sections with a thickness of 12 mm. The flange measured 150 mm, and the stem 45 mm. The braces had a slope of 2/3 with respect to the horizontal. Four pairs of braces reinforced each story in the NS direction. The floor plan was approximately 20 m in the EW direction and 33 m in the NS direction.

The storage at site RK41 was affected by large ground distortion (see Section 4). At this site, we observed buckling of flanges of beams at bolted connections (Fig. 5.15).

Steel frames are commonly used in the area to strengthen reinforced concrete structures. In the structures that use this system and we visited, the steel-concrete marriage seemed fruitful. Nevertheless, in one of these structures (Site SP30), spalling of plaster and concrete, and damage to architectural elements at construction joints caused disruption of operations.

Reinforced Concrete Structures

Initial reports did not mention damage to reinforced concrete structures. This was surprising initially given the measured ground motion intensity and the fact that, according to the Japan Building Disaster Prevention Association, the Niigata prefecture has one of the lowest rates of completion of mandated strengthening schedules in Japan. We therefore investigated in detail a number of reinforced concrete structures in the vicinity of the K-Net station at Kashiwazaki. We concentrated on public buildings because they had relatively regular floor plans and because they were accessible. We were allowed by the local government to inspect all public schools in the city. Photographs of each building inspected are linked to the Google Earth map accompanying this report.

We observed 1-mm thick inclined cracks in a column and 1 to 2.5-mm-thick inclined cracks in reinforced concrete walls in the Kashiwazaki High School (Site SP11), located at 100 m from the K-NET NIG018 station. The high school facilities included two reinforced concrete buildings (Figs. 5.16 to 5.20). We observed the south building to be a four-story building with shear walls in the NS direction and moment-resisting frames in the EW direction. The walls with cracks filled bays in one of the frames parallel to the EW direction in the south building and had a thickness of 12 cm. These walls were reinforced with bars with a diameter of 10 mm, spaced at 20 cm in the vertical and

horizontal directions. The inclined cracks described had the same orientation in the column and the walls, and indicated movement of the second level towards the west. The wall with the largest cracks had a door opening (bay 3-4). Refer to the Google Earth map accompanying this report for additional information.

The column observed to have an inclined crack had a clear height of 1.3 m. Other columns in the building had clear heights ranging from 1.3 to 3 m. The column with an inclined crack was located at the intersection of column lines C and 19. The cross section of column C-19 was rectangular with dimensions of 70 cm and 55 cm in the EW and NS directions, respectively (Fig. 5.21). Ties were specified to be 13 mm in diameter and to have an even spacing of 10 cm. A maximum tie spacing of 10 cm has been mandatory in Japan since 1972. In drawings of buildings built before 1972, one may find specifications calling for larger tie spacing (30cm). Cross ties with a diameter of 9 mm were to be provided every 50 cm. Column C-19 supported a single level (a slab that serves as roof beyond column line 18). Averages obtained for buildings from the same vintage indicate that concrete strength is likely to be close to 3 ksi. The yield stress of the reinforcement is estimated to be $f_y = 45$ ksi.

Inclined cracks were also observed in walls in the Kashiwazaki City Hall (Site SP 26), located 100 m from the K-NET NIG018 station and in a government building in Kariwa (Fig. 5.22 - Site SP33), which sits right next to the Kariwa JMA recording station. The building in Kariwa also showed damage to a sliding door and broken windows. Disruption of the soil surrounding the foundation was observed in this and other sites.

In general, the performance of the reinforced concrete buildings we visited was satisfactory with one exception. A three-story building used as a karaoke parlor in downtown Kashiwazaki suffered shear failures of columns in its first story (Figs. 5.23 and 5.24). From Figs. 5.23 and 5.24 it appears that the spacing of ties exceeded the specified maximum of 10cm.

The buildings we surveyed are not new buildings. The east wing of Kashiwazaki's Jr. High School 2 (Site SP3), for instance, was built in the 1960s. Nevertheless, the reinforced concrete structures we inspected performed well, except for the karaoke parlor. But in general, it is fair to say that the performance of reinforced concrete building structures was far superior to that of buildings in other seismic events. In an attempt to provide tangible information for interpretation of our observations, the ratios of column areas to total floor areas were computed for buildings inspected in or near Kashiwazaki (Table 5.3). The mean ratio of column to floor area is 0.59%.

Table 5.3. Ratios of column areas to total floor areas.

!"#%&'	(#)*	>8*.4'*/7.#-")4.N/6*&'); 60&'#)"%&4$ 9#.*?)#D&	7.4&28*.2* 9#.*?)#D&	7N:F50$', &/9# *&2#D&2 9*:);	< #%);	+", -*./01/()0.#2	34)#D/01/50$', &/)0)0/=$00./>.*4
		,	,	?,	?,		
@4.#A4/B08*.&, *&)/!"#%&'	(CDD	EFG	G	HI	HI	D	IHEJK
@42;#A4L4M#5#N/O4$	(CJP	QFG	GFG	RI	RI	G	IFGJK
7*?;&#P4$O#;/(?;00$	(CQI	G	Q	RI	GI	Q	IFGIK
@42;#A4L4M#O#;/(?;00$	(CSS	QFG	G	EI	GG	Q	IFQDK
@42;#A4L4M#T.F/O#/UJ/< *2)/!$%'F	(CS	QFG	QFG	RI	PE	D	IHRRK
@42;#A4L4M#T.F/O#/UJ/V42)/!$%'F	(CD	QFG	QFG	PG	QI	D	IFQDK
@42;#A4L4M#T.F/O#/US/	(CR	RFG	Q	RI	RI	D	IHPDK

It is worth noting that the Kashiwazaki High School and buildings surrounding the K-NET NIG018 station featured large reinforced concrete spandrels built integrally with girders and columns. These spandrels are common in Japan among buildings built before 1982. The spandrels in the high school had thickness varying from 12 to 30 cm and total depths (including the depth of the girder) ranging from 1.2 to 2.2 m. The longitudinal reinforcement in the spandrels (D10 bars at 10 cm from one another) runs through the column and flexural cracks in the spandrels suggested that they acted as integral parts of the girders.

5.3 References

Kilic, S., Sozen, M., (2003). Evaluation of Effect of August 17, 1999, Marmara Earthquake on Two Tall Reinforced Concrete Chimneys, ACI Structural Journal, Vol. 100, No. 3.

Figure 5.1: Layout of the Kashiwazaki-Kariwa nuclear reactors and locations of sites visited by the reconnaissance team within and near the facility.

Additional site information and imagery at http://walrus.wr.usgs.gov/infobank/n/nii07jp/html/n-ii-07-jp.sites.kmz

Figure 5.2: TEPCO Nuclear Power Plant (Sites SP35-SP39).

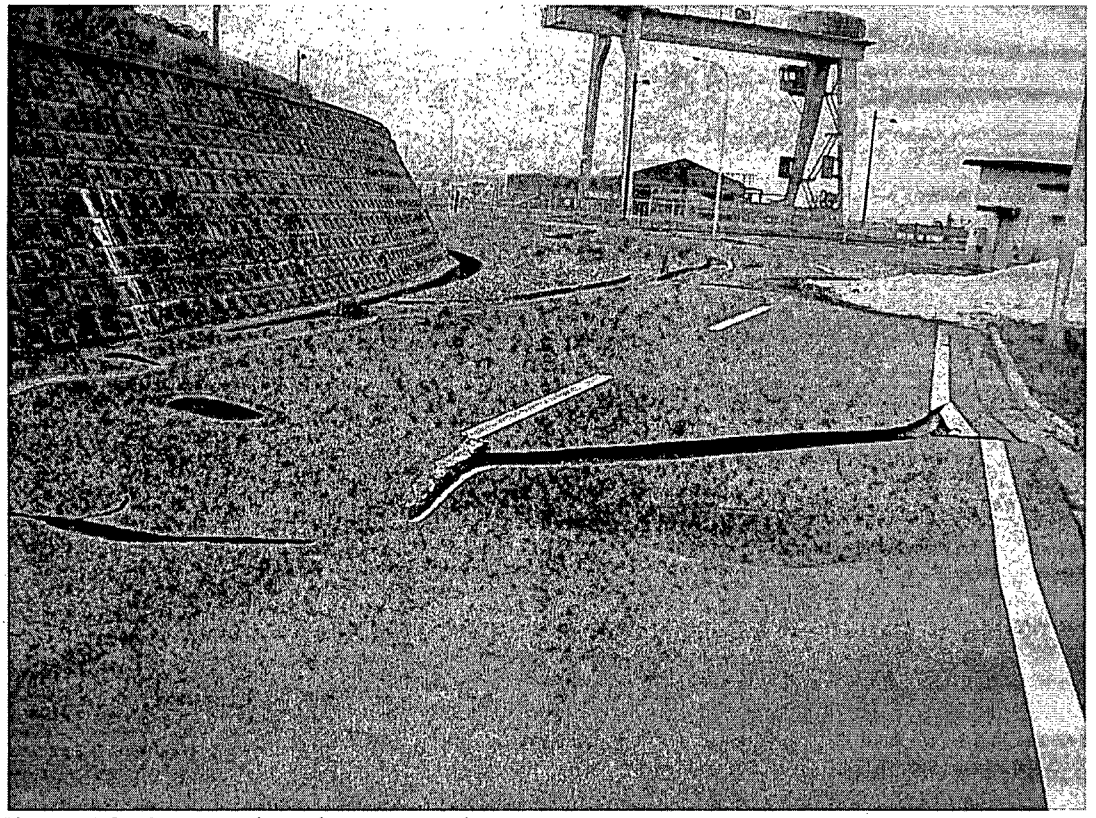

Figure 5.3: Damaged road at power plant.

Figure 5.4: Cracks in reinforced concrete element at ground level.

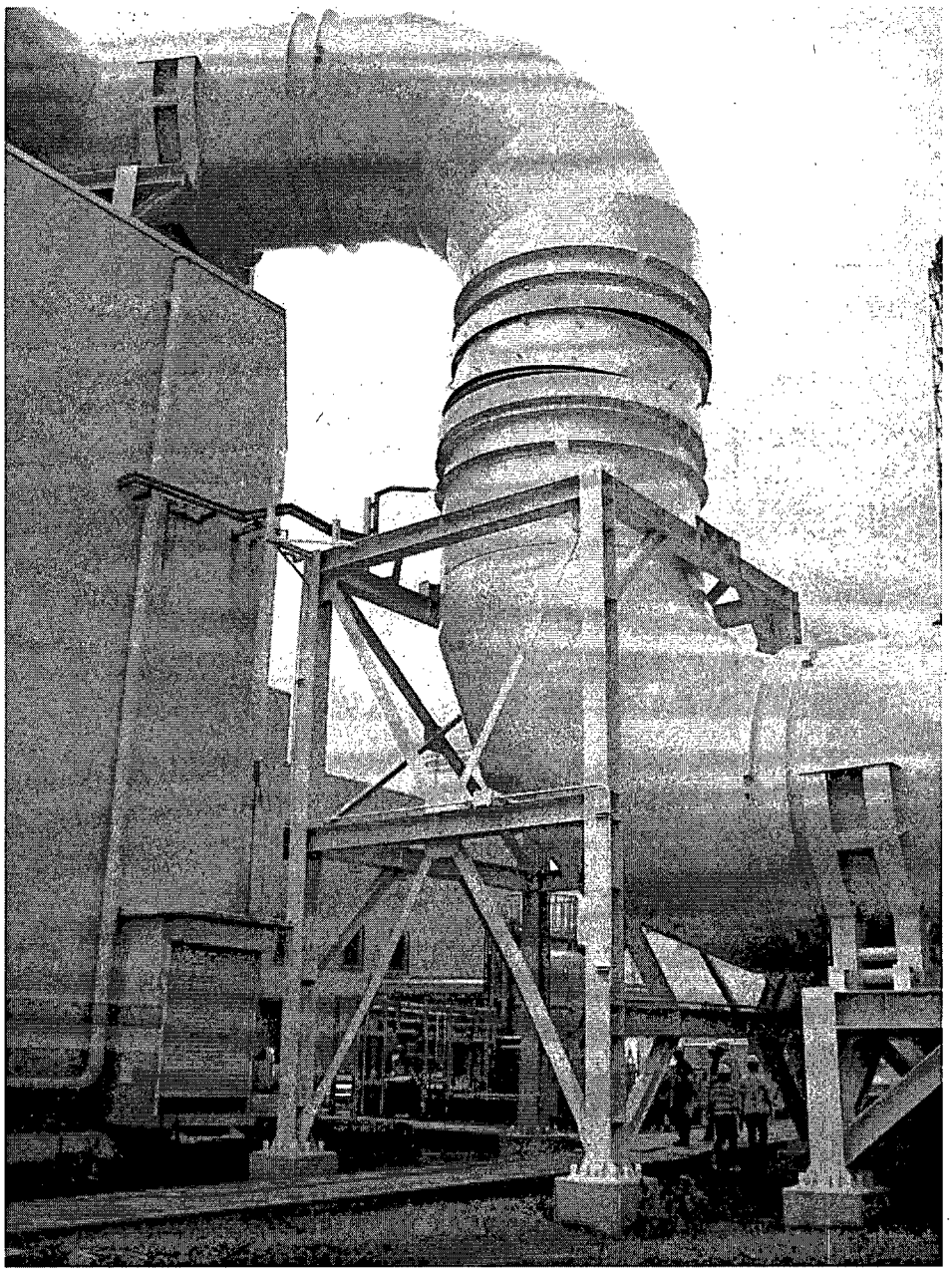

Figure 5.5: Failure of joint in exhaust pipe.

Figure 5.6: Rotation of isolated footings for equipment at nuclear power plant.

Figure 5.7: Ceiling damage in administration building of nuclear power plant.

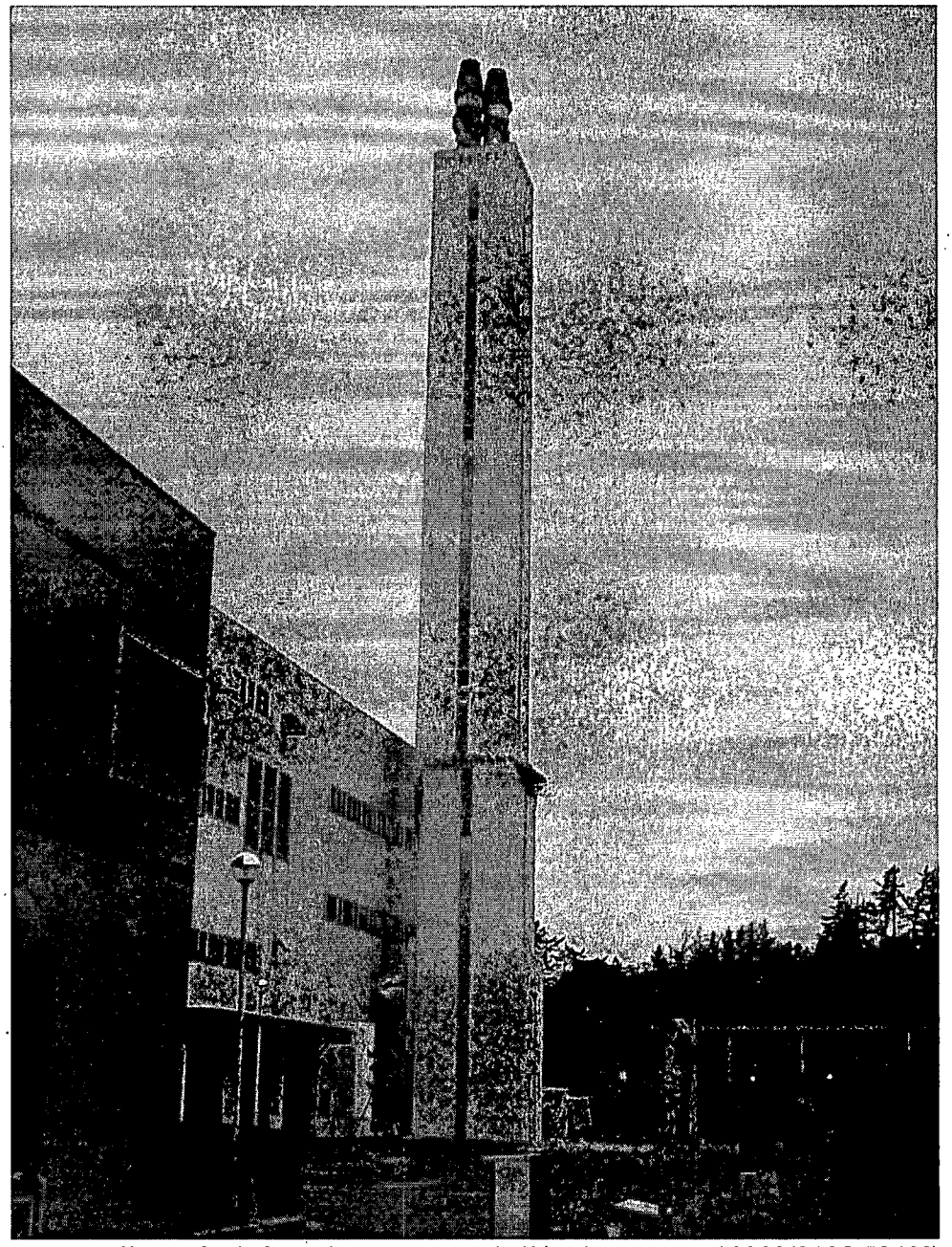

Figure 5.8: Failure of reinforced concrete stack (Site SP31, N37.3939° E138.5840°).

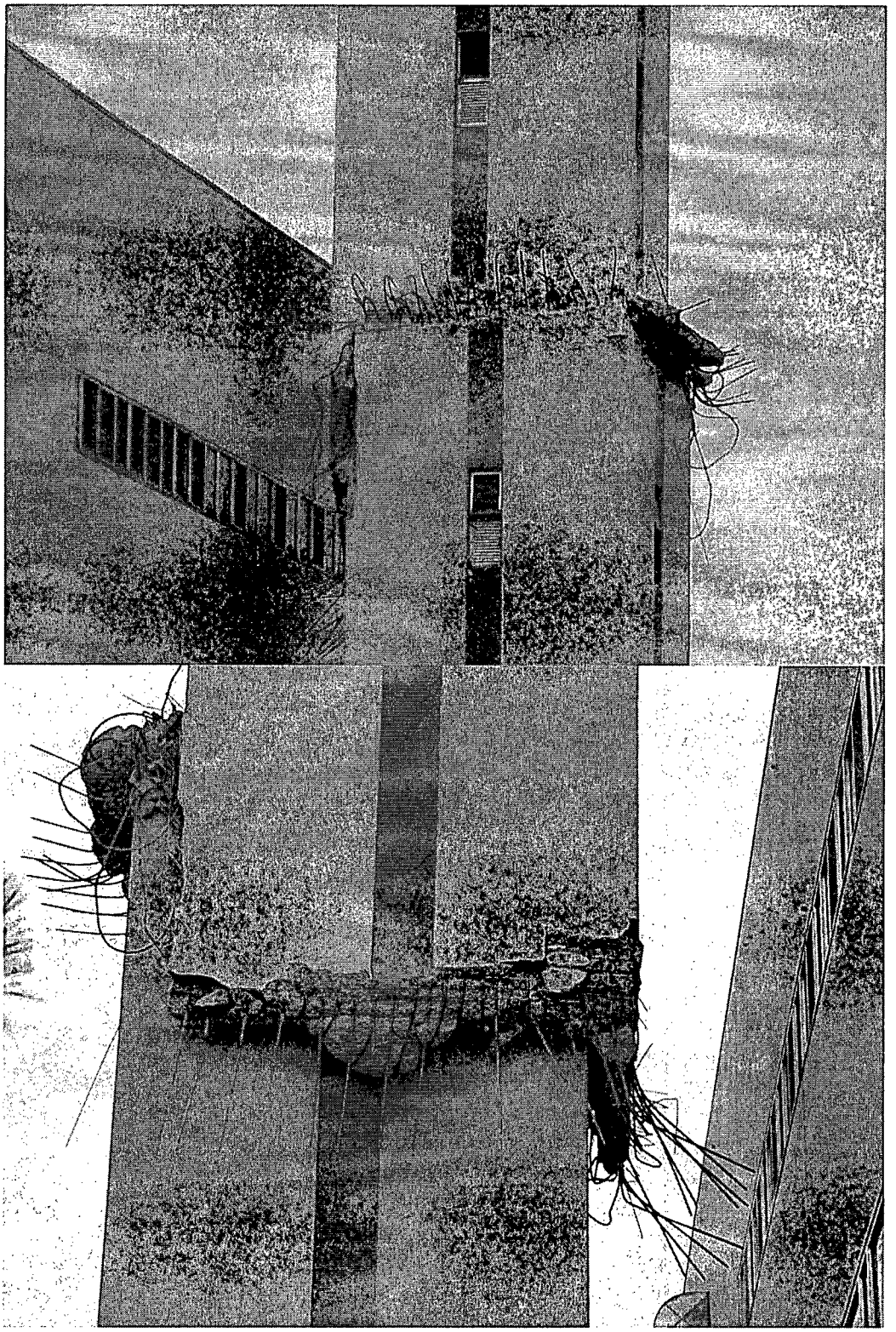

Figure 5.9: Details of failure of reinforced concrete stack (Site SP31, N37.3939° E138.5840°).

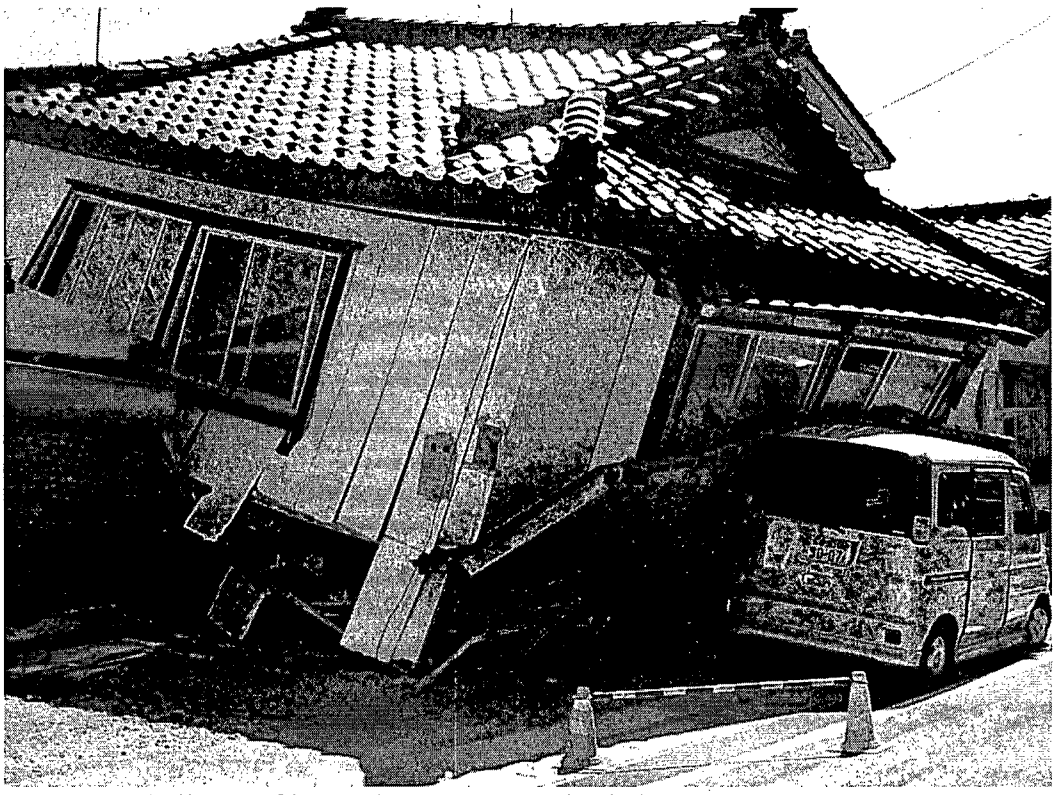

Figure 5.10: Collapse of house (N37.367°, E138.567°).

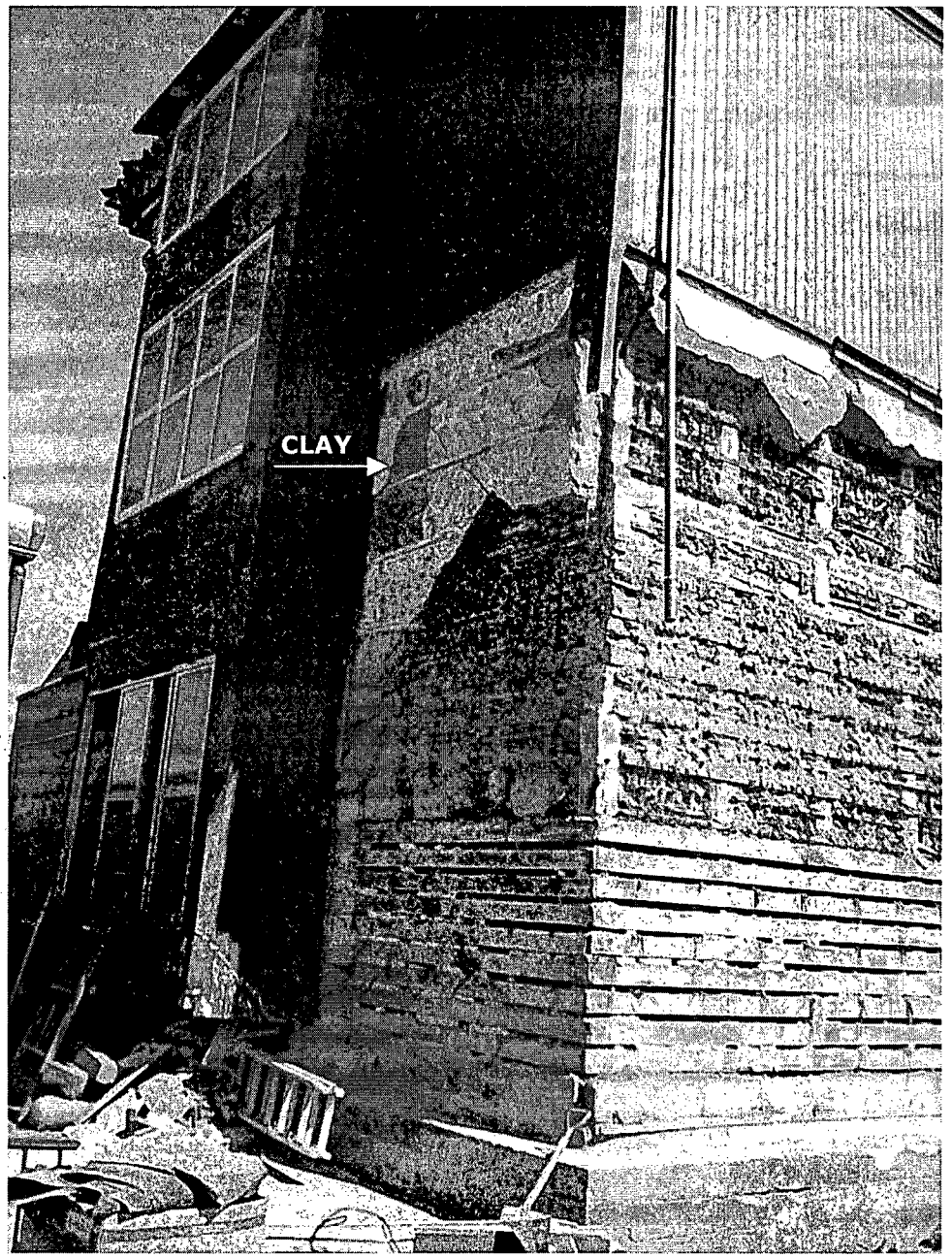

Figure 5.11: Traditional Japanese tsuchi-kabe ("soil wall") construction technique (Site SP13, N37.37056°, E138.55694°).

Additional site information and imagery at: http://walrus.wr.usgs.gov/infobank/n/nii07jp/html/n-ii-07-jp.sites.kmz

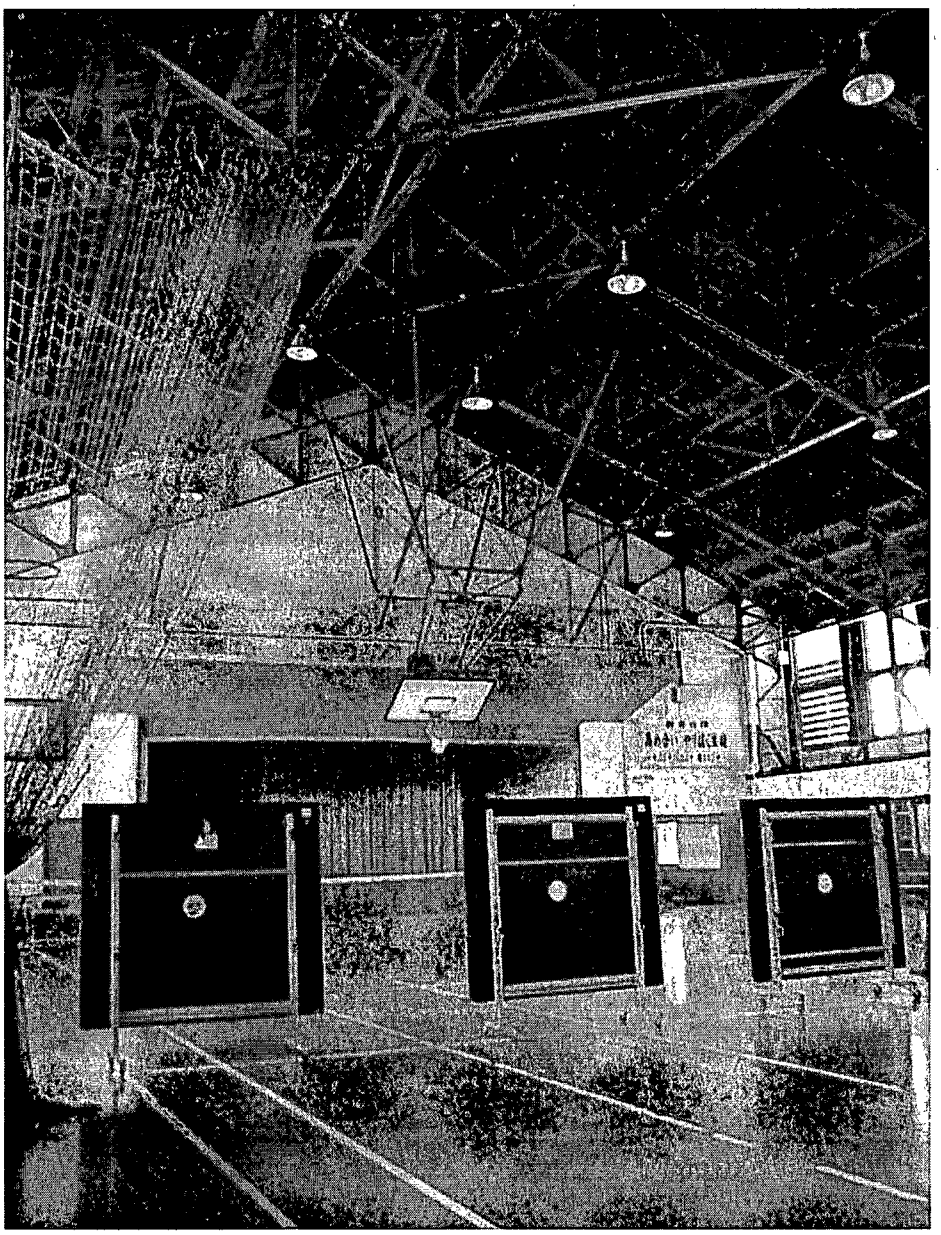

Figure 5.12: Gymnasium at Jr. High School No. 2, Kashiwazaki (Site SP2, N37.3728° E138.5709°).

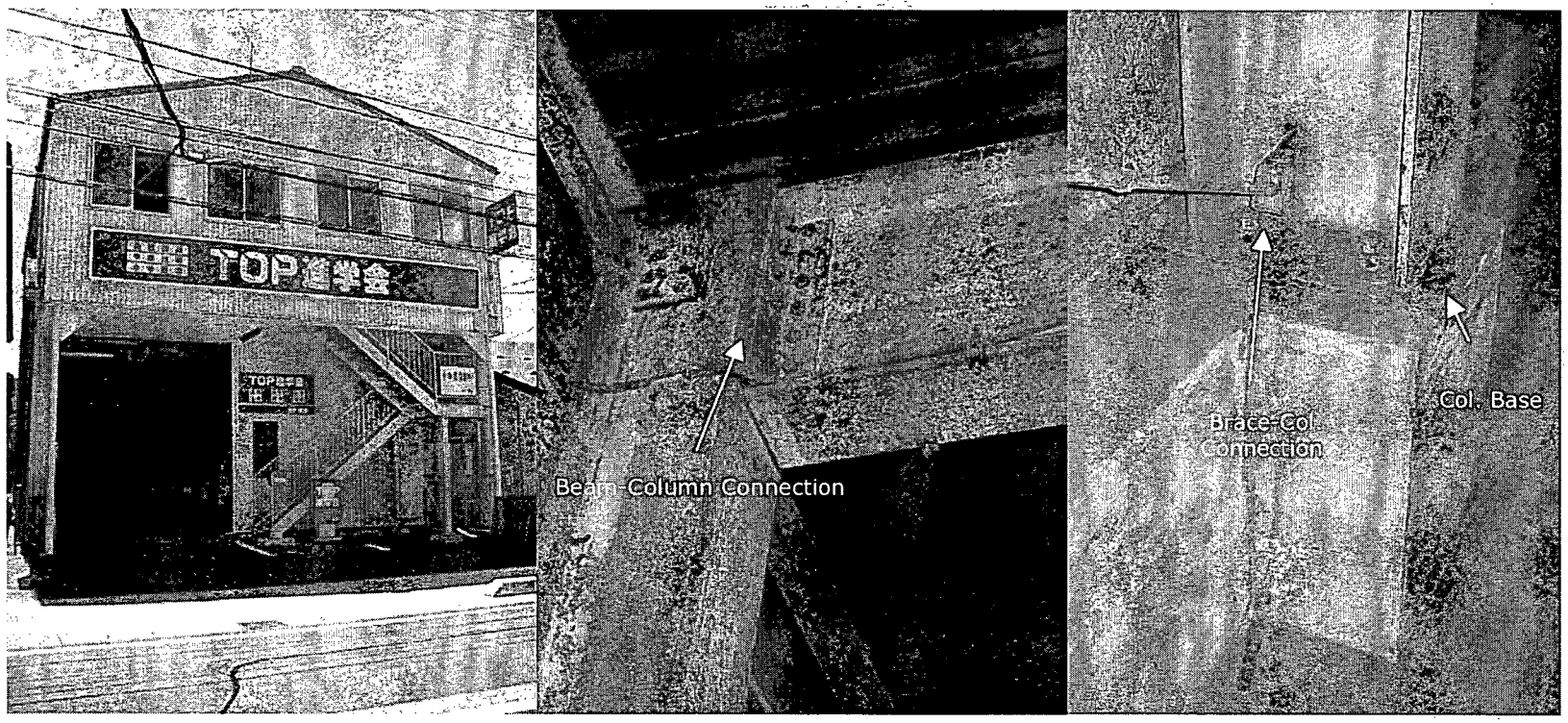

Figure 5.13: Parking structure in Kashiwazaki (Site SP29, N37.3707° E138.5566°).

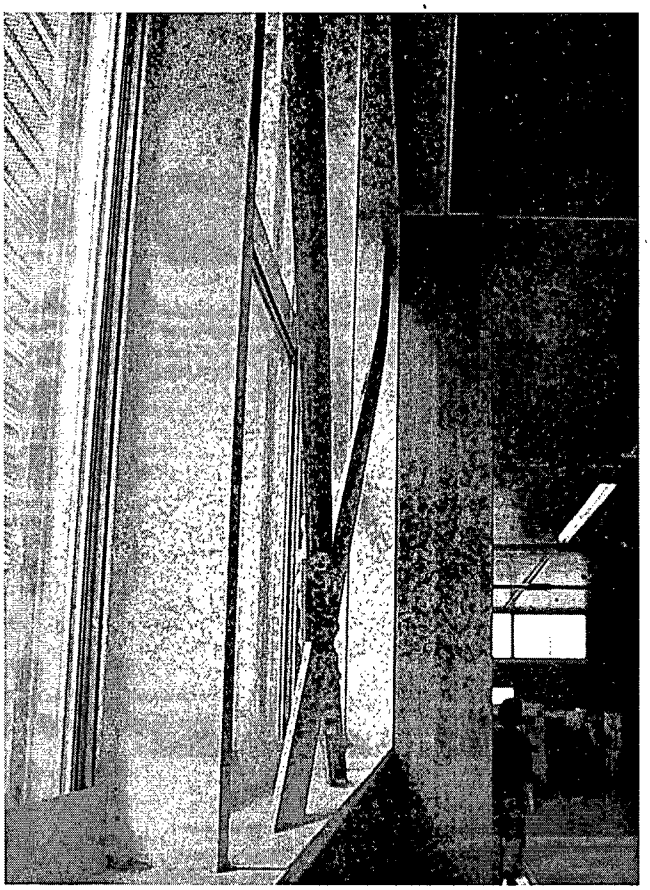

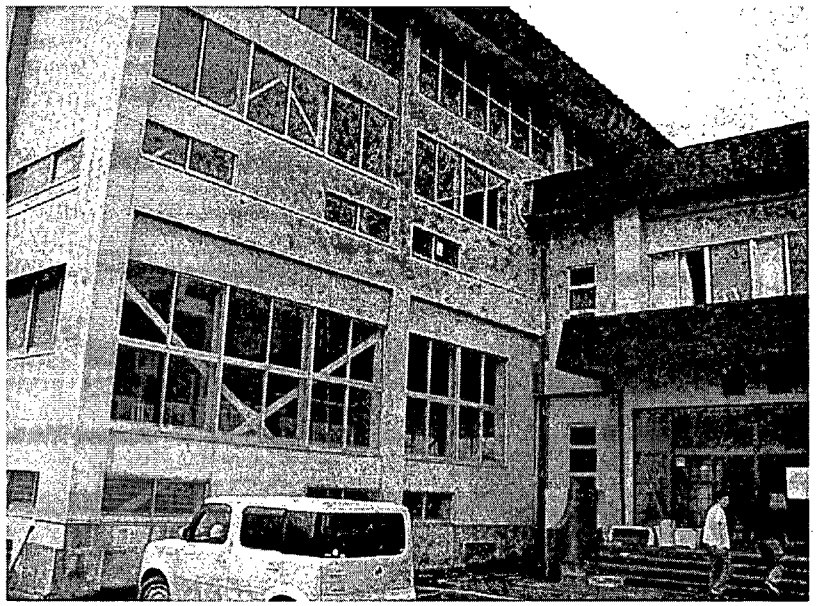

Figure 5.14: Buckling of braces in gymnasium in Kashiwazaki (Site SP7, N37.3755° E138.5541°).

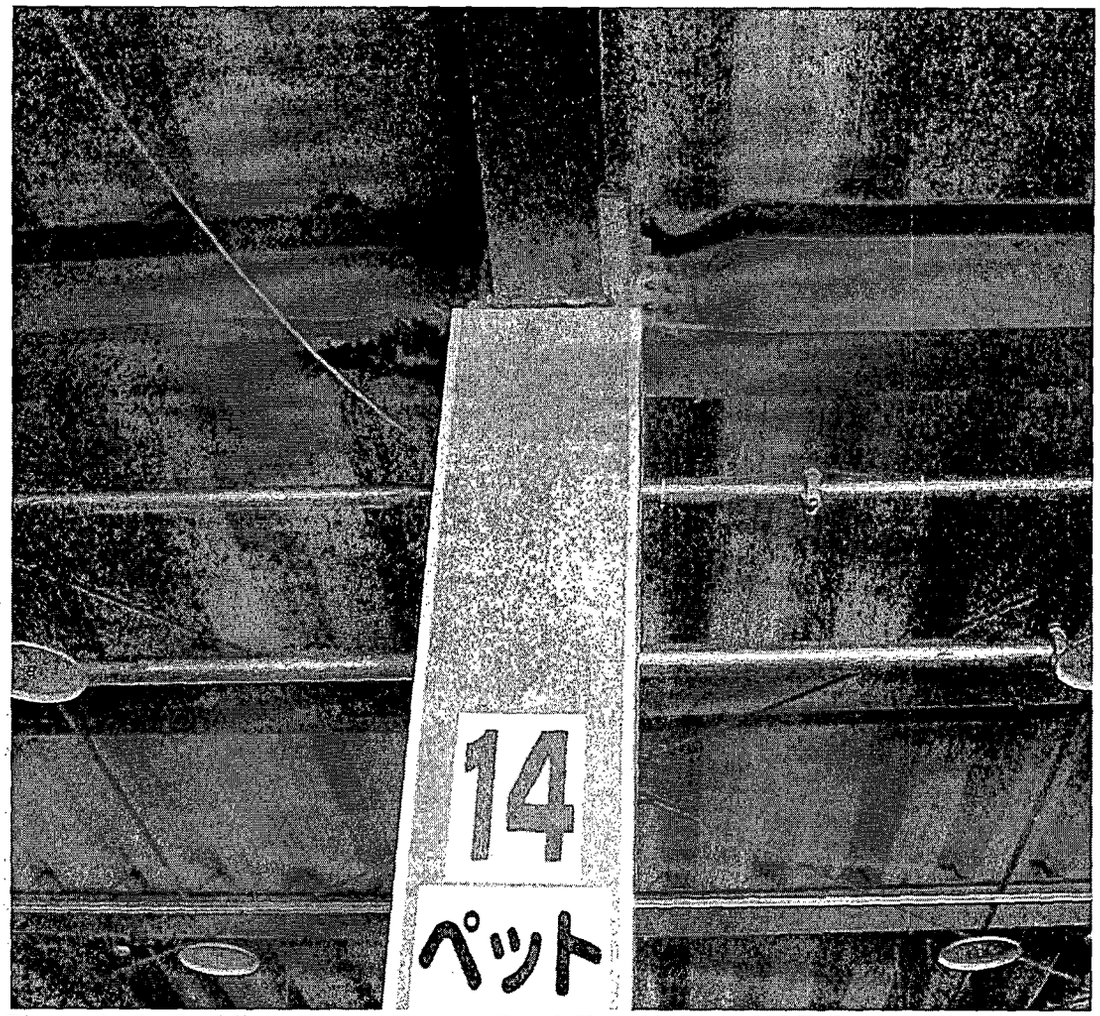

Figure 5.15: Buckling of beam flanges (Site RK41, N37.41472° E138.60833°, photo by Peter Yanev).

Figure 5.16: Kashiwazaki High School, south building (Site SP11, N37.3721° E138.5569°).

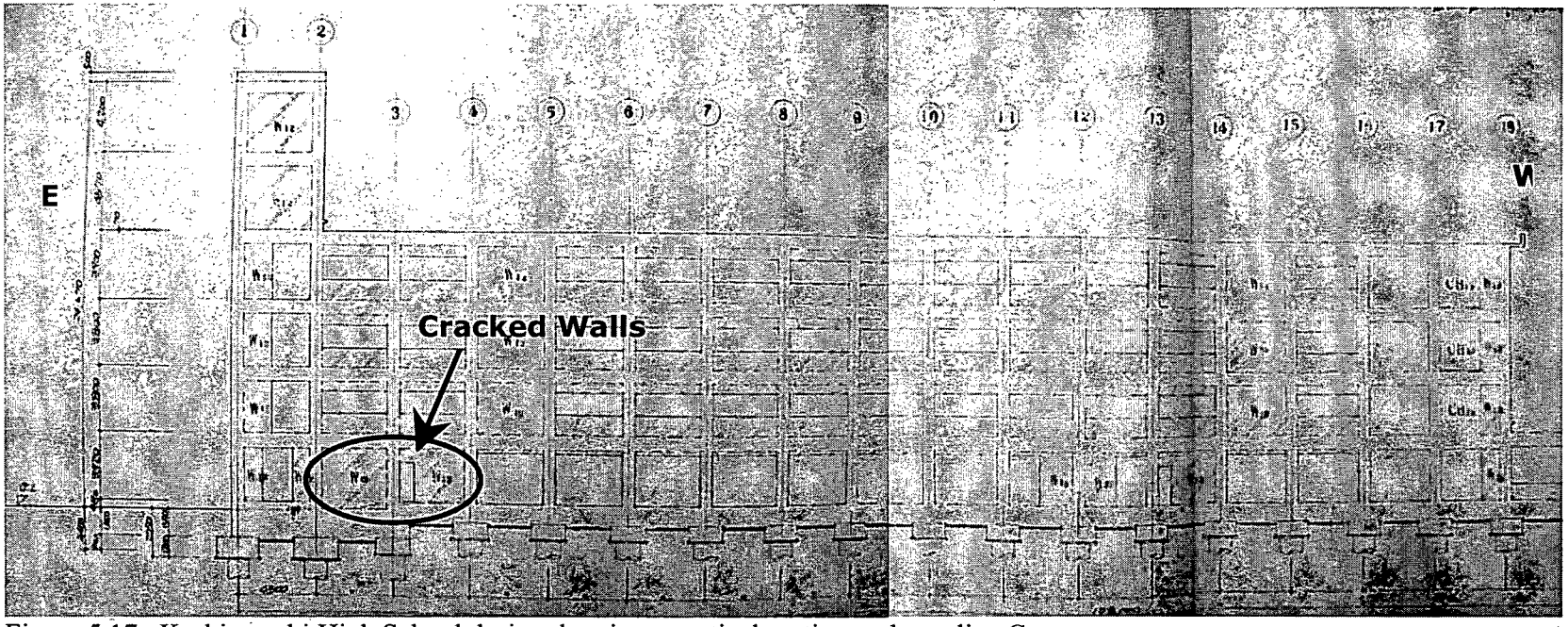

Figure 5.17: Kashiwazaki High School design drawings, vertical section, column line C.

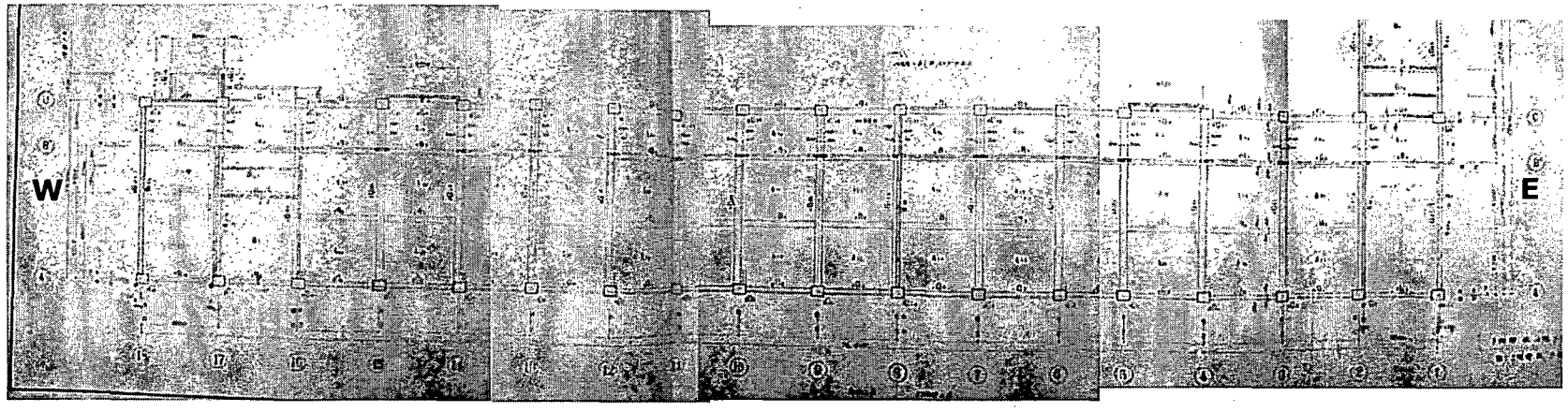

Figure 5.18: Kashiwazaki High School design drawings for typical floor plan.

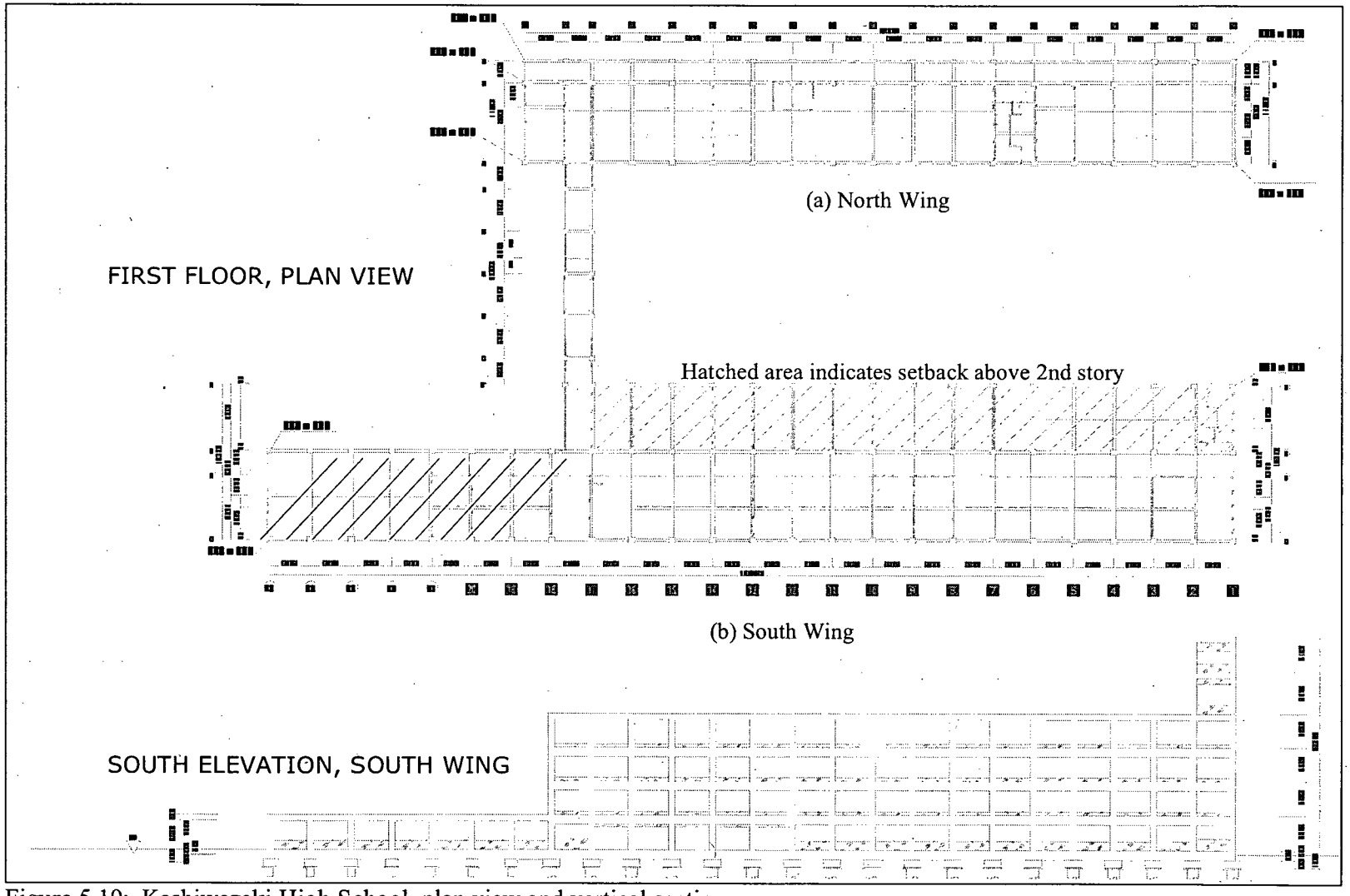

Figure 5.19: Kashiwazaki High School, plan view and vertical section.

Additional site information and imagery at http://walrus.wr.usgs.gov/infobank/n/nii07jp/html/n-ii-07-jp.sites.kmz

Main bars:	14-D24	18-D25
Hoops:	13ϕ-@100	13ϕ-@100
Sub-tie	9ϕ-@500	9ϕ-@500

(a) North Wing (b) South Wing

(c)

Figure 5.20: Typical column sections and reinforcing details, Kashiwazaki High School.

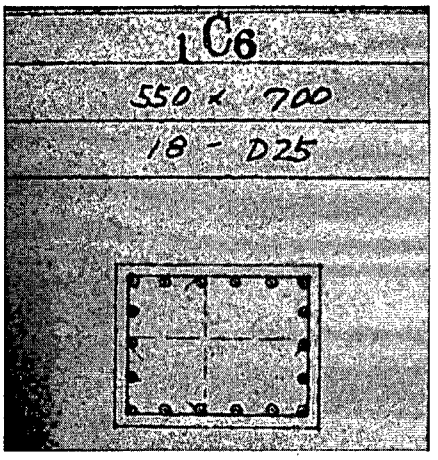

Figure 5.21: Column in first story of The Kashiwazaki High School, cross section and observed crack pattern (Site SP11, N37.3721°, E138.5569°).

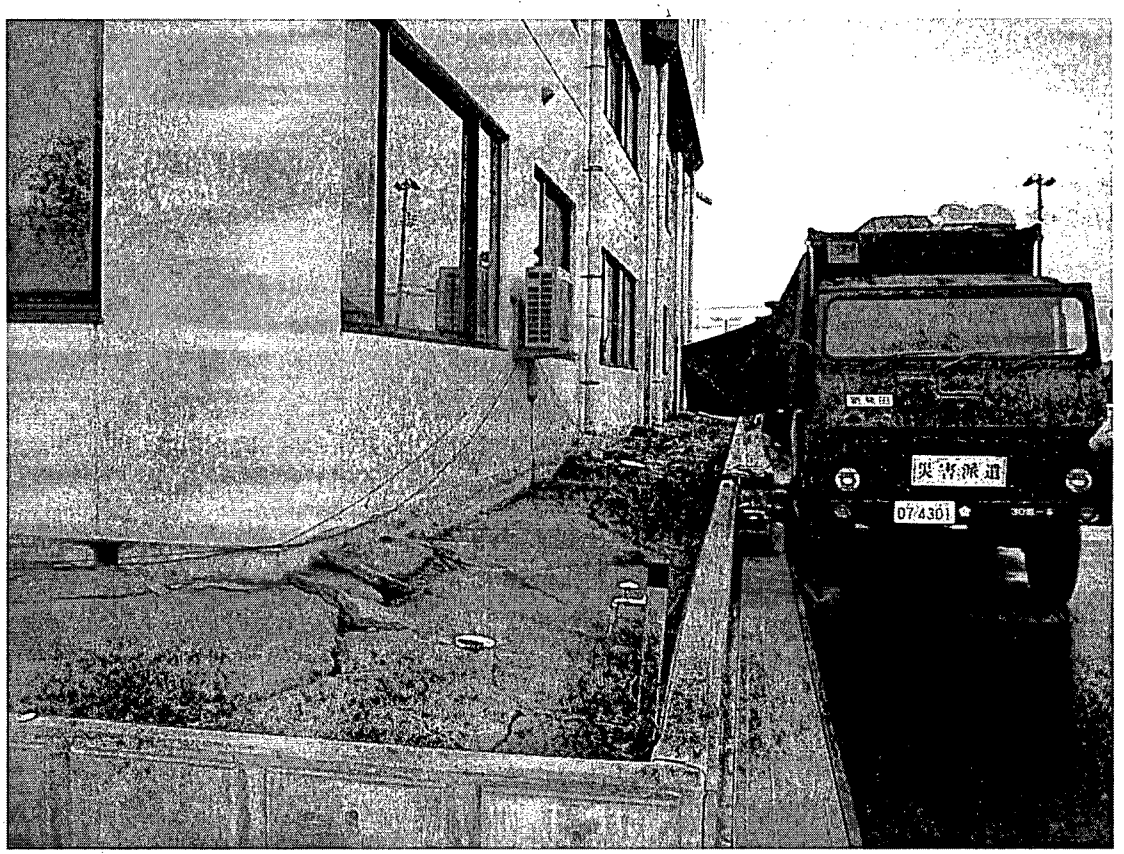

Figure 5.22: Disruption of soil surrounding a government building in Kariwa (Site SP33, N37.4223° E138.6222°).

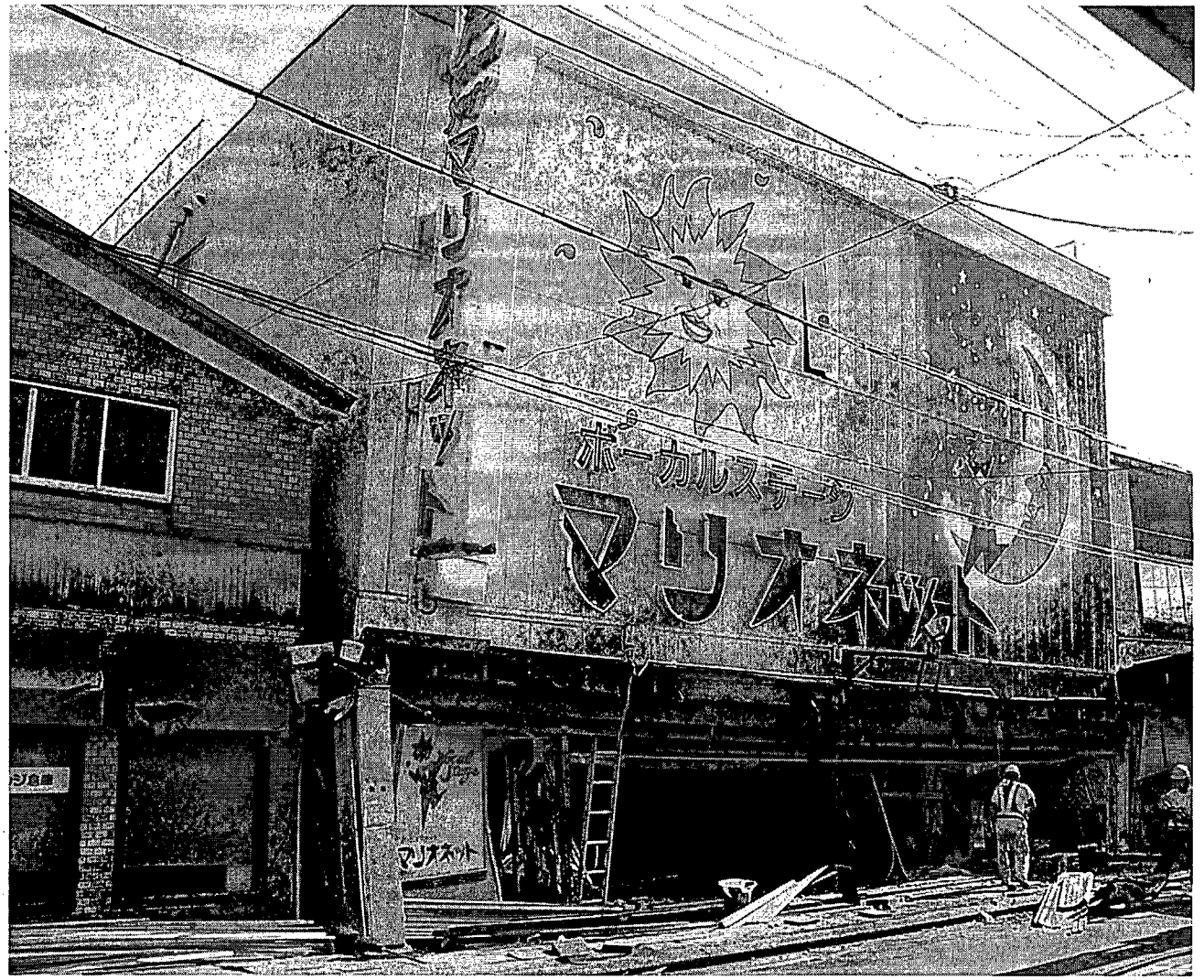

Figure 5.23: Karaoke parlor (Site NIT-81, N37.37000° E138.55825°, photo by Peter Yanev)

Figure 5.24: Shear failures of reinforced concrete columns (Site NIT-81, N37.37000° E13855825°, photo by Peter Yanev)

Section 6. Bridges

The GEER and the TCLEE teams investigated bridge damage on the Hokuriku Expressway, on National Highway 8, on bridges crossing the Sabaishi and the U Rivers, and on prefectural and city bridges. Most of the damage was the result of problem soils that caused lateral spreading or settlement to bridge approaches, making it impossible to use the bridge until repairs could be made. Damage to the bridges consisted of some combination of cracks in the abutments, vertical offsets at the approaches, and lateral offsets in the bearings. On longer bridges, there was also some damage to structural elements. Nearly every bridge was in service at the time of the investigations.

Table 6.1: Bridges observed during reconnaissance.

Name	Latitude (deg)	Longitude (deg)	Length (m)	Liquefaction	Landslides	Lateral Spreading	Bearing Distortion	Approach Offset	Severe Bridge Damage	Moderate Bridge Damage	Minor Bridge Damage	No Bridge Damage
Hokuriku Expressway												
Hachisaki Bridges	N37.315°	E138.437°	5-span 185 m			x	x	x		x		
Omigawa Bridges	N37.343°	E138.482°	3-span 300 m				x				x	
Yoshiigawa Bridges	N37.399°	E138.625°	7-span 200 m					x			x	
-	N37.4225°	E138.6412°	130 m					x				
National Highway 8												
Toyota Bridges	N37.389°	E138.592°	3-span 160 m				x	x	x	x		
Route 522	N37.364°	E138.570°	2-span 10 m						x			
Ugawa River Bridge	N37.3605°	E138.549°	2-span 60 m				x					
Yoneyama Bridge	N37.346°	E138.488°	5-span 280 m		x						x	
Yonahime Bridge	N37.3168°	E138.4348°	1-span 120 m		x		x			x		
Sabaichi River Crossings												
Ansei Bridge	N37.3864	E138.5693	106 m			x		x				
Heishi Hashi	N37.3894°	E138.5742°	22 m	x		x	x	x			x	
Heishi O-Hashi	N37.3888°	E138.5767°	118 m	x		x	x	x			x	
Kaiun Bridge	N37.3918°	E138.5806°	111 m	x		x	x	x			x	
Railway Bridge	N37.3917°	E138.5899°	65 m									x
Nagoma Bridge	N37.3904°	E138.5908°	112 m	x		x	x	x		x		
Uchara Ni Bridge	N37.3900°	E138.5960°	65 m			x	x	x		x		
Uchara Ichi Bridge	N3895°	E138.5966°	100 m			x	x	x		x		
Tsurugi Bridge	37.3921°	E138.6008°	43 m			x		x		x		
Genji Bridge	N37.3845°	E138.6017°	95 m			x	x	x		x		
U River Crossings												
Rinko Yasaka	N37.3675°	E138.5433°	81 m			x	x	x		x		
Yasaka Bridge	N37.3658°	E138.5438°	62 m			x						
Ukawa Bridge	N37.3641°	E138.5462°	66 m			x						
Osu Bashi	N37.3635°	E138.5478°	66 m			x	x	x		x		
Railway Bridges	N37.3619°	E138.5493°										x
Steel Bridge	N37.3547°	E138.5515°										x
Other Bridges												
Railway Bridge	N37.36896°	E138.56530°	20 m								x	
Rte 352 by NPP	N37.4248°	E138.6076°	20 m					x				
Highway 116 Bridge	N37.446°	E138.638°	20 m					x				

Additional site information and imagery at http://walrus.wr.usgs.gov/infobank/n/nii07jp/html/n-ii-07-jp.sites.kmz